

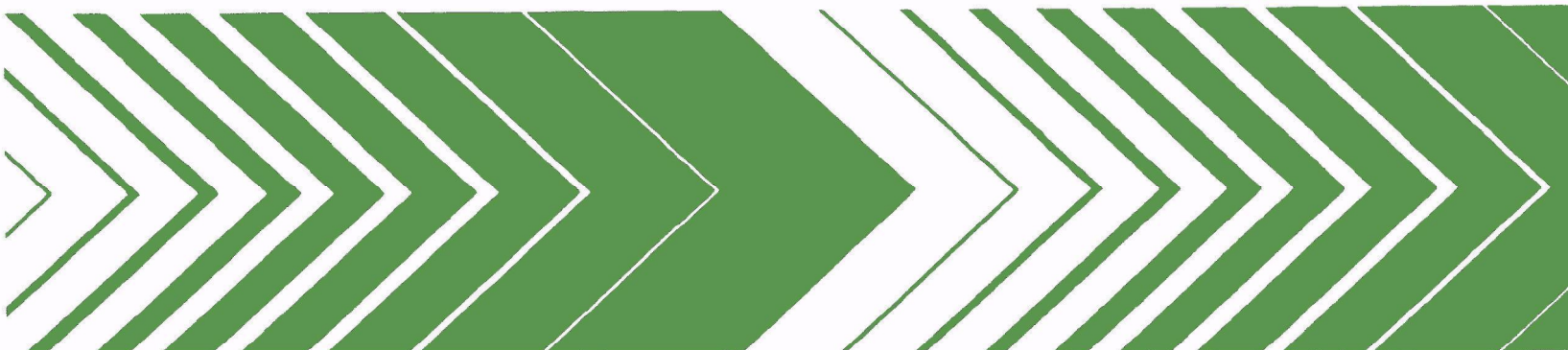
Research and Development



Environmental Monitoring Series

Optimum Meteorological and Air Pollution Sampling Network Selection in Cities

Volume I: Theory and Design for St. Louis



RESEARCH REPORTING SERIES

Research reports of the Office of Research and Development, U.S. Environmental Protection Agency, have been grouped into nine series. These nine broad categories were established to facilitate further development and application of environmental technology. Elimination of traditional grouping was consciously planned to foster technology transfer and a maximum interface in related fields. The nine series are:

1. Environmental Health Effects Research
2. Environmental Protection Technology
3. Ecological Research
4. Environmental Monitoring
5. Socioeconomic Environmental Studies
6. Scientific and Technical Assessment Reports (STAR)
7. Interagency Energy-Environment Research and Development
8. "Special" Reports
9. Miscellaneous Reports

This report has been assigned to the ENVIRONMENTAL MONITORING series. This series describes research conducted to develop new or improved methods and instrumentation for the identification and quantification of environmental pollutants at the lowest conceivably significant concentrations. It also includes studies to determine the ambient concentrations of pollutants in the environment and/or the variance of pollutants as a function of time or meteorological factors.

EPA-600/4-78-030
June 1978

OPTIMUM METEOROLOGICAL AND AIR POLLUTION SAMPLING NETWORK SELECTION
IN CITIES

Volume I: Theory and Design for St. Louis

Fred M. Vukovich, Walter D. Bach, Jr.,
and C. Andrew Clayton
Research Triangle Institute
P. O. Box 12094
Research Triangle Park
North Carolina 27709

Contract No. 68-03-2187

Project Officer

James L. McElroy
Monitoring Systems Research and Development Division
Environmental Monitoring and Support Laboratory
Las Vegas, Nevada 89114

ENVIRONMENTAL MONITORING AND SUPPORT LABORATORY
OFFICE OF RESEARCH AND DEVELOPMENT
U.S. ENVIRONMENTAL PROTECTION AGENCY
LAS VEGAS, NEVADA 89114

DISCLAIMER

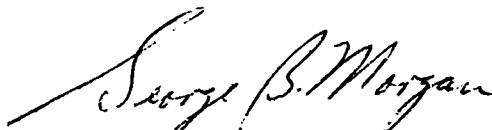
This report has been reviewed by the Environmental Monitoring and Support Laboratory-Las Vegas, U.S. Environmental Protection Agency, and approved for publication. Approval does not signify that the contents necessarily reflect the views and policies of the U.S. Environmental Protection Agency, nor does mention of trade names or commercial products constitute endorsement or recommendation for use.

FOREWORD

Protection of the environment requires effective regulatory actions which are based on sound technical and scientific information. This information must include the quantitative description and linking of pollutant sources, transport mechanisms, interactions, and resulting effects on man and his environment. Because of the complexities involved, assessment of specific pollutants in the environment requires a total systems approach which transcends the media of air, water, and land. The Environmental Monitoring and Support Laboratory-Las Vegas contributes to the formation and enhancement of a sound monitoring data base for exposure assessment through programs designed to:

- develop and optimize systems and strategies for monitoring pollutants and their impact on the environment
- demonstrate new monitoring systems and technologies by applying them to fulfill special monitoring needs of the Agency's operating programs

This report discusses the theoretical bases for a method of designing meteorological and air quality monitoring networks and the application of the method to the metropolitan St. Louis area. Regional or local agencies may find this method useful in planning or adjusting their aerometric monitoring networks. The Monitoring Systems Design and Analysis Staff at the EMSL-LV may be contacted for further information on the subject.



George B. Morgan

Director

Environmental Monitoring and Support Laboratory
Las Vegas

PREFACE

This document deals with the theoretical aspects of a methodology for optimum meteorological and air quality monitoring network selection and the application of the methodology to the metropolitan St. Louis area. Subsequent reports will be concerned with verification of the methodology for St. Louis with regard to the airflow and with regard to the air quality.

James L. McElroy
Project Officer
Environmental Monitoring and Support Laboratory
Las Vegas

ACKNOWLEDGEMENTS

This report was prepared by the Research Triangle Institute (RTI), Research Triangle Park, North Carolina, under Contract No. 68-03-2187 for the U.S. Environmental Protection Agency (EPA). A major portion of the funding of Phase I of this research project came from the National Science Foundation, Research Applied to National Needs. The support of these agencies is acknowledged. The Project Officer for EPA was Dr. James L. McElroy. Many individuals from RTI participated in this project. They are too numerous to cite here. However, certain individuals stand out and their efforts shall be acknowledged. Mr. J. W. Dunn was responsible for developing the computer algorithm for the three-dimensional primitive equation model. Mr. Bobby Crissman developed all the major parameters for the primitive equation model and helped in running the field program to verify the results of the entire modeling effort. Mr. Clifford Decker was responsible for the management of the field program.

Special acknowledgements are to be cited for the cooperation of various individuals and organizations allowing us to set up field stations on their property in St. Louis, Missouri. These are Sister Rosita Hyland of Incarnate Word Academy; Mr. E. M. Krings of the Chancery Office in St. Louis who allowed us to set up the site of Kenrick Seminary; Mr. Paul Mydlar of the St. Louis City Air Pollution Control Agency; and Mr. James Spanos, District Engineer of the East Side Levy and Sanitary District. Special thanks to Mr. Ashwin Gajjar of the St. Louis County Air Pollution Control Agency for not only allowing us to place our instruments in some of his air monitoring stations but also for providing us air pollution and meteorological data.

We would also like to acknowledge the cooperation of Mr. Robert Browning of the EPA, Research Triangle Park, for providing us with Regional Air Pollution Study (RAPS) data which will be used in a major part of our data analysis to follow.

TABLE OF CONTENTS

Foreword	iii
Preface	iv
Acknowledgements	v
Table of Contents	vii
List of Figures	viii
List of Tables	ix
Glossary of Terms	
Primitive Equation Model	x
Regression Model and Site Selection Algorithm	xii
Objective Analysis Model	xiv
Summary	xvi
1.0 Introduction	1
2.0 Theory	4
2.1 Applications of Model	6
3.0 Model Development	9
3.1 Primitive Equation Model	9
3.1.1 Grid, Finite Differencing and Boundary Conditions	11
3.1.2 Boundary Layer Parameterization	14
3.1.3 Initial Conditions and Integration	20
3.2 Determination of a Wind Monitoring Network	20
3.2.1 General	20
3.2.2 Development of Statistical Model Form	23
3.2.3 Selection of Candidate Sites	31
3.2.4 Design Selection Criteria	34
3.2.5 Design Selection Algorithm	39
3.2.6 Application of the Algorithm	41
3.2.7 Comparison of Alternative Wind-Monitoring Networks	44
3.3 Objective Variational Analysis Model	59
3.3.1 Description of the Model	62
3.3.2 Analysis Technique	67
3.3.3 Numerical Solutions	69
3.3.4 Weighting Factors	71
3.3.5 Test Results	72
4.0 Test and Evaluation	84
4.1 Operational Optimum Network	84
4.2 Field Programs	87
4.3 Analysis of Data	89
Appendix A - A Theoretical Study of the St. Louis Heat Island: The Wind and Temperature Distribution	91
Appendix B - Area Sources with Objective Variational Analysis Model	116
Appendix C - Sensitivity Analysis and Testing of the Variational Objective Analysis Model	121
References	133

LIST OF FIGURES

<u>Number</u>		<u>Page</u>
1	Flow diagram for developmental concept	7
2	Model grid points in the metropolitan St. Louis area	12
3	Distribution of $H(x,y)$ (m) field for the St. Louis, Missouri region	15
4	Distribution of the $\delta\theta(x,y)$ ($^{\circ}K$) field for the average heat island in St. Louis, Missouri	16
5	Design selection strategy	21
6	Thirty-point designs from square grid and diamond grid	43
7	Variance function for design A0	48
8	Variance function for design A1	49
9	Variance function for design A2	50
10	Variance function for design A3	51
11	Stations in the A2 network (the OSN) for St. Louis, Missouri	53
12	Variance function for the OSN*	58
13	Concentration isopleths ($\mu g/m^3$) at ground level from emissions (10 gm/s) normally distributed within the shaded area, at neutral stability and a constant wind, U , of 3 m/s	73
14	Horizontal distribution of ξ (—), S_z (— · — ·), and γ^{-1} (— — —) along $y = 5$ km for Case I ²	74
15	Concentration distribution ($\mu g/m^3$) with x as determined using R^{-2} interpolation of randomly selected observations (*) from the distribution of Figure 12	78
16	Concentration distribution ($\mu g/m^3$) with x for Case VI showing ψ^* (— · —), $\hat{\psi}(x — x)$, ψ from Case II (·····)* along $y = 5$ km	79
17	Analysis error variance versus iteration in Case VI (—) and Case VII (— — —).	81
18	Concentration isopleths ($\mu g/m^3$) determined from an R^{-2} interpolation of perturbed observations at randomly selected data points (*) of the distribution of Figure 25.	82
19	Concentration distributions with x for Case VII showing ψ^* (— · — ·), $\hat{\psi}(\cdot — \cdot)$ and ψ (—) along $y = 5$ km	83
20	Station array in the RAPS network and in the city/county network in St. Louis, Missouri	85
21	Stations in the OSN* for St. Louis, Missouri	86
22	Location, name and number of stations maintained by RTI	88

LIST OF TABLES

<u>Number</u>		<u>Page</u>
1	Terms Included in 49 Candidate Models	28
2	Means of R^2 and S^2 Over 48 Cases for 49 Models	29
3	Correlations Between Simulated and Predicted Values for Selected Models	30
4	Four 19-Point Networks Selected for Evaluation	45
5	Average Correlation and Sums of Squares of Deviations for Each Network	45
6	Symbol Key to Variance Function Plots	46
7	Summary of Correlations Between Observed and Predicted Values Over 441 Points of Innermost Grid--By Wind Shear and Design	56
8	Specification of Design Points for The OSN and OSN*	57

GLOSSARY OF TERMS
Primitive Equation Model

- x ~ horizontal coordinate in a Cartesian coordinate system which is positive in the direction of the initial flow field
- y ~ horizontal coordinate perpendicular to the x axis in the Cartesian coordinate system which is positive to the left of the initial flow field
- z ~ vertical coordinate
- u ~ x -component of the horizontal wind field
- v ~ y -component of the horizontal wind field
- w ~ vertical velocity
- p ~ pressure
- θ ~ potential temperature
- p_0 ~ 100 centibar
- R ~ gas constant for dry air
- f ~ Coriolis parameter
- ρ ~ density
- g ~ the acceleration of gravity
- A_x ~ x -component of the exchange coefficient for heat and momentum
- A_y ~ y -component of the exchange coefficient for heat and momentum
- A_{xz} ~ vertical component of the exchange coefficient for the x -component of momentum
- A_{yz} ~ vertical component of the exchange coefficient for the y -component of the momentum
- A_{Hz} ~ vertical component of the exchange coefficient for heat
- $()'$ ~ perturbation quantities
- $(\bar{ })$ ~ initial values
- $H(x,y)$ ~ the height of the natural and manmade topography above the river height at a grid point
- z^* ~ the height of any grid point above H
- $\Delta\theta$ ~ the temperature associated with the heat island at any time
- $\delta\theta$ ~ the total amplitude of the heat island
- γ ~ rate constant for the production of the heat island

$u_* \sim$ x-component of the friction velocity

$v_* \sim$ y-component of the friction velocity

$T^* \sim$ the scale temperature

$U^* \sim \sqrt{u_*^2 + v_*^2}$

$z_0 \sim$ roughness length

$k \sim$ von Kármán constant

$\kappa = 0.287$

$\alpha = 18$

$\ell \sim$ mixing length for momentum

$\ell_H \sim$ mixing length for heat

$Ri \sim$ Richardson number

$\alpha_1 = 18$

$\alpha_2 = 11$

GLOSSARY OF TERMS

Regression Model and Site Selection Algorithm

x ~ horizontal coordinate in a Cartesian coordinate system; increasing from west to east

y ~ horizontal coordinate in a Cartesian coordinate system; increasing from south to north

$H(x,y)$ ~ height (above Mississippi River) of the natural and manmade topography at the point (x,y)

$P_j(x,y)$ ~ a polynomial term (identified by the index j) of the form $x^\alpha y^\gamma$ where α and γ take on non-negative integral values

$Z_k(x,y)$ ~ the k th wind speed component ($k=1$ for WE and $k=2$ for SN) at the point (x,y)

B_{kj} ~ the estimated regression coefficient associated with P_j when component Z_k is used as a dependent variable

$Q_j(x,y,H)$ ~ a polynomial term (identified by the index j) of the form $x^\alpha y^\gamma [H(x,y)]$

C_{kj} ~ the estimated regression coefficient associated with Q_j when component Z_k is used as a dependent variable

$\hat{Z}_k(x,y)$ ~ the predicted value for wind component k at the point (x,y)

s^2_{ikm} ~ the residual variance for wind component Z_k from fitting a particular model (index m) to a particular set of data (index i)

R^2_{ikm} ~ the proportion of total variation in wind component Z_k accounted for by a particular model (index m), when applied to a particular set of data (index i)

$b_j(k)$ ~ the j th estimated regression coefficient in a particular (13-term) model which relates wind component Z_k to geographic location and elevation

X_D ~ the matrix of independent variables for a particular design (network of stations) D

$b_k^{(D)}$ ~ the vector of $b(k)$ values obtained from a design D

$\hat{Z}_k^{(D)}(x,y)$ ~ the predicted value of the k th wind component at the point (x,y) obtained from applying a particular model to data from a design D

σ^2_k ~ the (unknown) error variance associated with component Z_k

$v_D(k,x,y)$ ~ the variance of $\hat{Z}_k^{(D)}(x,y)$

$s_D(x,y) = v_D(k,x,y)/\sigma_k^2$, the value of the variance function associated with design D, evaluated at the point (x,y)

$w(x,y) \sim$ the value of a weighting function at the point (x,y)

$R \sim$ a set of 521 grid points contained in the region $\{(x,y): |x| \leq 16, |y| \leq 16\}$

$\Gamma_D = \frac{1}{521} \sum_R w(x,y) s_D(x,y)$, the value of the design selection criterion for design D

$\Delta_r \sim$ a class of r-point designs

$D_\ell^{(r)} \sim$ a particular element (identified by the index ℓ) of Δ_r

GLOSSARY OF TERMS
Objective Analysis Model

- x ~ horizontal coordinate in a Cartesian coordinate system; increasing from west to east
- y ~ horizontal coordinate in a Cartesian coordinate system; increasing from south to north
- z ~ vertical coordinate in a Cartesian coordinate system increasing with distance from earth's surface
- u ~ x-component of the horizontal wind vector
- v ~ y-component of the horizontal wind vector
- w ~ vertical velocity
- ψ ~ pollutant concentration
- Q ~ pollutant emission rate
- σ_y ~ standard deviation of the pollutant concentration in the horizontal crosswind plane from a point-source emission
- σ_z ~ standard deviation of the pollutant concentration in the vertical plane from a point-source emission
- U ~ mean wind speed
- ϕ ~ an arbitrary, unspecified variable
- Ω ~ the domain of the integration; relaxation coefficient
- K_H ~ eddy diffusivity in the horizontal plane
- K_z ~ eddy diffusivity in the vertical plane
- Z ~ maximum altitude of the surface layer
- S_z ~ local standard deviation of pollutant concentration in the vertical plane
- L ~ characteristic length of the pollution system
- Σ ~ characteristic value of σ_z
- q_x, q_y ~ standard deviation of the area emission distribution
- R ~ turbulent Reynolds number ($= K/UL$)
- $(-)$ ~ characteristic magnitude of a variable
- $(\wedge) \sim = \int_0^z dz$
- $(*)$ ~ analytic solution to the pollution distribution
- (\sim) ~ "observed" quantity

$(\psi_B) \sim$ "background" value
 $i,l \sim$ indices of increments in the x direction
 $j,m \sim$ indices of increments in the y direction
 $v \sim$ iteration number

SUMMARY

This report describes the theory and the models which have been developed to establish an optimum meteorological and air pollution sampling network in urban areas. The theory and models are generalized so that they can be applied to any urban area. However, the network developed is specific for a given urban region. The network yields both meteorological and air pollution data so that not only may the distribution of a pollutant be obtained over the domain of the network, but that the distribution may be predicted over short time intervals.

The optimum network provides a basis whereby the distribution of any given pollutant may be obtained at a given time over the domain of the network. The data may be used to determine long-term statistics or short-term analysis. Long-term statistics may be determined from the background or maximum pollutant concentrations. The short-term analysis will provide a means whereby regions may be determined where a pollutant concentration exceeds the standards.

Three specific models are required in order to determine the optimum network and acquire the air pollution distribution over the domain of the network. These are: a three-dimensional hydrodynamic model; a statistical model; and an objective variational analysis model.

The basis of the network is the wind field in the urban area rather than the air pollution distribution. The wind field was chosen because it provided a solution with longer-term stability than the air pollution distribution. The addition of two or three major sources in an urban area can markedly changed the statistics of the air pollution distribution in a short period of time. Any network based on today's air pollution distribution may become inadequate with the addition of major sources.

The primitive hydrodynamic model is used to simulate the wind field over a variety of cases in which the major factors influencing the flow (essentially the urban heat island, surface roughness variability, topography, etc.) are included in the model. With proper definition of the urban forcing functions, a reasonable approximation to the statistical nature of the flow

can be obtained. By statistical nature of the flow, we mean that the specification of the exact magnitude of the flow is not necessary if its order of variability is reasonably well represented. This further asserts that the magnitude of the difference between minima and maxima in the flow may not be exact, but the location of minima and maxima be reasonably well represented. More specifically, the simulation data were used to develop the form of a statistical model which could be used to describe the wind distribution over the domain of the network. The magnitude of the flow and wind speed maxima and minima are determined after the parameters of the model are estimated. In the applied sense, observed wind speeds and directions from stations in the network would be used to estimate parameters (i.e., actual data will be used to determine the magnitude of the flow and of the wind speed maxima and minima).

These simulated data were used to determine the form of a regression model which approximates the various wind fields generated by the hydrodynamic model. The regression model form was then used, along with a set of potential network sites and a criterion for judging alternative networks (e.g., minimizing the average variance of predicted values), to derive an "optimum" network for sampling winds. The method used to develop the network involved the successive elimination of candidate sites--until a reasonably sized network was achieved.

The air pollution distribution is obtained through an objective variational analysis model. The model simultaneously minimizes the error variance by comparing the observed pollution concentration field with the derived pollution field and the error variance of the constraint equation. In order for the variance to be a minimum, it is shown that a second-order Euler-Lagrange equation must be satisfied under specific boundary conditions. The model requires as input parameters: the wind field derived from the optimum sampling network, the observed pollutant concentration data from the optimum sampling network, and the source emissions.

The models were applied to develop an optimum network for St. Louis, Missouri. St. Louis was chosen as a test case because the Environmental Protection Agency's (EPA) Regional Air Pollution Study (RAPS) provided

corollary data to evaluate the optimum network. After the optimum network was determined, existing stations were included as part of the optimum network which coincided or nearly coincided with those in the RAPS or city/county network. Of the nineteen (19) stations in the optimum network, sixteen (16) coincided or nearly coincided with existing stations.

In the summer of 1975 and winter of 1976, field programs were conducted concurrent with a RAPS intensive study period to collect data in order to test and evaluate the optimum network. Besides the sixteen (16) stations that overlapped with the city/county and RAPS network, three (3) stations had to be set by the Research Triangle Institute. At each of these stations, wind speed and direction, carbon monoxide, methane, and total hydrocarbon data were collected. Carbon monoxide was considered the principal pollutant to be used in the evaluation of the network. The results of this evaluation will be presented in a future report.

1.0 INTRODUCTION

The establishment of the air quality standards has brought about the need to develop air quality sampling networks in urban areas. Such networks have two primary purposes. The first is to provide data for analysis of air pollution over the urban region to determine if and where a particular pollutant concentration exceeds the standard and to determine the effectiveness of long-term control strategies. The former information is required to implement control measures to reduce the concentration of the particular pollutant to an acceptable level. The second purpose is to provide a data base for both the short- and long-term prediction of the concentration of a particular pollutant over the urban region. This information provides a base for the development of long-term control strategies. Diagnosis and prediction of air pollution is particularly necessary now that the energy crisis has made it probable that some industries and power plants will burn high sulfur coal.

Sweeney (1969) attempted to establish objective guidelines for determining the number and location of sampling stations in an optimum sampling network (OSN) for urban areas purely by statistical means. He concluded that the present state-of-the-art of statistical theory does not provide a basis for a general solution to the problem. The basis for this conclusion lies in the fact that the air pollution distribution and meteorological conditions are dynamic phenomena that vary in space and time in an urban region and vary from one urban region to the next. However, Sweeney indicated that a solution specific for a particular urban region can be obtained if a representative and statistically significant data set is available for the urban region. This data set should be made up of observations of n number of pollutants and m number of meteorological parameters. For most urban regions, n is greater than or equal to three, and m is at least one (the wind distribution) but can be larger, depending on the accuracy required.

In order to acquire this data set, Sweeney suggested that a high resolution sampling network be set up in a given urban region for the collection of data on pollution concentrations and meteorological conditions over a period of years. Though this is scientifically appealing, it is economically unfeasible. The Regional Air Pollution Study (RAPS) being sponsored by the

Environmental Protection Agency (EPA) in the metropolitan St. Louis area will cost millions of dollars and does not yield the high resolution data required by Sweeney. Sweeney required a resolution of the order of 2 to 4 km. To obtain data at those resolutions would require from 64 to 256 sampling stations. It is unreasonable to ask each urban region to support such programs.

In order to ease the economic pressure, Sweeney suggested that the urban region should be divided into sections. A high resolution network should be set up in one section and data collected over a number of years. When sufficient data are obtained in the first section, the sampling network would be moved to another, and data collection would commence and continue until sufficient data were obtained. This iterative process would continue until the data set was complete.

There is, however, a dilemma that arises when one determines an OSN based solely, or in part, on air pollution data. Most, if not all, urban regions are constantly changing. New industries are moving in, old industries are moving out; that is, new point sources move in and old point sources move out. It is important to note that the location of the old and new point sources are very often different. Furthermore, over the years, rural roads which often have insignificant traffic, become major line sources with the establishment of housing projects and accompanying commercial areas near or along the road. Other kinds of urban expansion results in similar changes. Urban expansion can produce a major change in the air pollution distribution in a 5- to 10-year period. Any OSN based on today's representative air pollution data sets may soon become obsolete. This effect would prevent Sweeney's suggested technique for obtaining a representative data set from being practical. In the intervening time between collecting data in the first segment of the urban region and collection of data in the last segment, major changes in source configurations may have occurred, making the segmented data sets totally independent of each other.

It is obvious for economic reasons that the basis of the OSN must be very stable over a relatively long period of time. A technique to establish an OSN on a more stable basis than is provided by the air pollution distribution is described in this report. The models developed have been completed and an OSN

for St. Louis, Missouri has been created. St. Louis, Missouri was chosen as a test case because the RAPS program will provide corollary data to evaluate the OSN.

2.0 THEORY

The conservation equation for any pollutant, ψ , defined for a point in space away from the earth's surface, yields the exact nature of the variables necessary to completely specify the distribution of the pollutant, i.e.,

$$\frac{\partial \psi}{\partial t} = -V \cdot \nabla \psi + \nabla \cdot (K \nabla \psi) + \psi \sum_n k_n \psi_n^* + S \quad ,$$

The first two terms on the right yield the meteorological influence on the distribution of ψ . The first term is the advective term where V is the wind vector, and the second term is the diffusion term where K is the exchange coefficient. The third term is the chemical reaction term where k is the reaction constant, ψ^* is the pollutant with which reactions take place in the case of second-order reactions, and n is the index of the summation indicating that more than one, second-order reaction may take place. The last term is the source (S) term. In this development, it was assumed that the pollutant was inert; i.e., $\psi \sum_n k_n \psi_n^* = 0$.

For a given urban region, the source parameters [source strength, source location, source type (line, point, etc.)] are known or can be determined. Any changes in the source parameters due to urban expansion or industrial relocation can also be specified. In the case of an inert gas, therefore, the unknowns are the meteorological parameters, i.e., the wind field and the distribution of K . Since a reasonable estimate of the diffusion coefficients can be obtained through wind observations and estimates of the stability, it is only necessary to establish the wind field.

The wind field should be relatively unaffected by urban expansion and industrial relocation in comparison to the effect on the pollution distribution. The changes in surface roughness that occur when a rural area is converted into a residential area will be important, but will not completely alter the nature of the flow. For example, winds from the north over a formerly rural area will have a slight westerly component over the rougher residential area, but the major wind component will be from the north; that is, something as significant as the wind turning and becoming southerly due to the roughness will not occur.

Urban expansion increases the areal dimensions of the urban heat island, which is probably the major forcing function affecting the mesoscale flow in an urban region. However, this expansion should be an effect manifested over many years (20 to 30 years) and would not alter the flow significantly if the location and heat content of the center of the heat island did not change markedly. The expansion of the suburban residential area would tend to flatten the temperature gradient in the suburbs, which would reduce accelerations due to pressure forces rather than intensify them. The establishment of another heat island center would be an important factor which would affect the flow, but the creation of such a center with an affective areal extent in most cases would also take many years (again 20 to 30 years). This would indicate that the urban wind field should be stable in the mesoscale over a relatively long period of time compared to changes that could take place in the air pollution distribution due to urban expansion.

If the parameters in the conservation equation are specified over an urban region, then it is possible to determine the distribution of a particular pollutant using an Objective Variational Analysis Model (OVAM) (Sasaki, 1970). This technique provides the pollution distribution by making proper use of limited observed data and the governing equation. In terms of the air pollution distribution, the governing equation (the conservation equation), in effect, allows the sources to be treated similarly to observations of the particular pollutant and thus, a higher order variability of the particular pollutant can be ascertained than would otherwise be obtained using limited observed data. Therefore, an OSN for the wind field would suffice to determine the distribution of a particular pollutant if: 1) air pollution data were also available at the stations in this network, 2) a proper source inventory were available, and 3) the above data (1 and 2) including the wind field, were incorporated in an OVAM. These data may also be used to predict the air pollution distribution over a short period of time.

However, we are still left with the prospect of establishing a representative data set for the wind field in order to determine an optimum network. A numerical simulation of the wind field in an urban region under the action of a multitude of synoptic meteorological conditions circumvents the economic problem of high resolution data collection over long periods of time.

With proper definition of the urban forcing function, a reasonable approximation to the statistical nature of the flow can be obtained. By statistical nature of the flow, we mean that specification of the exact magnitude of the flow is not necessary if the order of variability is reasonably well represented. This further asserts that the magnitude of the difference between minima and maxima be reasonably represented. The simulation data would be specifically used to develop the form of a statistical model which could be used to determine the flow over the domain of the network. Actual magnitudes for the wind speed components and between wind speed maxima and minima are determined after the parameters of the statistical model have been established. In the applied sense, parameters of the statistical model would be determined using observed data from stations in the network. Since only the form of the statistical model is developed using the simulation data, it is not necessary that the simulation data precisely describe the exact magnitude of the flow. Only the order of variability must be well represented. These simulated data can then be used to obtain an approximation to the OSN by integrating them with a model based on regression and sampling theory.

2.1 Applications of Model

Figure 1 is a flow diagram for the entire development concept. The primitive equation model is used to establish a representative data set for the wind field in a given urban area. In the case of St. Louis, Missouri, the data set was composed of forty-eight (48) case studies. The data are used to determine the form of a regression model that adequately characterizes the wind field for the given urban region. The resultant model form is then used in the site selection algorithm to yield the OSN. The theoretical development phase of the modeling ends here; that is, in the figure the theoretical development phase is the region above the lower dashed line.

The applied phase is the region below the upper dashed line. For this phase, it is assumed that the OSN for the wind field has been set up in the urban region. Wind and air pollution data are obtained at the stations in the OSN. The wind data are used to develop the wind distribution through the same regression model determined in the theoretical development phase. The wind distribution, the observed air pollution data, and the emissions

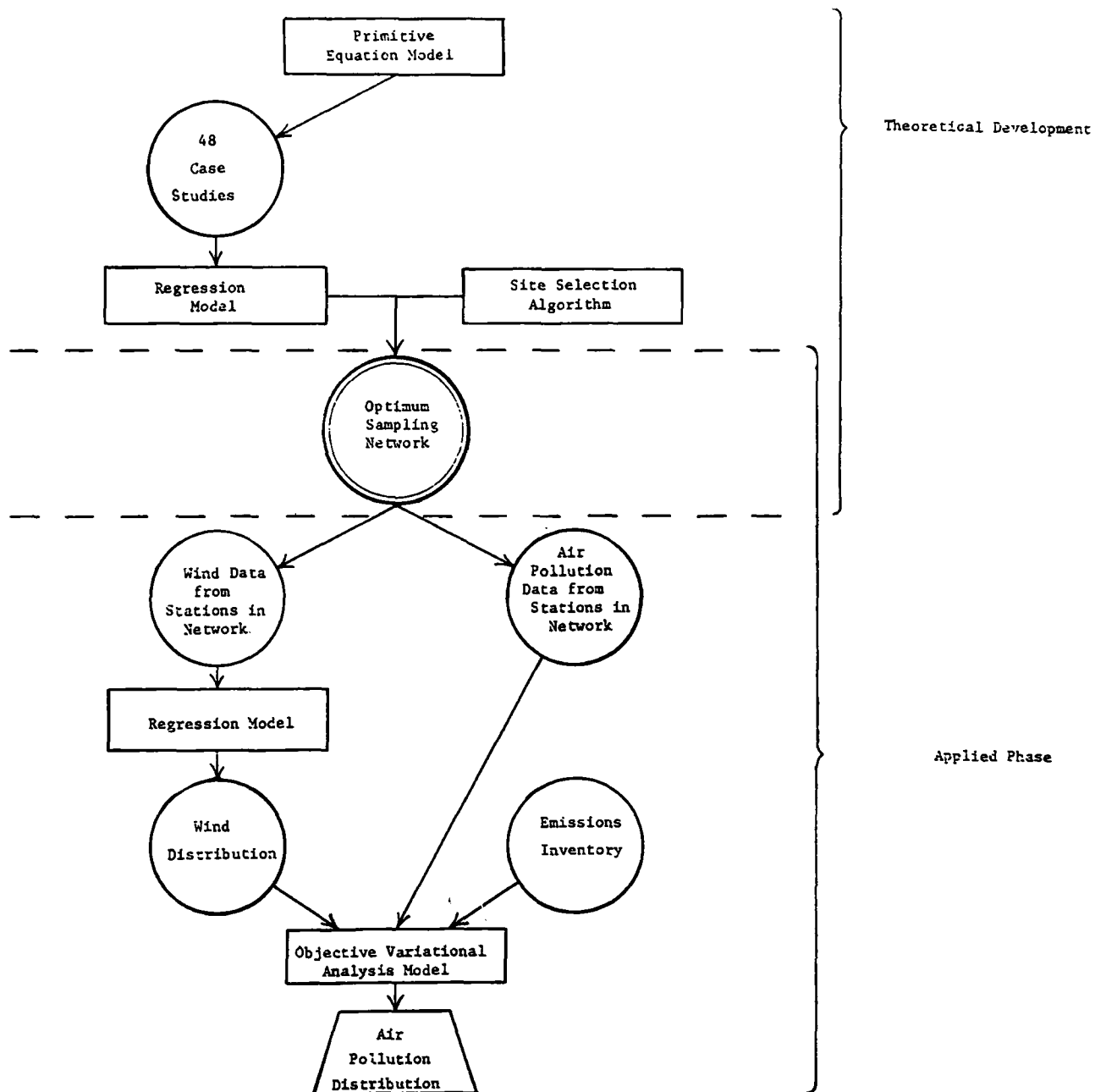


Figure 1. Flow diagram for developmental concept.

inventory are input data for the OVAM, which subsequently yields the air pollution distribution.

3.0 MODEL DEVELOPMENT

The principal purpose of this phase of the research project was to develop the models necessary 1) to yield an approximation to the statistical nature of the wind field, 2) to determine an OSN for the wind field, and 3) to establish the air pollution distribution using the wind distribution, air pollution data from the OSN and the source parameters.

3.1 Primitive Equation Model

A three-dimensional primitive equation model was developed to simulate the flow in an urban region. The model included those factors (essentially the urban heat island, surface roughness variability, and topography--including effective building heights) which would significantly change the synoptic-scale flow. Solutions were obtained for forty-eight (48) synoptic cases. These included variations in wind direction (8 points on the compass), three wind speed distributions (weak, medium and strong wind speeds with corresponding weak, medium and strong vertical wind shear in the boundary layer), and two categories of stability (stable and adiabatic boundary layer). These solutions were specific for the city of St. Louis, Missouri in that the topography and the parameters needed to generate the urban heat island were obtained from data specific for that city. The city of St. Louis is located in rather flat terrain and is not affected by large bodies of water. In order to obtain solutions for other urban regions, it is only necessary to supply the model with these parameters for the desired urban regions.

The forty-eight (48) cases mentioned above on which the optimum network was based were made up of surface wind speed categories which range from approximately 0.5 m/s to 5.0 m/s. There was no apparent increase in the order of variability when the wind speed was further increased. Analysis also showed that increasing the stability or decreasing the stability beyond the range depicted had no appreciable affect on the order of variability. Since the form of the statistical model which would be used to describe the flow over the domain of the network using the data obtained from the network, requires that the order of variability is well represented in the data set used to determine the model form, it was concluded that the wind speed

categories and stability categories were sufficient to yield a reasonable estimate of the model form.

The basic equations governing the dynamics and thermodynamics for dry convection in the primitive equation model are listed below:

$$\begin{aligned} \frac{\partial u}{\partial t} + u \frac{\partial u}{\partial x} + v \frac{\partial u}{\partial y} + w \frac{\partial u}{\partial z} = - \frac{R\theta}{p} \left(\frac{p}{p_0} \right)^\kappa \frac{\partial p}{\partial x} + f_v \\ + \frac{\partial v}{\partial x} (A_x \frac{\partial u}{\partial x}) + \frac{\partial}{\partial y} (A_y \frac{\partial u}{\partial y}) + \frac{\partial}{\partial z} (A_{xz} \frac{\partial u}{\partial z}) , \end{aligned} \quad (1)$$

$$\begin{aligned} \frac{\partial v}{\partial t} + u \frac{\partial v}{\partial x} + v \frac{\partial v}{\partial y} + w \frac{\partial v}{\partial z} = - \frac{R\theta}{p} \left(\frac{p}{p_0} \right)^\kappa \frac{\partial p}{\partial y} - f_u \\ + \frac{\partial}{\partial x} (A_x \frac{\partial u}{\partial x}) + \frac{\partial}{\partial y} (A_y \frac{\partial v}{\partial y}) + \frac{\partial}{\partial z} (A_{yz} \frac{\partial v}{\partial z}) , \end{aligned} \quad (2)$$

$$\frac{\partial \theta}{\partial t} + u \frac{\partial \theta}{\partial x} + v \frac{\partial \theta}{\partial y} + w \frac{\partial \theta}{\partial z} = \frac{\partial}{\partial x} (A_x \frac{\partial \theta}{\partial x}) + \frac{\partial}{\partial y} (A_y \frac{\partial \theta}{\partial y}) + \frac{\partial}{\partial z} (A_{Hz} \frac{\partial \theta}{\partial z}) \quad (3)$$

$$\begin{aligned} \rho \frac{\partial^2 w}{\partial z^2} + 2 \frac{\partial \rho}{\partial z} \frac{\partial w}{\partial z} + w \frac{\partial^2 \rho}{\partial z^2} = - \frac{\partial}{\partial z} \{ \rho \left(\frac{\partial u}{\partial x} + \frac{\partial v}{\partial y} \right) \} \\ - \frac{\partial}{\partial z} \left(u \frac{\partial \rho}{\partial x} + v \frac{\partial \rho}{\partial y} \right) , \end{aligned} \quad (4)$$

$$\frac{\partial p}{\partial z} = - \frac{p g}{R\theta} \left(\frac{p_0}{p} \right)^\kappa . \quad (5)$$

The model is dry. Long- and short-wave radiation is also not included. In the above equations, the horizontal diffusion coefficients for momentum and heat were considered identical. The local rate of density change was set to zero ($\frac{\partial \rho}{\partial t} = 0$). This assumption yielded equation (4) for the vertical velocity. The most important approximation used in the model is the hydrostatic assumption through which the pressure field was derived. This assumption is justified since we are dealing with a relatively shallow atmosphere; i.e., the top of the atmosphere is 4.0 km in the model. It is expected that the pressure perturbations produced by the forcing functions in the urban areas should be less than 10^{-5} g which suggests that the hydrostatic approximation is a reasonable approximation.

Preliminary computations of the vertical velocity using equation (4) indicated that the contribution of the second term on the righthand side is negligible. The simplified version of (4) was used in this study; i.e.,

$$\rho \frac{\partial^2 w}{\partial z^2} + 2 \frac{\partial \rho}{\partial z} \frac{\partial w}{\partial z} + w \frac{\partial^2 \rho}{\partial z^2} = - \frac{\partial}{\partial z} \left\{ \rho \left(\frac{\partial u}{\partial x} + \frac{\partial v}{\partial y} \right) \right\} \quad (6)$$

Perturbation principles were applied to the above equation. In the perturbation analysis, variables designated by the overbar (\bar{p} , for instance) are used to represent the synoptic state which was assumed to be both in geostrophic and hydrostatic equilibrium. Primed variables are used to represent the perturbations produced by the available forcing functions in the city area.

3.1.1 Grid, Finite Differencing and Boundary Conditions

The horizontal dimensions of the grid are 144 km by 144 km, which more adequately covers the urban and suburban regions of St. Louis. A nested grid was employed in which the central region (21 x 21 grid points) centered about the city had a grid spacing of 1 km. Outside the central region, the grid spacing increased in both x and y according to the expression 2^i km, where $i = 1, 2, 3, 4$ until the grid spacing equalled 16 km. Then the grid spacing was held constant for three grid points. Figure 2 shows a graphical description of the grid. The three equally spaced grid points 16 km apart are not included in the figure.

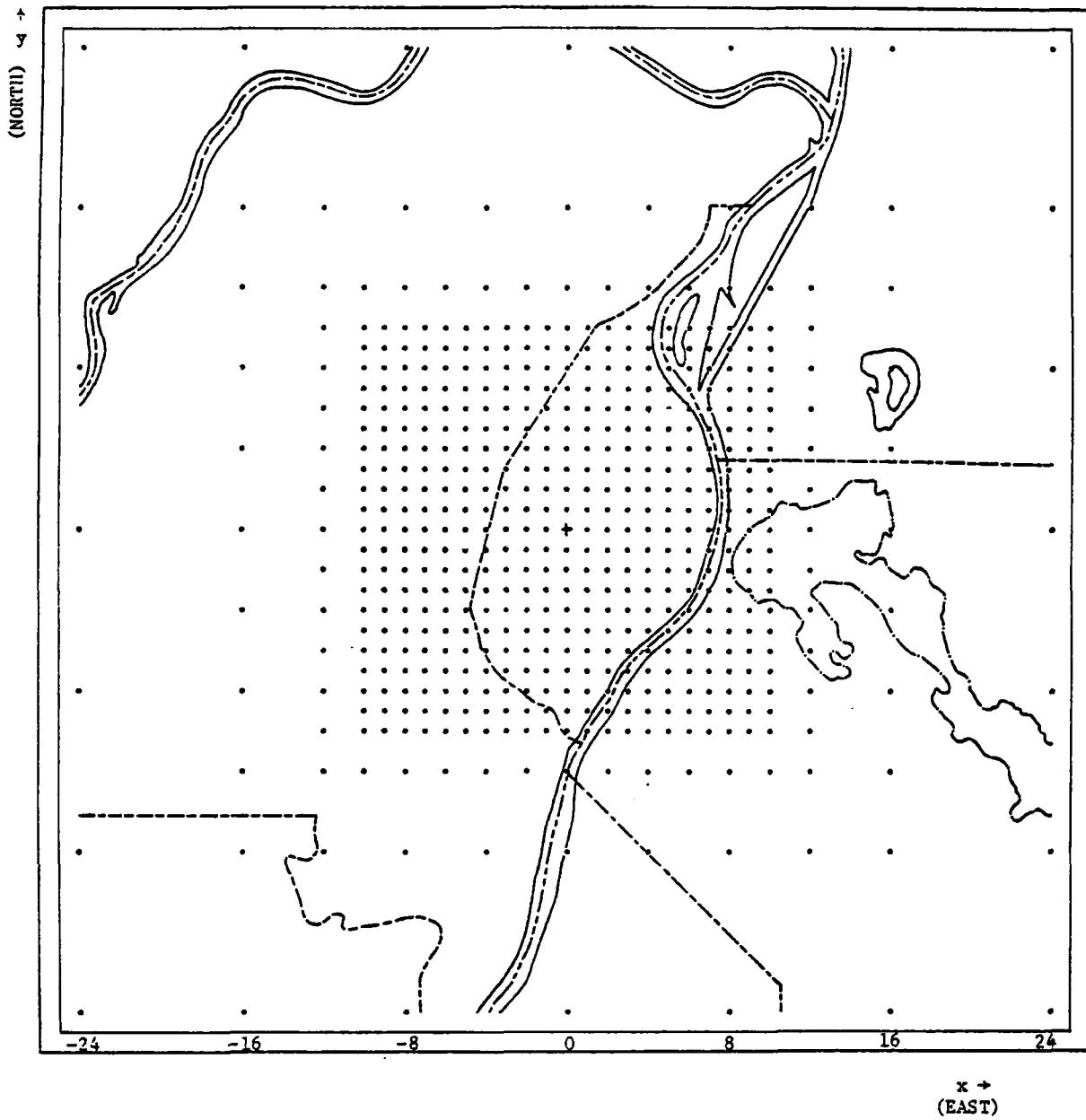


Figure 2. Model Grid Points in the metropolitan St. Louis area.

In regions where grid space was constant, center difference formulas were used for first- and second-order space derivatives. In the region of changing grid spacing, upstream differencing was employed to give first-order space derivatives, and second-order, non-centered derivatives were used to determine the diffusion terms. Since upstream differencing is dissipative, the horizontal diffusion terms were adjusted in the region of unequal grid spacing so that overdampening did not occur.

At the horizontal boundaries, mass, momentum, and heat were allowed to flow in or out except at the upstream boundary; i.e.,

at $x = - 72$ km,

$$u' = v' = \theta' = p' = 0$$

at $x = + 72$ km,

$$\frac{\partial u}{\partial x} = \frac{\partial v}{\partial x} = \frac{\partial \theta}{\partial x} = \frac{\partial p}{\partial x} = 0, \text{ and}$$

at $y = \pm 72$ km,

$$\frac{\partial u}{\partial y} = \frac{\partial v}{\partial y} = \frac{\partial \theta}{\partial y} = \frac{\partial p}{\partial y} = 0.$$

There were eight vertical levels in the model. The vertical levels were: $z = 0, 100$ m, 300 m, 600 m, 1000 m, 1500 m, 2500 m and 4000 m. Heights are with respect to the $z = 0$ plane which will be defined in Section 3.1.2. Upstream differencing was used exclusively in the vertical. The upper boundary conditions were

$$\left. \begin{array}{l} w' = v' = u' = \theta' = p' = 0 \\ \text{and} \\ u = \bar{u}, p = \bar{p}, \text{ and } \theta = \bar{\theta} \end{array} \right\} z = 4 \text{ km.}$$

The lower boundary conditions will be discussed in detail in Section 3.1.2.

3.1.2 Boundary Layer Parameterization

The primary forcing functions in urban areas are the surface heat flux and local terrain effects. In order to describe the effect of terrain, the topographic distribution was parameterized for the model. The average height of the local terrain plus the average building heights were computed in areas about each grid point. The building heights were determined from Sanborn Maps, courtesy of the St. Louis City Planning Office. The size of the area depended on the grid-spacing, i.e., for a 1-km grid-spacing, the area about the grid point was 1 km^2 , and for a 2-km grid-spacing, it was 4 km^2 , etc. The minimum averaged terrain height was determined from the set of average values and this value was subtracted from each terrain height. Then the building heights were added to yield average deviations from the reference height. The $z = 0$ plane is defined where $H(x,y) = 0$.

At $z = H(x,y)$ and at the side walls of an obstacle that may be higher than the first grid point above $z = 0$ where the prediction equations are integrated, the boundary conditions were

$$u = v = w = 0.$$

If $z^* - H(x,y) < 15 \text{ m}$, where z^* is the height of any grid point above H , the prediction equations become unstable for the time increment used. Therefore, values of $H(x,y)$ which did not satisfy this criteria were reduced to $H(x,y) = z^* - 15$. For St. Louis, all values of $H(x,y)$ were less than 100 m which is the height of the first level in the model; about six $H(x,y)$ values exceeded the stability criteria and were reduced (Figure 3).

In order to characterize the effects of an urban heat island and/or large bodies of water (sea or lake breeze), a field of potential temperature departures, $\delta\theta(x,y)$ at $z = H(x,y)$, were used. The $\delta\theta(x,y)$ field for St. Louis was due entirely to the heat island influence. The field was obtained from data presented in a Stanford University report (1953) and available surface weather data for the region (Figure 4).

The urban heat island represented by the $\delta\theta(x,y)$ values was allowed to develop gradually with time by letting

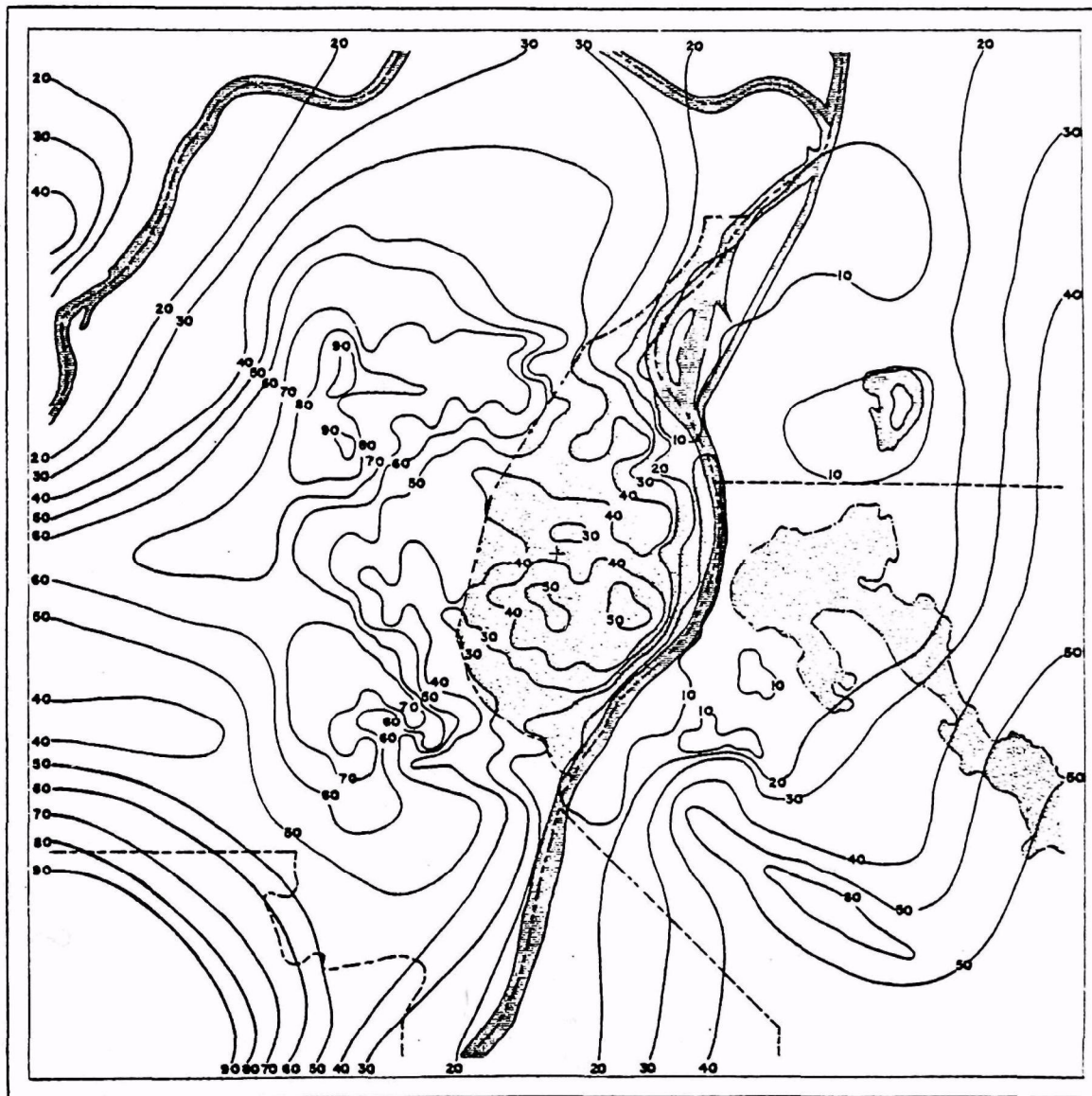


Figure 3. Distribution of $H(x,y)$ (m) field for the St. Louis, Missouri region. See text for definition of $H(x,y)$.

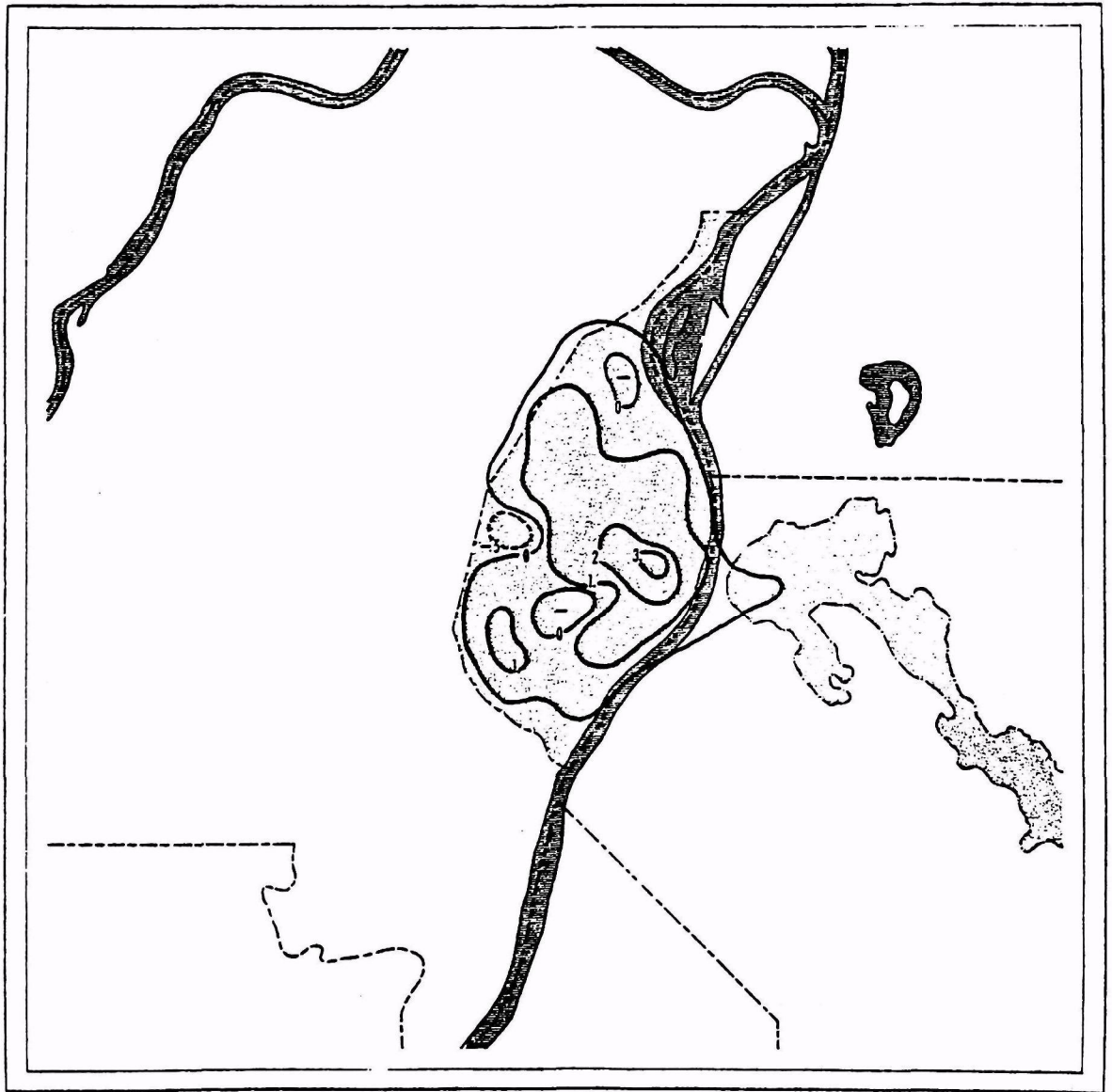


Figure 4. Distribution of the $\delta\theta(x,y)$ ($^{\circ}\text{K}$) field for the average heat island in St. Louis, Missouri. See text for definition of $\delta\theta(x,y)$.

$$\Delta\theta(x,y) = \delta\theta(x,y) [1-\exp(-\gamma t)]$$

where

γ is the rate constant and for this study was such that $\Delta\theta(x,y) \approx \delta\theta(x,y)$ in three hours

The boundary condition at $z = H(x,y)$ on the potential temperature was

$$\theta(x,y,H) = \bar{\theta}(y,0) + \Delta\theta(x,y) \quad .$$

If an obstacle was higher than one or more grid levels, then at $z = H(x,y)$ and at the side walls of the obstacle (which was not the case in St. Louis):

$$\theta(x,y,H) = \bar{\theta}(y,H) + \Delta\theta(x,y) \quad .$$

The initial synoptic field represented by the overbar is determined as if the terrain were not present.

The heat and momentum flux at $z = H(x,y)$ were determined through simultaneous solution of the boundary layer profile equations for the friction velocities, u_* and v_* , and the scale temperature, T^* . These parameters are proportional to the momentum and heat fluxes, respectively, at the surface. The profile equations used were:

$$u = \frac{u_*}{k} \left[\ln\left(\frac{z-H}{z_o}\right) + \frac{\alpha T^* k \{g(z-H)\}^{1/2}}{\theta U^*} \right] \quad ,$$

$$v = \frac{v_*}{k} \left[\ln\left(\frac{z-H}{z_o}\right) + \frac{\alpha T^* k \{g(z-H)\}^{1/2}}{\theta U^*} \right] \quad , \text{ and}$$

$$\theta = \theta(H) + \frac{T^*}{k} \left[\ln\left(\frac{z-H}{z_o}\right) + \frac{\alpha T^* k \{g(z-H)\}^{1/2}}{\theta U^*} \right]$$

where $U^* = \sqrt{u_*^2 + v_*^2}$, and $\alpha = 18$. The above equations are adaptations of those used by Estoque and Bhumralkar (1969). The roughness length, z_o , was allowed to vary in the following manner. In regions other than the built-up sections of the city

$$z_o = 0.0015 H(x,y)$$

Using the above expression and for the given values of $H(x,y)$ in the St. Louis area other than in the built-up sections, $1 \text{ cm} \leq z_o \leq 13 \text{ cm}$. In the built-up sections,

$$z_o = .02 H(x,y)$$

which yielded values as large as 1 meter. In the model only one major built-up section was designated. This region was bounded by Forest Park to the west, the Mississippi River to the east, approximately St. Louis Avenue to the north, and Russell Avenue to the south. This technique is an adaptation of a technique suggested by Lettau (1969).

The formulas for the vertical eddy diffusion coefficients were

$$A_{xz} = \ell^2 \left| \frac{du}{dz} \right| ,$$

$$A_{yz} = \ell^2 \left| \frac{dv}{dz} \right| ,$$

$$A_{Hz} = \ell_H^2 \left| \frac{dV}{dz} \right| ;$$

where $V^2 = u^2 + v^2$. The mixing lengths, ℓ , were given by

$$\left. \begin{aligned} \ell &= k(z-H) (1-\alpha_1 Ri)^{1/4}, \\ \ell_H &= \ell (1-\alpha_1 Ri)^{1/4}, \end{aligned} \right\} \frac{\partial \theta}{\partial z} \leq 0$$

and

$$\left. \begin{aligned} \ell &= k(z-H) (1+\alpha_2 Ri)^{-1/2}, \\ \ell_H &= \ell (1+\alpha_2 Ri)^{-1/2}, \end{aligned} \right\} \frac{\partial \theta}{\partial z} > 0$$

where $\alpha_1 = 18$, $\alpha_2 = 11$, and Ri is the Richardson number. The above equations were derived from expressions given by Rossby and Montgomery (1935) and Holzman (1943). The vertical profile of the vertical diffusion coefficients was constrained to have a second-order variability with height, and the coefficients were set at zero above 800 m.

The horizontal diffusion coefficients were assumed to be proportional to the square root of mean grid spacing; i.e.,

$$\begin{aligned} A_x &= b_o \sqrt{\frac{\Delta x_u + \Delta x_d}{2}}, \\ A_y &= b_o \sqrt{\frac{\Delta y_u + \Delta y_d}{2}}; \end{aligned}$$

where the subscripts, u and d define the upstream and downstream grid-spacing of the grid point, respectively. The constant b_o depended on the initial boundary layer stability. Though A_x and A_y increase as Δx or Δy increase,

the ratio $A_x/\Delta x^2$ or $A_y/\Delta y^2$ decreases markedly, which reduces the horizontal diffusion in the unequal grid spacing regions. This was done to compensate for the dampening produced by the upstream differencing in that region.

3.1.3 Initial Conditions and Integration

The initial wind field was assumed to have a wind direction parallel to the x axis and a speed which varied in z alone. An initial potential temperature distribution was given at $x = -72$ km and $y = -72$ km. Since the synoptic state (initial conditions) was in geostrophic and hydrostatic equilibrium, the necessary initial pressure and potential temperature field were derived through integration of the geostrophic and hydrostatic equations.

In order to study air flow in the city for various wind directions, the $H(x,y)$ and $\delta\theta(x,y)$ fields which define the city area were rotated to effectively yield a new angle for the wind. In order to accomplish this, two $H(x,y)$ and $\delta\theta(x,y)$ fields had to be developed. One field was used for the northwest, southwest, southeast and northeast wind directions. The other for north, west, south and east wind directions.

For the time integration, forward time differencing was combined with the leap-frog method to control the divergence of the solution at even and odd time steps. Forty-eight (48) different simulations were performed for St. Louis; these included variations of synoptic wind direction and wind speed and of boundary layer stability. Exact specifications of the initial stability and wind field and other model parameters used in the simulation is presented in Appendix A. The Appendix presents a paper published in the Journal of Applied Meteorology.

3.2 Determination of a Wind Monitoring Network

3.2.1 General

The basic strategy for selecting a network of wind monitoring stations is illustrated in Figure 5. The objectives of this procedure are twofold:

- 1) to determine a statistical model form which could be used to characterize the horizontal wind field over the St. Louis area for a variety of meteorological conditions, and
- 2) to determine a network of sites for monitoring winds.

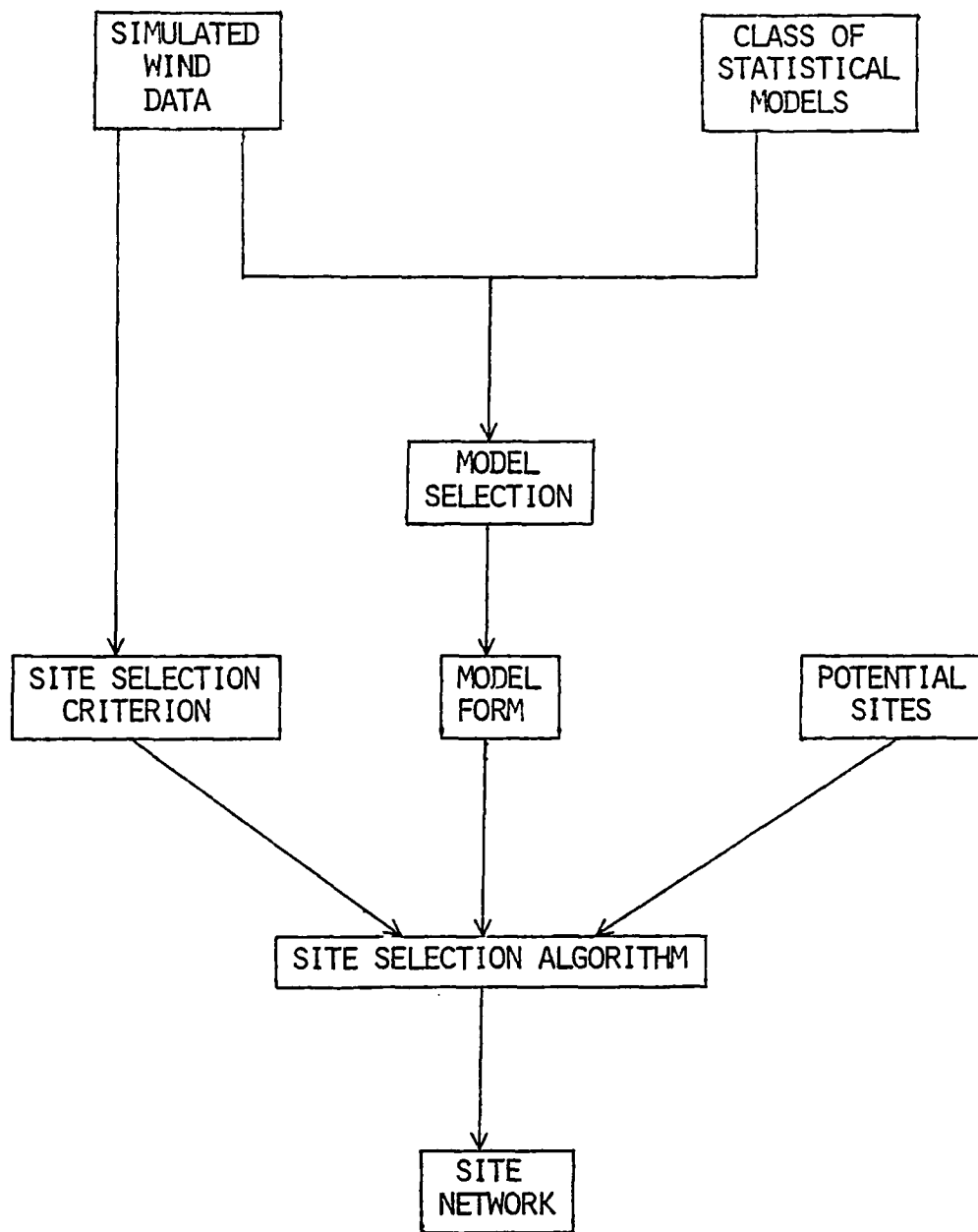


Figure 5. Design selection strategy.

Once such a network is selected and set up, actual wind data would be collected at each site in order to estimate the parameters of the statistical model. This fitted model would produce an estimated wind field over the region which would be combined with the emissions source inventory (in the OVAM) to produce an estimated pollutant concentration field.

As indicated in Figure 5, the three basic ingredients required for selecting a wind-monitoring network are

- (a) a statistical model form (which relates winds to geographic location),
 - (b) a set of M candidate sites (from which a subset of n is to be selected as a wind monitoring network), and
 - (c) an objective criterion for comparing alternative networks.
- Items (a), (b) and (c) are discussed, respectively, in Subsections 3.2.2, 3.2.3, and 3.2.4.

Given the set of M candidate sites, there are

$$\binom{M}{n} = \frac{M!}{n!(M-n)!}$$

possible networks which should be compared via the chosen criterion. In order to make any reasonable claim of optimality, it is clear that M should be much larger than n (i.e., the class of possible networks is large). On the other hand, the evaluation all possible networks in such a situation is computationally unfeasible. (For instance, if M is only 50, there are 47,129,212,243,960 possible networks containing 20 stations which can be selected. Ideally, of course, M would be much larger). Hence, it was necessary to develop an algorithm which evaluates only some of the possible networks. This algorithm is described in Subsection 3.2.5. Results of its application are given in Section 3.2.6. In general, application of this algorithm would yield a set of sites for monitoring winds which would permit good wind field estimation. Because of several economic and practical constraints, it was necessary to make several modifications to the strategy depicted in Figure 5. First, it was necessary to apply the algorithm to two different sets of candidate sites. Secondly, it was necessary to combine the two resulting networks into a single network.

Finally, for validation purposes, it was necessary to make some modification to this network in order to take advantage of data available from existing stations. These modifications to the general strategy are described in Section 3.2.7 along with the resulting network.

3.2.2 Development of Statistical Model Form

In general, the development of the statistical model form involved two basic steps:

- (1) specification of a class of models which, for any given set of meteorological conditions (covered by the simulated data, since these are the available data), is assumed to contain a model which will permit an adequate approximation of the wind field,
- (2) determination of a single model form from within this class which will provide a reasonable approximation of the wind fields under all such conditions.

Selection of a statistical model form was based on data generated by the primitive equation model. These data consisted of quasi-steady-state values for the west-east (WE) and south-north (SN) wind speed components at various geographical points (grid points). Forty-eight (48) sets of initial conditions were used to create 48 data sets as indicated by the cells in the table below:

Wind Shear Code	Initial Wind Speed	Stability Condition*	Prevailing Wind Direction							
			0°	45°	90°	135°	180°	225°	270°	315°
1	1.5	1								
2	3.0	1								
3	6.0	1								
4	1.5	2								
5	3.0	2								
6	6.0	2								

*1 = stable boundary layer (nighttime)

2 = neutral boundary layer (daytime)

For each cell in the 0°, 90°, 180°, and 270° columns of the table, wind speed data were available at each of the points shown in Figure 2. For the other prevailing wind directions, the data were available for the points obtained by rotating the grid points in Figure 2 by 45°. These sets of points will be referred to as square grids and diamond grids, respectively. Primary interest was in the central portions of the areas defined by these grids. Hence, the model fitting was based only on the data at the 521 grid points within:

- (a) the square: $\{(x,y) : -16 \leq x \leq +16, -16 \leq y \leq +16\}$, or
- (b) the diamond: $\{(x,y) : |x| + |y| \leq 16\sqrt{2}\}$.

Two classes of statistical models were considered. The first of these permitted models of the form

$$Z_k(x,y) = \sum B_{kj} P_j(x,y) \quad (1)$$

where

$Z_k(x,y)$ = the kth wind speed component (k=1 for WE and k=2 for SN)
at the point (x,y)

B_{kj} = coefficients to be estimated

$P_j(x,y)$ = a term of form $x^\alpha y^\gamma$, where α and γ can take on non-negative integral values.

This first class of models consisted of all terms $P_j(x,y)$ such that

$$0 \leq \alpha + \gamma \leq 9$$

and

$$0 \leq \alpha \leq 6$$

$$0 \leq \gamma \leq 6.$$

These 43 terms are represented by the products of row and column headings in the following array:

	1	x	x ²	x ³	x ⁴	x ⁵	x ⁶
1
y
y ²
y ³
y ⁴
y ⁵
y ⁶

Since there are 43 such terms, this class contains 2^{43} subsets of terms (i.e., 2^{43} candidate model forms).

The second class of model forms differs from the first in that it permits models involving the topographic evaluation. In particular, this class contains models of the following form:

$$Z_k(x,y) = \sum C_{kj} Q_j(x,y, H(x,y)) \quad (2)$$

where the Z_k are as in (1), the C_{kj} are parameters to be estimated, $H(x,y)$ denotes the elevation (above a base plane) at the point (x,y) , and the Q_j represent terms of the form

$$H^\delta x^\alpha y^\gamma .$$

The exponents are restricted to be non-negative integers in the ranges

$$\begin{aligned} 0 &\leq \delta \leq 2 \\ 0 &\leq \alpha \leq 6 \\ 0 &\leq \gamma \leq 6 . \end{aligned}$$

In addition, the following restrictions were employed:

$$\begin{aligned} 0 &\leq \alpha + \gamma + \delta \leq 5 \\ \text{or} \\ \text{if } \alpha &= 6, \text{ then } \gamma = \delta = 0 \\ \text{if } \gamma &= 6, \text{ then } \alpha = \delta = 0 . \end{aligned}$$

Thus, the second class of model forms is represented by the following arrays of terms:

$\delta = 0$	1	x	x^2	x^3	x^4	x^5	x^6
1
y		
y^2			
y^3	.	.	.				
y^4	.	.					
y^5	.						
y^6	.						

$\delta = 1$	1	x	x^2	x^3	x^4
1
y	
y^2	.	.	.		
y^3	.	.			
y^4	.				

$\delta = 2$	1	x	x^2	x^3
1
y	.	.	.	
y^2	.	.		
y^3	.			

There are, thus, 2^{48} potential model forms in this second class, some of which are also in the first class.

In order to determine a "good" model for a particular simulated case and a particular wind component, stepwise regression was applied twice--once for each of the two classes of terms. This procedure allowed a determination of which of the B_{kj} and C_{kj} could reasonably be assigned a zero value (i.e., determine which terms in (1) and (2) should be included). In all, 192 stepwise regressions were performed (2 components x 48 sets of conditions x 2 classes of terms). The Statistical Analysis System (SAS) (Service, 1972) was used to perform these analyses.

As might be expected, different models appeared "best" for the different situations and components. In order to arrive at a single model form (i.e., a single set of terms) for each component, the results of the 192 stepwise regression analyses were tabulated in terms of how frequently the various terms were picked by the procedure as being of significance. The lower order terms, as might be expected, were judged significant in virtually all of the cases whereas, the higher order terms occurred only rarely. This analysis led to a set of 49 potential model forms which were judged to warrant further consideration (see Table 1).

Each of these 49 models was fitted to the wind component data for each set of conditions. For each model form and each case, the following summary statistics were computed in order to determine the adequacy of the least squares fit:

- 1) s_{ikm}^2 = residual mean square for the kth component ($k = 1$ for WE, $k = 2$ for SN when the mth model ($m = 1, 2, \dots, 49$) is fitted to case i ($i = 1, 2, \dots, 48$)).
- 2) R_{ikm}^2 = the proportion of the total variation in component k accounted for when model m is used for the i th case.
- 3) $s_{i \cdot m}^2 = s_{i1m}^2 + s_{i2m}^2$
- 4) $R_{i \cdot m}^2 = (R_{i1m}^2 + R_{i2m}^2) / 2$

Thus, for the mth model form, 48 values of s_{i1m}^2 , s_{i2m}^2 , $s_{i \cdot m}^2$, R_{i1m}^2 , R_{i2m}^2 , and $R_{i \cdot m}^2$ were determined. The means of these 48 values are shown in Table 2. Table 3 shows, for selected cases and models, the correlations between the simulated data and the predicted values.

Selection of a model form from among these 49 candidates was, to a large degree, subjective. One would prefer one of the simpler (i.e., smaller) models in that fewer observations would generally be necessary for estimating the model parameters (i.e., smaller networks would be possible). On the other hand, one must be assured that all major variations in the wind field--within the region of interest--can be characterized by such a model. Results such as those shown in Tables 2 and 3 indicated that the 13-term model might satisfactorily achieve these two conflicting goals. This was verified by visual comparisons of several simulated wind fields and the corresponding wind fields predicted via this model (Model #2 of Table 1).

TABLE 1. TERMS INCLUDED IN 49 CANDIDATE MODELS ^{1/}

Model No.	No. Terms	1	x^3	y^3	xy^2	x^2y	xy^2	x^3y	x^5	x^6	x^2y^2	hy	hx	h^2	x^3y^3	x^4y
		xy	h	y^4	xy^3	y^5	y^6									xy^4
1	7	x	x													
2	13	x	x	x												
3	14	x		x				x								
4	14	x	x	x								x				
5	15	x		x				x			x					
6	15	x	x	x								x	x			
7	15	x	x	x	x											
8	15	x	x	x				x								
9	16	x		x				x			x				x	
10	16	x		x	x			x								
11	16	x		x				x								
12	16	x	x	x								x	x	x		
13	16	x	x	x	x							x				
14	16	x	x	x				x				x				
15	17	x		x	x			x			x					
16	17	x		x				x			x					
17	17	x	x	x							x					
18	17	x	x	x	x							x	x			
19	17	x	x	x				x				x	x			
20	17	x	x	x	x			x								
21	17	x	x	x				x								
22	18	x		x	x			x			x				x	
23	18	x		x	x			x			x				x	
24	18	x		x	x			x								
25	18	x		x	x			x								x
26	18	x	x	x	x							x	x	x		
27	18	x	x	x				x				x	x	x		
28	18	x	x	x	x							x				
29	18	x	x	x				x				x				
30	19	x		x	x			x			x					
31	19	x		x	x			x			x					x
32	19	x	x	x	x						x		x	x		
33	19	x	x	x				x			x		x	x		
34	19	x	x	x	x			x				x	x			
35	19	x	x	x				x				x	x			
36	19	x	x	x	x			x								
37	20	x		x	x						x				x	
38	20	x		x	x						x				x	x
39	20	x		x	x			x								x
40	20	x	x	x	x							x	x	x		
41	20	x	x	x				x				x	x	x		
42	20	x	x	x	x			x				x				
43	21	x		x	x			x			x					x
44	21	x	x	x	x			x			x	x	x			
45	21	x	x	x	x			x			x	x	x			
46	21	x	x	x	x			x				x	x			
47	22	x		x	x			x			x				x	x
48	22	x	x	x	x			x				x	x	x		
49	23	x	x	x	x			x			x	x	x			

^{1/} An x indicates that the term, or set of terms, in the column heading is included in the model.

TABLE 2. MEANS OF R^2 AND S^2 OVER 48 CASES FOR 49 MODELS

No. Terms	Model No.	R^2_{11m}	R^2_{12m}	S^2_{11m}	S^2_{12m}	$R^2_{1 \cdot m}$	$S^2_{1 \cdot m}$
7	1	.506690	.505472	.0329170	.0273231	.506081	.0602401
13	2	.612684	.601470	.0250040	.0226008	.607077	.0476048
14	3	.610855	.602028	.0243881	.0228007	.606441	.0471888
14	4	.619309	.608337	.0247029	.0222233	.613823	.0469242
15	5	.621956	.610881	.0237868	.0224006	.616418	.0461874
15	6	.626621	.620353	.0245117	.0217743	.623487	.0462860
15	7	.628498	.627543	.0241404	.0208269	.628220	.0449672
15	8	.632817	.625636	.0234719	.0214662	.629227	.0449381
16	9	.631938	.627727	.0232632	.0211935	.629833	.0444566
16	10	.628740	.630877	.0234377	.0207780	.629808	.0442157
16	11	.637016	.619352	.0226128	.0220495	.628184	.0446622
16	12	.632402	.625615	.0242622	.0214110	.629009	.0456732
16	13	.633396	.631836	.0218663	.0206676	.632616	.0445339
16	14	.639205	.632182	.0231702	.0211175	.635693	.0442877
17	15	.639841	.639730	.0228322	.0203724	.639785	.0432046
17	16	.649766	.629442	.0219225	.0216140	.639604	.0435366
17	17	.641896	.632942	.0216405	.0209432	.637419	.0445837
17	18	.641776	.643474	.0236537	.0202812	.642625	.0439349
17	19	.647259	.644662	.0229790	.0206673	.645960	.0436463
17	20	.649483	.651902	.0225609	.0197121	.650693	.0422730
17	21	.660507	.643192	.0215896	.0206260	.651849	.0422156
18	22	.643447	.644561	.0227069	.0200606	.644004	.0427675
18	23	.659748	.646289	.0213931	.0204004	.653019	.0417935
18	24	.654901	.648201	.0216514	.0200157	.651551	.0416672
18	25	.644181	.645746	.0225244	.0200003	.644963	.0425247
18	26	.648129	.649922	.0233922	.0198670	.649925	.0432592
18	27	.652812	.648361	.0227316	.0204065	.650586	.0431380
18	28	.654352	.655630	.0222756	.0195608	.654991	.0418363
18	29	.667180	.649763	.0212449	.0202740	.658472	.0415188
19	30	.667651	.658291	.0209566	.0195745	.662971	.0405312
19	31	.655282	.654599	.0219146	.0195914	.654940	.0415060
19	32	.654789	.655356	.0229084	.0194937	.655072	.0424021
19	33	.662321	.655880	.0220989	.0199057	.659100	.0420046
19	34	.663166	.668411	.0220731	.0191196	.665788	.0411927
19	35	.673714	.659408	.0210597	.0199041	.666561	.0409636
19	36	.676539	.668854	.0206323	.0189649	.672696	.0395972
20	37	.671257	.663122	.0208271	.0192599	.667190	.0400871
20	38	.658887	.659430	.0217872	.0192769	.659159	.0410641
20	39	.670341	.663070	.0207275	.0192319	.666706	.0399594
20	40	.668447	.673431	.0218383	.0187527	.670939	.0405910
20	41	.679120	.662787	.0207915	.0196717	.670953	.0404632
20	42	.682313	.672308	.0203177	.0188329	.677310	.0391506
21	43	.683092	.673161	.0200279	.0187873	.678126	.0388152
21	44	.674997	.678870	.0213450	.0183824	.676934	.0397273
21	45	.690203	.671031	.0200606	.0191709	.686617	.0392316
21	46	.687850	.681627	.0201613	.0184982	.684739	.0386555
22	47	.686697	.677992	.0198961	.0184698	.682344	.0383659
22	48	.693491	.686474	.0199033	.0181627	.689983	.0380660
23	49	.702166	.692708	.0193341	.0177598	.697437	.0370935

TABLE 3. CORRELATIONS BETWEEN SIMULATED AND PREDICTED VALUES
FOR SELECTED MODELS^{1/}

Wind Shear Code	Angle	Model Number (No. of Terms Shown in Parenthesis)									
		#1 (7)	#2 (13)	#14 (16)	#36 (19)	#48 (22)					
		WE	SN	WE	SN	WE	SN	WE	SN	WE	SN
1	0	.69	.59	.80	.73	.82	.76	.87	.80	.87	.81
	90	.67	.53	.78	.69	.82	.77	.82	.80	.82	.80
	180	.47	.61	.58	.72	.67	.77	.71	.77	.71	.77
	270	.67	.58	.81	.67	.83	.75	.86	.77	.88	.77
2	0	.68	.56	.77	.69	.79	.72	.84	.78	.85	.79
	90	.74	.60	.85	.73	.87	.75	.89	.78	.89	.79
	180	.47	.75	.56	.82	.64	.83	.69	.83	.70	.83
	270	.56	.66	.73	.73	.75	.76	.80	.80	.81	.80
3	0	.62	.75	.72	.78	.73	.79	.77	.84	.77	.84
	90	.75	.56	.78	.64	.79	.68	.80	.71	.80	.71
	180	.51	.75	.56	.77	.64	.78	.68	.80	.70	.80
	270	.55	.57	.65	.64	.68	.67	.74	.70	.75	.71
4	0	.79	.81	.84	.84	.84	.86	.85	.87	.87	.87
	90	.76	.74	.80	.83	.81	.83	.84	.84	.84	.84
	180	.90	.74	.92	.78	.92	.80	.92	.82	.93	.83
	270	.60	.70	.68	.76	.68	.77	.71	.77	.72	.78
5	0	.89	.86	.90	.88	.91	.89	.92	.91	.92	.91
	90	.75	.72	.78	.80	.78	.82	.81	.83	.81	.84
	180	.65	.76	.76	.79	.82	.80	.82	.82	.85	.83
	270	.83	.41	.86	.65	.86	.66	.88	.69	.89	.69
6	0	.80	.89	.85	.91	.86	.92	.87	.93	.88	.94
	90	.78	.76	.80	.78	.81	.79	.82	.79	.82	.79
	180	.62	.78	.69	.82	.70	.83	.72	.86	.73	.86
	270	.76	.88	.80	.89	.80	.89	.82	.90	.82	.90

^{1/} Estimation of the model parameters was based on the simulated data at the 521 points of the square grid [± 16 , ± 16]. The correlations were computed using the 521 pairs of simulated and predicted wind components.

Thus, the form of the prediction model chosen for input to the site selection algorithm was

$$\begin{aligned}\hat{Z}_k(x,y) = & b_0(k) + b_1(k)x + b_2(k)y + b_3(k)H(x,y) \\ & + b_4(k)x^2 + b_5(k)y^2 + b_6(k)xy + b_7(k)x^3 \\ & + b_8(k)y^3 + b_9(k)x^2y + b_{10}(k)xy^2 \\ & + b_{11}(k)x^4 + b_{12}(k)y^4,\end{aligned}\tag{3}$$

where $k = 1$ for the WE component and $k = 2$ for the SN component. It is assumed that the $b_j(k)$ would be estimated, for a given case, by ordinary (least squares) regression.

3.2.3 Selection of Candidate Sites

A second required input for the network selection algorithm, in addition to the model form, is a set of candidate sites or candidate design points. The choice of a large number of such points is obviously preferable, in that a large number of potential networks covering a wide range of possibilities should be included in the evaluation.

The set of points selected should encompass, and extend somewhat beyond, the geographic area for which good estimation of wind fields is desired. On the other hand, all of the points should fall within an area over which the model can be expected to hold. This is particularly important, since the design selection criteria (see Section 3.2.4) are aimed at minimization of variance as opposed to bias. Such criteria not only assume the correctness of the model but also tend to select some design points at the extremities of the allowable region.

It should also be noted that many practical restrictions can, in general, be incorporated into the algorithm via the specification of candidate sites. For instance, one can force certain points to be in the design (e.g.,

previously existing stations); similarly, certain areas not amenable to the establishment of wind/pollution monitoring can be taken into account by simply not including any candidate points within such areas. In the context of this study, a natural restriction on the set of candidate sites was introduced by the fact that the model includes the elevation $H(x,y)$. This dictated that one know the elevation of any candidate site. For this reason, any candidate site was required to be coincident with a point from either the diamond or square grid.

As previously indicated, the model fitting was judged on the basis of two regions (actually, on a discrete set of points within each of two regions). These were (the 521 grid points in)

$$\{ (x,y) : |x| \leq 16 \text{ and } |y| \leq 16 \} \quad (4)$$

and

$$\{ (x,y) : |x| + |y| \leq 16 \sqrt{2} \} .$$

As indicated above, the set of potential design points should, therefore, fall within a subregion of these regions. This subregion should also cover the urban area. One option for the set of candidate sites would be the union of the grid points within the following two sets:

$$\{ (x,y) : |x| \leq 10 \text{ and } |y| \leq 10 \} \quad (5)$$

$$\{ (x,y) : |x| + |y| \leq 10 \} . \quad (6)$$

It should be noted that each of these regions is contained in the intersection of the two regions given by (4). There were 441 points in each of these regions; since there was little exact overlap of the grid points in these two regions, a large number of points are contained in this union. This number of points not only would be computationally impractical in the design selection algorithm, but also would include many essentially redundant points because

of near-overlap. A second approach would, therefore, be to select a subset of this union--for example, removing points which nearly overlapped other points.

Both of these approaches, however, involve a problem which stems from the fact that the set of candidate sites would be made up of points from both the square and the diamond grids. Hence, a design selected via the algorithm would typically involve points which originated from the two grids.

Consequently, evaluation of such a design with respect to the simulated data would be difficult since simulated data would be unavailable for some of the design points. For instance, suppose that a 20-point design were obtained and that 10 of the points originated from the square grid and the remaining 10, from the diamond grid. Suppose one wished to fit model (3) to the simulated data for a particular case (say, a north wind case) using these 20 sites. Since simulated data for a north wind case would be available only at the 10 points originating from the square grid, one would not be able to perform this evaluation (or would need to use some type of interpolation to produce data at the remaining 10 points in order to do it).

In order to avoid these types of problem, it was determined that:

- 1) the design selection algorithm would be applied twice using two different sets of candidate sites (namely, grid points in the region (5) and those in region (6)),
- 2) the two resultant networks would be combined into a single design by clustering together points which were close together, and
- 3) the points of the single design would be forced to coincide with points of one of the original grids (so that evaluation of half of the 48 simulated cases could be carried out).

It should be noted that modifications are currently being made to the simulation program which will permit it to generate wind data over a single grid for all cases. This will eliminate many of the somewhat subjective or arbitrary decisions which were required to circumvent problems arising from the use of two grids.

3.2.4 Design Selection Criteria

In addition to the model form (3) and the above-described sets of candidate sites from which potential sampling networks (i.e., designs) can be chosen, the design selection algorithm requires a statistical criterion for objectively evaluating various designs. The objective of the algorithm is, thus, to optimize the given criterion by choice of design. Such design optimality criteria are generally concerned with one (or both) of two sources of error: bias and variance. In the present case, two sources of bias are actually involved: (1) the failure of (3) to represent the simulated data; and (2) the failure of the simulation model to portray reality. The model selection strategy was directed toward choosing a model form for which the first of these bias components is sufficiently small. Most practical design selection strategies are aimed toward the variance source of error (i.e., variation about the fitted model) since assessing bias requires knowledge of the correct model. Some protection against large bias is necessary and is achieved indirectly by restriction of the region of interest to a smaller area than that covered by the initial grid; unless the selection of design points are constrained in such a manner, variance criteria will typically yield unrealistic designs in that some points will be selected at the extremities of the allowable region. The model (3), or any similar model, will obviously not be appropriate over too large a region.

In order to discuss design selection criteria, it is convenient to rewrite the fitted model (3) in vector notation:

$$\hat{Z}_k(x,y) = \underline{x}' \underline{b}_k \quad (7)$$

where $\underline{x}' = (1, x, y, H, x^2, y^2, xy, x^3, y^3, x^2y, xy^2, x^4, y^4)$,

$\underline{b}_k' = (b_0(k), b_1(k), \dots, b_{12}(k))$, and

$k = 1$ for the WE component, $k = 2$ for the SN component.

The vector \underline{b}_k' is the least squares estimate of the corresponding parameter vector

$$\underline{\beta}_k' = (\beta_0(k), \beta_1(k), \dots, \beta_{12}(k)) , \quad (8)$$

i.e., the underlying model for the observed wind component data is assumed to be

$$Z_k(x,y) = \underline{x}' \underline{\beta}_k + e_k \quad (9)$$

where the deviations e_k from the surface $\underline{x}'\underline{\beta}_k$ are assumed to be uncorrelated and randomly distributed with zero mean, and with variance σ_k^2 , which does not depend on the point (x,y) .

A design of size n consists of a set of n points (x,y) . The coordinates, elevation, and observed value, respectively, for the i th such point are denoted as (x_i, y_i) , $H_i = H(x_i, y_i)$ and $Z_{ki} = A_k(x_i, y_i)$. Corresponding to each such point is the vector:

$$\underline{x}'_i = (1, x_i, y_i, H_i, x_i^2, y_i^2, x_i y_i, x_i^3, y_i^3, x_i^2 y_i, x_i y_i^2, x_i^4, y_i^4).$$

The following notation is made:

$$X_D = \begin{bmatrix} \underline{x}'_1 \\ \underline{x}'_2 \\ \vdots \\ \underline{x}'_n \end{bmatrix}, \quad Z_k^{(D)} = \begin{bmatrix} Z_{k1} \\ Z_{k2} \\ \vdots \\ Z_{kn} \end{bmatrix}$$

where the subscript (or superscript) D is used to indicate that a matrix (or vector) depends on the design (i.e., the particular set of points involved).

The estimates $\underline{b}_k^{(D)}$ are determined as:

$$\underline{b}_k^{(D)} = (X_D' X_D)^{-1} X_D' Z_k^{(D)}.$$

At an arbitrary point (x,y) , then, the predicted value for the k th wind speed component, based on the particular design, D , is

$$\hat{z}_k^{(D)}(x,y) = \underline{x}' \underline{b}_k^{(D)} .$$

The variance of $\hat{z}_k^{(D)}(x,y)$, denoted by $v_D(k,x,y)$ is given by

$$\text{Var} [\hat{z}_k^{(D)}(x,y)] \equiv v_D(k,x,y) = \underline{x}' (\underline{X}_D' \underline{X}_D)^{-1} \underline{x} \sigma_k^2 .$$

For the given model form and a particular design, the variance of the predicted value at the point (x,y) is, thus, proportional to the variance function $s_D(\cdot)$ evaluated at the point (x,y) :

$$s_D(x,y) = \underline{x}' (\underline{X}_D' \underline{X}_D)^{-1} \underline{x} ;$$

that is, $v_D(k,x,y) = \sigma_k^2 s_D(x,y)$.

Various functions of $s_D(\cdot)$ can be used for evaluating designs of size n . For example, one may regard D as "better than" design D^* if

- (a) $s_D(x_0, y_0) \leq s_{D^*}(x_0, y_0)$ for a particular point (x_0, y_0) ,
- (b) $\max s_D(x,y) \leq \max s_{D^*}(x,y)$ where R is a specified continuous region of the x - y plane or a specified set of discrete points, or
- (c) $\text{average } s_D(x,y) \leq \text{average } s_{D^*}(x,y)$.

The criterion chosen was similar to (c) above. Note that the criterion (c) depends on

- (i) a class of n-point designs (containing at least two designs).
- (ii) a set R (either continuous or discrete)^{1/}, and
- (iii) the model form.

In the present case, however, the availability of the simulated data provided some additional information. If certain areas within the St. Louis region consistently tended to experience lower (or higher) wind speeds than other areas, regardless of the initial set of conditions, then the fitted surfaces should reflect this pattern. Unless one or more design points fall within such an area, however, then it would be unlikely that the fitted surfaces would behave in this manner. Because such patterns were expected, it appeared that a criterion which incorporated this additional information should be developed for use in the selection of designs. Accordingly, the following criterion was chosen for evaluating designs of size n:

Design D is better than design D* if

$$\text{average}_{(x,y) \in R} w(x,y) s_D(x,y) \leq \text{average}_{(x,y) \in R} w(x,y) s_{D^*}(x,y) . \quad (10)$$

The weight $w(x,y)$ attached to a point (x,y) was chosen to reflect patterns which were consistent over varying conditions, i.e., if, at a particular point (x_0, y_0) , the wind speed was consistently higher and/or lower than was typical for most points, then the weight $w(x_0, y_0)$ would be large relative to the weights for other points. Intuitively, the form of (10) suggests that a "good" design will attempt to make $s_D(x,y)$ small when $w(x,y)$ is large in order to yield a small average value. The construction of the weights and design selection criterion is described below for the square grid. A completely analogous development holds for the diamond grid.

Twenty-four cases were available (6 wind shear codes x 4 prevailing wind directions) which provided values of the wind speed components for each of the 521 grid points contained in the region $\{(x,y) : |x| \leq 16, |y| \leq 16\}$. This set of points is denoted by R. Let $Z_{kj}(x,y)$ denote the observed (simulated)

^{1/}

The use of a continuous region R, while somewhat more appealing, was regarded as infeasible because the elevation H was not available on a continuous basis (but rather, only at the grid points).

value for the k th component ($k = 1$ for WE, $k = 2$ for SN) at the point (x,y) for the j th case ($j = 1, 2, 3 \dots, 24$). The wind speeds were then calculated:

$$Z_j(x,y) = \sqrt{Z_{1j}^2(x,y) + Z_{2j}^2(x,y)} \quad \begin{array}{l} (x,y) \in R \\ j=1,2,\dots,24 \end{array}$$

The mean and sum of squares were then computed for each case.

$$\left. \begin{array}{l} \bar{Z}_j = \frac{1}{521} \sum_R Z_j(x,y) \\ SS_j = \sum_R (Z_j(x,y) - \bar{Z}_j)^2 \end{array} \right\} j = 1, 2, \dots, 24.$$

The individual deviations from the mean, $(Z_j(x,y) - \bar{Z}_j)$, were then squared and standardized by SS_j :

$$w_j(x,y) = \frac{(Z_j(x,y) - \bar{Z}_j)^2}{SS_j} \quad \begin{array}{l} (x,y) \in R \\ j = 1, 2, \dots, 24. \end{array}$$

Finally, the weights were determined by averaging the $w(x,y)$ over conditions:

$$w(x,y) = \frac{1}{24} \sum_{j=1}^{24} w_j(x,y) \quad (x,y) \in R.$$

The criterion for selecting designs of size n is, thus, minimization of Γ_D with respect to designs, where

$$\Gamma_D = \frac{1}{521} \sum_R w(x,y) s_D(x,y). \quad (11)$$

Thus, the function of the weights is essentially to reduce, in a probabilistic sense, the size of the class of models of the form (3). Obviously, particular models of this form can yield wind component surfaces (over the x-y plane) with several hills, valleys, ridges, etc. The complete class of models of this form would allow such patterns to occur in any part of the region. Many of these particular models (i.e., specific $\underline{\beta}$ vectors in (9)) may never occur--e.g., regardless of wind conditions, the surfaces may tend to be flat over subareas of the region of interest. Obviously, several design points in such a subregion would be unnecessary. On the otherhand, in subregions where hills, valleys, or ridges are common, the presence of several design points is essential in order to characterize the surfaces.

The above-described strategy was repeated for the diamond-grid situation. Criterion (11) with $w(x,y) = 1$ (i.e., criterion (c), as previously described) was also examined.

3.2.5 Design Selection Algorithm

As previously indicated, the potential designs points (i.e., candidate sampling sites) were restricted to a smaller region than the initial grid in order to achieve protection against bias. In particular, for the square-grid situation, the set of candidate sites was restricted to the set of grid points contained in the region $\{(x,y) : |x| \leq 10, |y| \leq 10\}$. This set contains 441 points (see Figure 2).

In the process of site selection, if one wished to consider all possible designs containing 19 stations, one would need to evaluate the criterion 9.737×10^{32} times in order to obtain the best design. For designs of other sizes, another enormous number of criterion evaluations would be required. Since $s_D(\cdot)$, and most other design optimality criteria depend on the inverse of the matrix $X_D' X_D$, a tremendous number of matrix inversions would be required, which would result in insufferably long computer runs. Hence, there was a need to develop an algorithm which would yield a good design without evaluating all possible designs of a given size. It was also desirable to program this algorithm so that it would be adaptable to various choices of models, criteria and potential points.^{1/}

^{1/} This flexibility is achieved by requiring the user to specify the model and criterion (in user-supplied subroutines) and the set of candidate sites (as input to the program).

A "backward elimination" algorithm satisfying these objectives was developed. Basically, the algorithm works in the following manner. Consider M candidate sites (numbered 1 through M) and suppose a design of size n is desired. Let Δ_{M-1} be the class of designs $\{D_1^{(M-1)}, D_2^{(M-1)}, \dots, D_M^{(M-1)}\}$ containing $M-1$ points, where $D_i^{(M-1)}$ denotes the design of size $M-1$ obtained from the set of M points by omitting the i th point. Let $r_i^{(M-1)}$ be the value of the criterion for this design.^{1/} The programmed algorithm evaluates the criterion for all M designs in the class, Δ_{M-1} , and determines that the minimum value is achieved for the design $D_k^{(M-1)}$, i.e., $r_k^{(M-1)} = \min \{r_1^{(M-1)}, r_2^{(M-1)}, \dots, r_M^{(M-1)}\}$. The k th point is then removed from consideration as a possible design point. Hence, the set of candidate sites now consists of $M-1$ points and there are $(M-1)$ possible designs of size $M-2$ in the class Δ_{M-2} . The designs in this class are obtained by omitting the i th point (assuming the set of points has been renumbered from 1 to $M-1$). In the same manner as above, the program evaluates the criterion for each design. The minimum value $r_k^{(M-2)}$ is determined, and the set of points in $D_k^{(M-2)}$ becomes the set of candidate points for the next iteration; this process continues until n points remain. It should be emphasized that such a technique cannot guarantee that the "best" design of a given size is found (where "best" is defined in terms of the particular optimality criterion). Although the resultant design should be reasonably good, the term "optimal sampling network" should not be interpreted in a rigorous mathematical sense.

The backward elimination procedure requires

$$(M-n)(M+n+1)/2$$

evaluations of the criterion. For instance, for $M = 441$ and $n = 19$, the design selection criterion would be evaluated 97,271 times. Explicit inversion of matrices is largely avoided by the use of recurrence relationships which express the inverse of a matrix in terms of previously computed matrices.

^{1/}It is assumed in this discussion that optimization is achieved by minimizing, as opposed to maximizing, the particular criterion.

3.2.6 Application of the Algorithm

The design selection algorithm was first applied to the square grid using the weighted average variance criterion (11) where the average was taken over the set of 521 grid points in $\{(x,y) : |x| \leq 16, |y| \leq 16\}$. The 13-term model (3) was employed and the initial set of candidate sites was restricted to the set of 441 grid points in the square $\{(x,y) : |x| \leq 10, |y| \leq 10\}$. The resulting designs of sizes 13, 14, ..., 30 are specified below:

<u>13-Point Design</u>		<u>Number of Points</u>			<u>Number of Points</u>		
<u>x</u>	<u>y</u>		<u>x</u>	<u>y</u>		<u>x</u>	<u>y</u>
-10	-10	14	7	-7	23	10	-10
-10	0	15	0	6	24	7	10
-10	7	16	-7	0	25	-7	6
-7	-7	17	7	0	26	-7	-10
-7	7	18	0	-1	27	6	-7
-7	10	19	-10	10	28	5	1
0	-10	20	0	-7	29	-10	-7
0	10	21	7	7	30	-7	-6
6	7	22	10	7			
7	-10						
10	-7						
10	0						
10	10						

The points in the 14-point design consist of those in the 13-point design plus the point labeled "14". The 15-point design contains the points in the 14-point design plus point number "15", etc.

The algorithm was then applied to the diamond grid. The average was taken over the rotated set of 521 grid points in the region $\{(x,y) : |x| + |y| \leq 16\sqrt{2}\}$ and the initial set of candidate sites consisted of the grid points in $\{(x,y) : |x| + |y| \leq 10\sqrt{2}\}$. The resulting design points were as follows:

<u>13-Point Design</u>		<u>Number of Points</u>	<u>Number of</u>				
<u>x</u>	<u>y</u>		<u>x</u>	<u>y</u>	<u>Points</u>	<u>x</u>	<u>y</u>
-14.14	0.00	14	-9.19	-4.95	23	-2.12	12.02
-4.95	-9.19	15	-4.95	9.19	24	0.71	13.44
0.00	-14.14	16	5.66	8.49	25	1.41	8.49
-7.78	-0.71	17	7.78	0.71	26	-0.71	-2.12
1.41	-8.49	18	2.12	-0.71	27	0.71	-9.19
-9.19	4.95	19	0.00	7.07	28	-13.44	-0.71
2.12	-2.12	20	9.90	-4.24	29	-9.90	2.83
7.07	-7.07	21	2.12	-7.78	30	7.07	-1.41
7.07	0.00	22	-7.78	0.71			
0.71	7.78						
0.00	14.14						
8.49	5.66						
14.14	0.00						

The two 30-point designs are shown in Figure 6. It should be noted that many of the selected sites occur on the boundaries of the allowable region. As previously indicated, this is typical of variance-minimization criteria. Consequently, the choice of the shape and size of the region of interest is very important since it will typically have significant influence on the resulting design. It was for this reason that the design points were constrained to be in the innermost grids, and it is assumed that interest in estimating wind fields is confined to this region. It should also be noted that since, for a given value of y , the model form is a quartic in x (apart from the H term), one requires a minimum of five distinct levels (values) of x in a design in order to be able to estimate the model parameters. Projection of the design points arising from the square grid, for example, into the x axis shows a clear pattern of five essentially distinct levels (at -10, -7, 0, 7 and 10 km). A similar pattern holds for the y coordinate. That such patterns persist even with the inclusion of the H term in the model form and the inclusion of weights

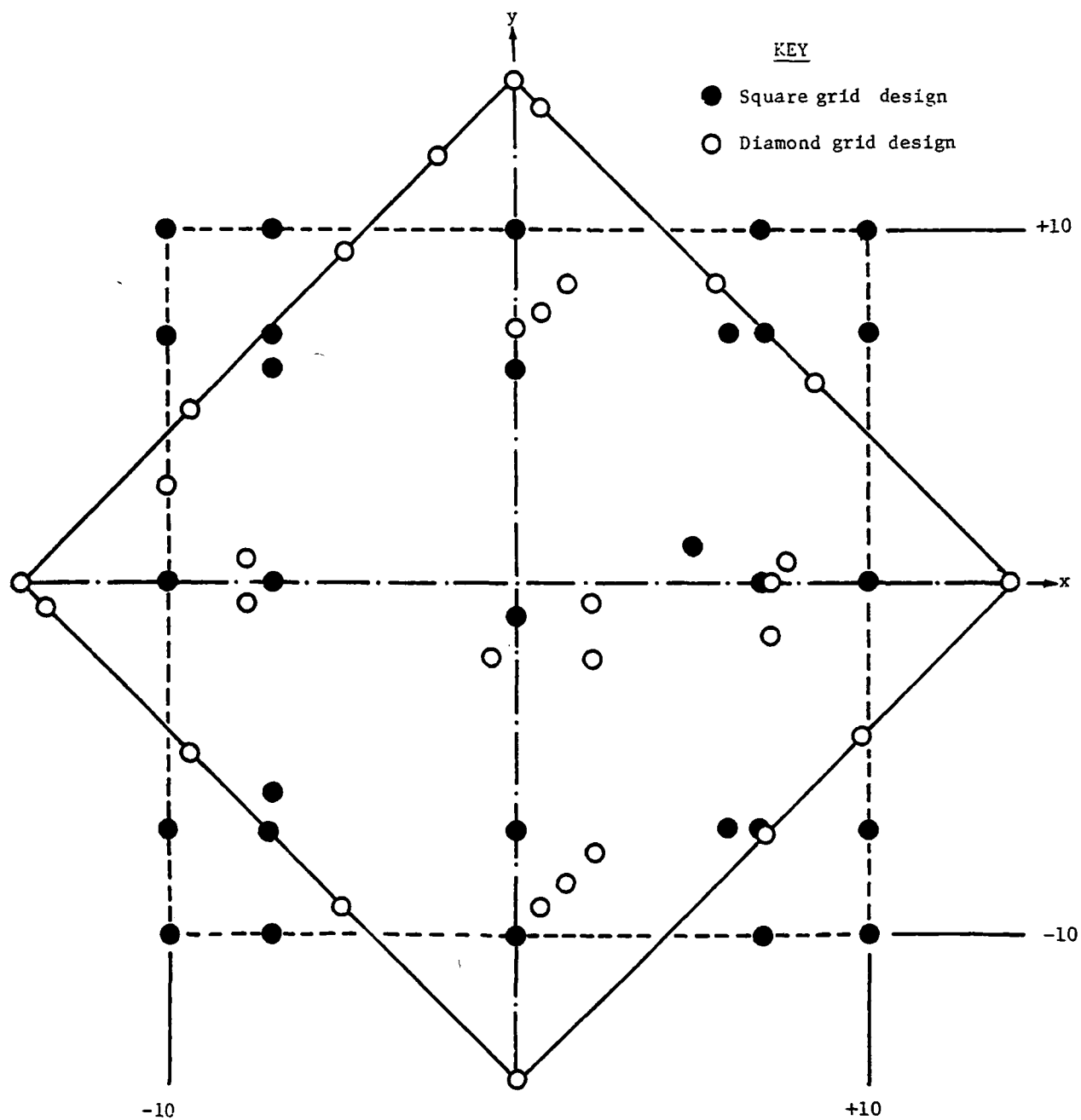


Figure 6. Thirty-point designs from square grid and diamond grid.

in the design selection criterion suggests that neither of these was overwhelmingly important in affecting the site selections. With regard to the influence of the weights in (11), this was substantiated by applying the algorithm with an unweighted criterion (i.e., $w(x,y) = 1$ in (11)). The chief influence of the weights, as might be expected, was a slight shift of some points near the urban St. Louis area into or closer to this urban area.

It should be emphasized that the influence of topography and/or the value of a weighted criterion could be much greater for other areas of the country--for instance, in areas of more complex terrain. In such areas, one would also expect that a more complex model form would be required (assuming the same size region of interest) to characterize the more complex wind-component surfaces that would generally occur in such an area.

3.2.7 Comparison of Alternative Wind-Monitoring Networks

To arrive at a single design consisting of less than twenty stations, as dictated by economic considerations, the clusters of points evident in Figure 6. were reduced to single points. In particular, four 19-point designs were chosen for further evaluation. In order to have simulation data available for evaluating these networks, the points of these designs were forced to be points contained in the full square grid.^{1/} The four designs, designated as A0, A1, A2 and A3, are indicated in Table 4. The designs A0, A1 and A2 were the result of subjective clusterings of points. Note that A0 and A1 differ by only one point and that A2 tends to concentrate more design points in the urbanized area. Design A3 was determined by applying an objective statistical technique (hierarchical fusion) for clustering the sixty points shown in Figure 6.

^{2/} BMD statistical programs package contains the clustering routine employed. The 19 points listed under A3 in Table 4 represent the subset of square grid points closest to the centroids of the resulting nineteen clusters determined by the procedure.

For each of the four designs, the 13-term model was applied to WE and SN wind speed components for the 24 sets of simulation data associated with the

^{1/} The choice of the square grid, as opposed to the diamond grid, was arbitrary. The rationale for forcing design points to coincide with points contained in a single grid was described in Section 3.2.3.

^{2/} Biomedical Computer Programs, Health Science Computing Facility, Department of Biomathematics, School of Medicine, University of California, Los Angeles, March, 1971, (Supported by NIH, Special Research Resources Grant RR-3).

TABLE 4. FOUR 19-POINT NETWORKS SELECTED FOR EVALUATION

A0		A1		A2		A3	
x	y	x	y	x	y	x	y
-16	0	-16	0	-16	0	-16	0
16	0	16	0	16	0	16	0
0	-16	0	-16	0	-16	0	-16
0	16	0	16	0	16	0	16
-10	-10	-10	-10	-10	-10	-10	-10
-10	10	-10	10	-10	10	-10	10
-7	0	-7	0	-7	0	-8	1
-7	-7	-7	-7	-7	-7	-8	-6
-7	7	-7	7	-7	7	-8	6
0	-10	0	-10	0	-10	1	-8
0	-7	0	-7	6	-2	-6	-10
1	-2	1	-2	1	-2	1	-1
0	6	0	6	1	8	0	8
7	-7	7	-7	7	-7	7	-8
7	0	7	0	5	1	7	0
5	6	5	6	5	6	-6	10
8	6	10	-10	10	-10	10	-10
10	-4	10	-4	10	-4	10	-6
10	10	10	10	10	10	8	8

TABLE 5. AVERAGE CORRELATION AND SUMS OF SQUARES OF DEVIATIONS FOR EACH NETWORK

Network	Average Correlation Coefficient	Average Sums of Squares of Deviations
A0	.703	13.7
A1	.705	13.2
A2	.684	15.1
A3	.711	14.2

TABLE 6. SYMBOL KEY TO VARIANCE FUNCTION PLOTS^{1/}

<u>Plotted Symbol</u>	<u>Value of Variance Function $s_D(x,y)$</u>
0	$\leq 1/2$
1	1/2-1
2	1-2
3	2-4
4	4-8
5	8-16
6	16-32
7	32-64
8	64-128
9	> 128

^{1/} Given in Figures 7, 8, 9, 10 and 11.

square grid (6 wind shear codes times 4 prevailing wind directions: 0° , 90° , 180° , 270°). Average correlations and sums of squares of deviations between "observed" and predicted values (over the innermost grid) are given in Table 5. The differences between the average correlation coefficients and between the sum of squares of deviations were too small to make these results conclusive.

Comparison of the designs by use of the variance function $s_D(x,y)$, however, revealed a clear preference for design A2. Plots of these functions are given in Figures 7 through 10. Table 6 yields the key to the plots. Figure 7 indicates that A0 is likely to provide poor prediction in the south-east corner of the innermost grid; design A3 suffers a similar deficiency at the northeast corner (see Figure 10). Actual plots of wind vectors using these networks showed that, indeed, very large errors were found in the respective regions. For this reason, designs A0 and A3 were dropped from further consideration. The regions of large errors apparently did not produce smaller correlations and larger sums of squares of deviations because these designs permitted sufficiently good estimates to be obtained elsewhere on the grid.

A comparison of the variance function plots for designs A1 and A2 indicated a preference for A2; in particular, A2 appeared to provide for better prediction in the urbanized area. The following frequency distributions of the variance functions $s_{A1}(x,y)$ and $s_{A2}(x,y)$, for instance, can be derived from Figures 8 and 9.

Range of $s_D(\cdot)$	Region: $\begin{cases} -10 \leq x \leq 10 \\ 10 \leq y \leq 10 \end{cases}$		Region: $\begin{cases} 0 \leq x \leq 7 \\ -8 \leq y \leq 8 \end{cases}$	
	A1	A2	A1	A2
$\leq 1/2$	219	224	80	100
$1/2$ to 1	205	211	54	36
1 to 2	17	6	2	0

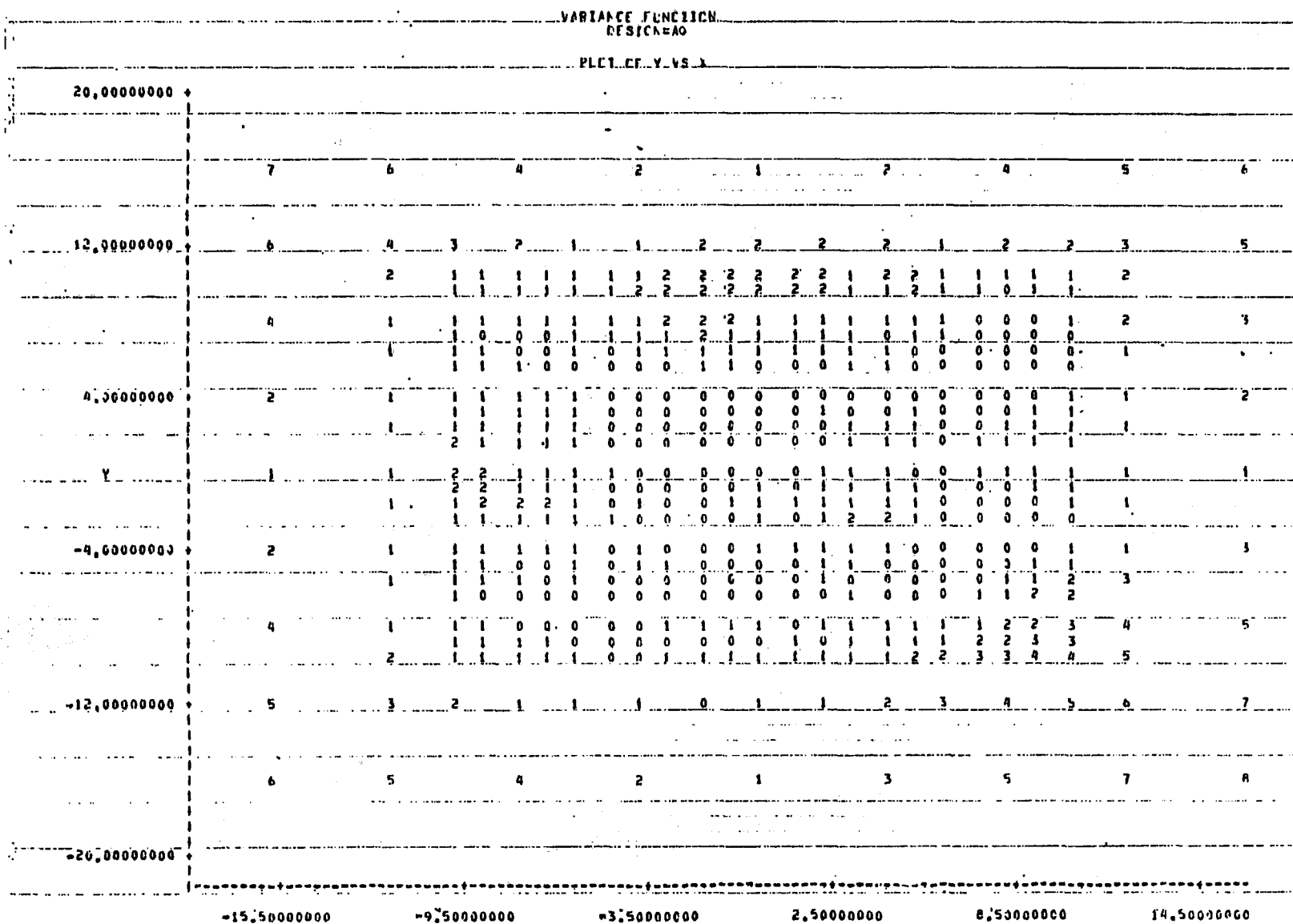


Figure 7. Variance function for design A0.

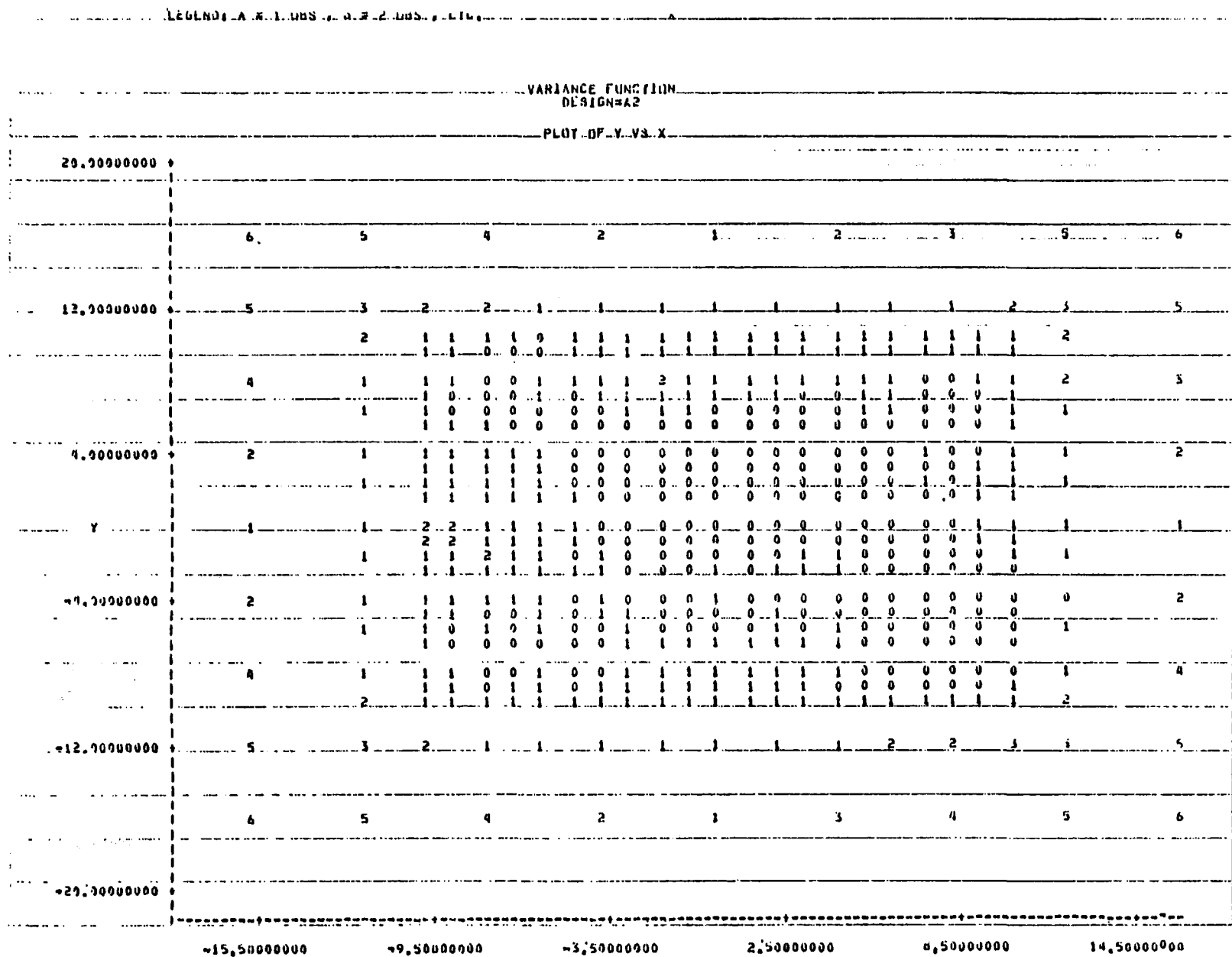


Figure 9. Variance function for design A2.

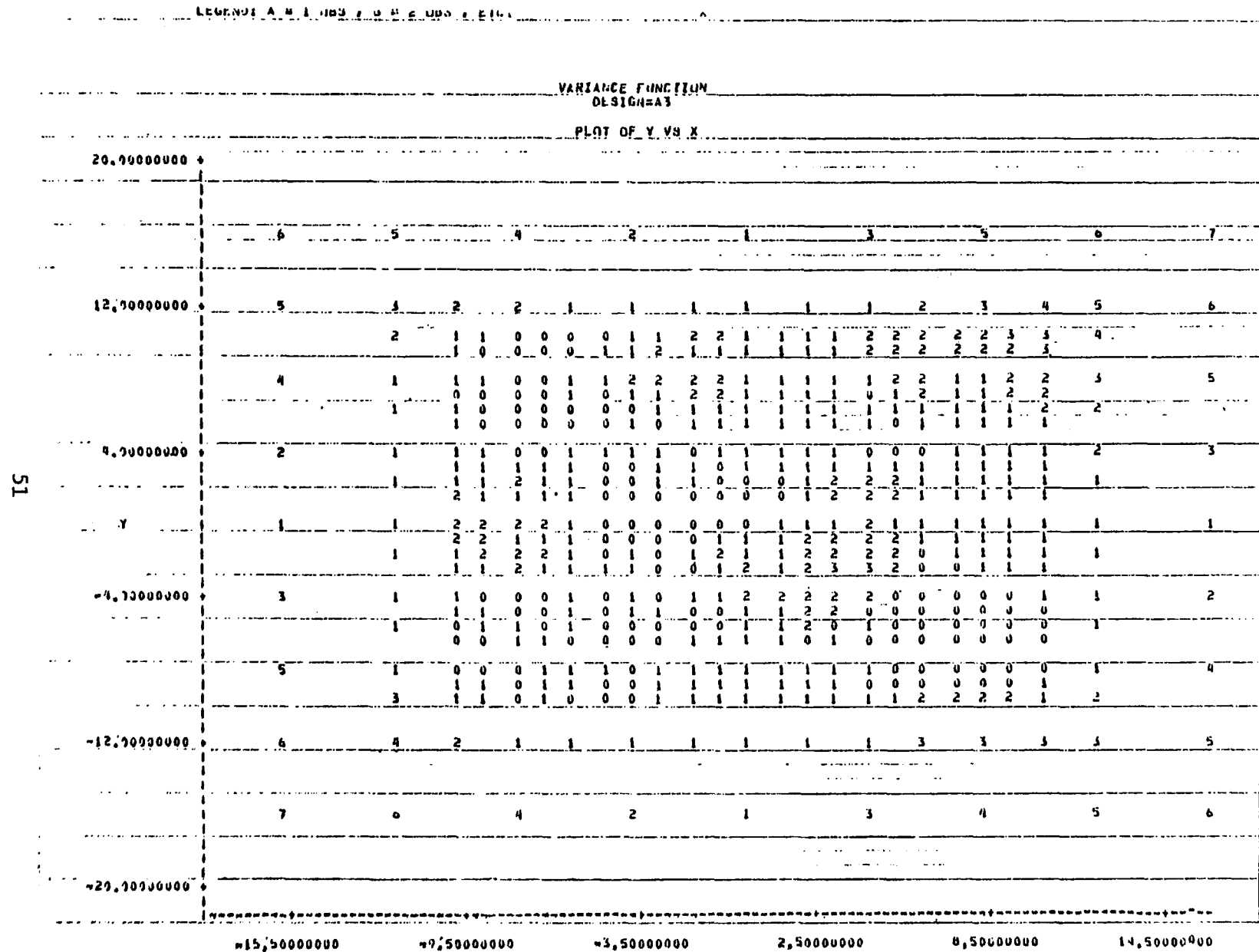


Figure 10. Variance function for design A3.

The preference for A2 was further demonstrated by comparisons between predicted and simulated wind fields. The predicted wind fields were generated, for several cases, by estimating the model parameters from simulated data at the design points of these two networks. Hence, A2 was chosen as the best 19-point design. All of the evaluation criteria (average correlations, sums of squares of deviations, variance function plots, and direct examination of predicted versus observed wind fields) indicated that wind field prediction outside the region $[\pm 10, \pm 10]$ was highly unreliable (for any of the designs). Figure 11 is a plot of network A2 which will, from this point on, be referred to as the OSN (Optimum Sampling Network).

Implementation of this 19-point design would typically proceed on a sequential basis; consequently, it may be important to know

- 1) the order in which stations should be established, and
- 2) the minimum number of stations which must furnish wind data (i.e., at what point in the sequential implementation can one begin to utilize the data to estimate wind fields?)^{1/}

Also, even after full implementation of the network, not all 19 stations would always be able to furnish wind data. Hence, it was also important to have some idea of the impact of missing data (non-reporting stations) on the wind field estimation. The results below, though not specifically directed toward this latter problem, do provide some insight into how many stations must be functioning at a particular point in time in order for the network data to be useful.

To obtain designs containing fewer than 19 points, the design selection algorithm was applied once again using the same model and criterion as before (i.e., Model (3) and Criterion (11)). The initial set of candidate sites for this run, however, were the 19 points of the OSN (i.e., $M=19$). The resultant designs can be specified as follows:

^{1/}Estimation of the parameters of model (3), of course, requires a minimum of 13 stations; the questions here are concerned with how many additional stations are needed for reliable estimation and which stations should these be.

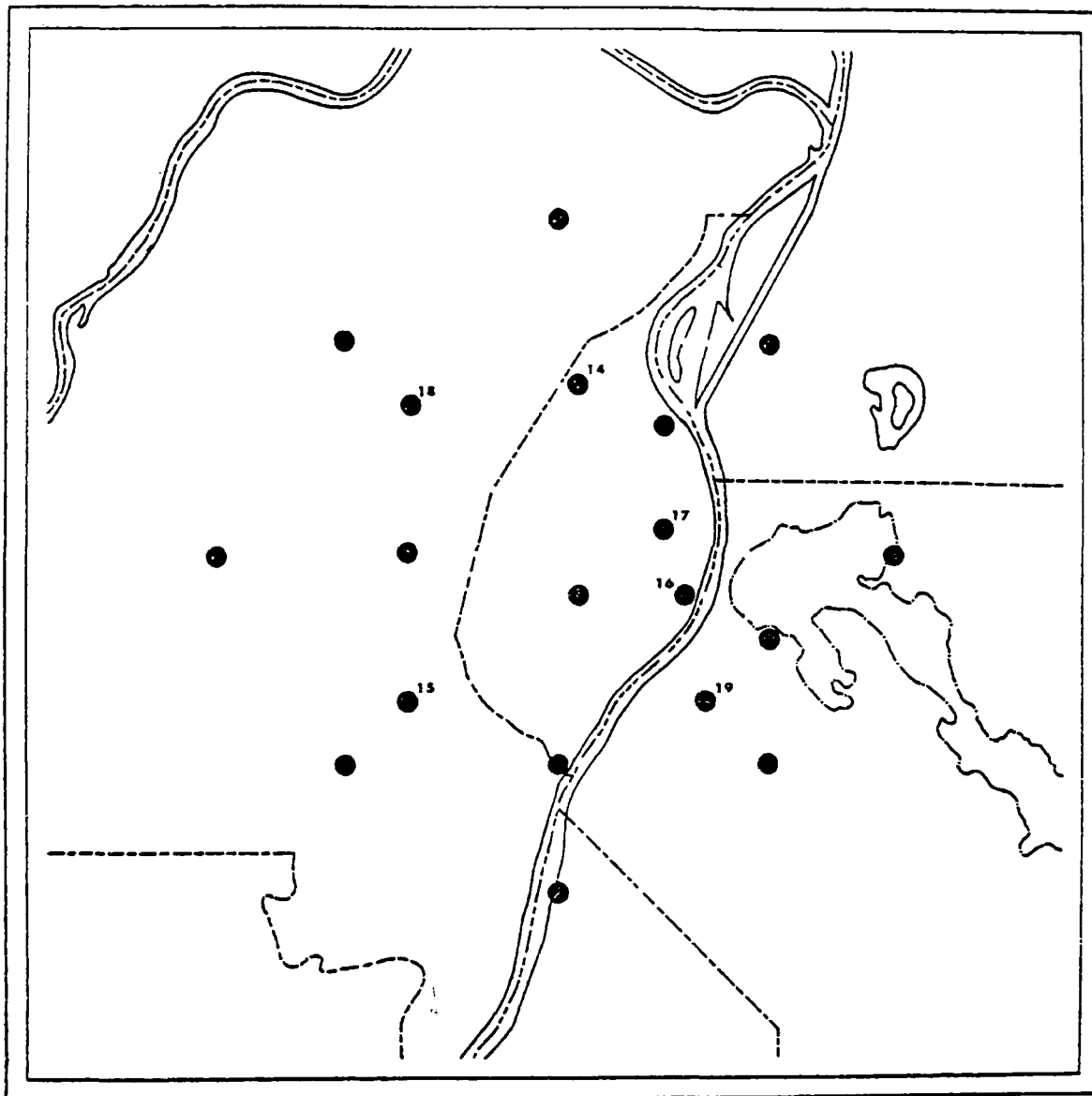


Figure 11. Stations in the A2 network (the OSN) for St. Louis, Missouri. See text for discussion of numbered stations.

<u>Design</u>	<u>No. Points</u>	<u>Specification</u>
B	18	Remove (7,-7) from OSN
C	17	Remove (-7,7) from Design B
D	16	Remove (5,1) from Design C
E	15	Remove (5,-2) from Design D
F	14	Remove (-7,-7) from Design E
G	13	Remove (1,8) from Design F

The distributions for the variance functions for the above designs over 441 points in the innermost grid are characterized in the table below:

<u>Design</u>	<u>No. of Sampling Stations</u>	<u>Frequency Distribution</u>					<u>Mean</u>	<u>Standard Deviation</u>	<u>Maximum</u>
		<u><1/2</u>	<u>1/2-1</u>	<u>1-2</u>	<u>2-4</u>	<u>4-8</u>			
G	13	0	229	158	41	13	1.25	0.82	5.21
F	14	18	316	106	1	--	0.84	0.25	2.09
E	15	50	337	54	--	--	0.74	0.22	1.60
D	16	96	309	36	--	--	0.67	0.21	1.53
C	17	149	274	18	--	--	0.61	0.20	1.30
B	18	202	232	7	--	--	0.55	0.17	1.17
OSN	19	224	211	6	--	--	0.53	0.17	1.16

Sums of squares of deviations between simulated and predicted wind components over this same set of points were calculated for 24 cases, where the estimation of the model (3) parameters was based only on data at those points in the particular design.^{1/} Let SSD_{ijkm} represent this sum of squares for the i^{th} prevailing wind direction (0° , 90° , 180° , 270°), the j^{th} wind shear (1,2,...,6), the k^{th} component (WE, SN) and the m^{th} design (OSN, B, C, D, E, F, G); then one can compute the average over prevailing wind directions as:

^{1/} Data from the remaining 24 cases could not be utilized since these cases provided data at the grid points of the diamond-shaped grid. Hence, simulated data at the design points for these cases was unavailable.

$$SSD_{.j.m} = \frac{1}{4} \sum_{i=1}^4 (SSD_{ij1m} + SSD_{ij2m}). \quad (12)$$

Values of this quantity are shown below:

Design	No. Points	Wind Shear Code					
		1	2	3	4	5	6
G	13	39.9	81.8	113.9	6.4	19.9	76.1
F	14	32.7	58.5	85.2	4.6	12.6	43.8
E	15	27.5	50.4	63.2	3.1	8.7	26.5
D	16	27.8	49.7	63.3	3.2	9.9	29.3
C	17	26.2	50.6	65.0	3.4	10.1	30.6
B	18	25.6	48.9	63.5	3.4	10.0	31.4
OSN	19	25.3	48.5	64.7	3.3	9.4	30.2

The above tables, and the results shown in Table 7 (which presents a summary of the correlations between observed and predicted values for each design) are quite consistent. They indicate that the 13- and 14-point designs are substantially inferior to the larger networks. The 15-point design, however, does not appear to be unduly bad with respect to the 19-point OSN.

Because it was economically unfeasible for RTI to establish a 19-station field program for validating the results, it was necessary to make a further modification of the basic strategy (Figure 5). This modification, which is described further in Section 4.0, involved some shifting of the points in the OSN (in order to be coincident with existing RAPS stations or city/county stations). The resultant design points, referred to as the operational OSN and denoted by OSN*, are shown in Table 8 along with the corresponding points of the OSN. The variance function plot for the OSN* is given in Figure 12. The distribution of the variance function for the OSN (Figure 9) and the OSN*, over two regions of interest, are given below:

TABLE 7. SUMMARY OF CORRELATIONS BETWEEN OBSERVED AND PREDICTED VALUES
OVER 441 POINTS OF INNERMOST GRID--BY WIND SHEAR AND DESIGN

Wind Shear Code	Design	No. Points	Correlations for 4 angles x 2 components		
			<u>Minimum</u>	<u>Mean</u>	<u>Maximum</u>
1	G	13	.02	.50	.72
	F	14	.44	.63	.79
	E	15	.47	.65	.79
	D	16	.48	.65	.79
	C	17	.48	.66	.79
	B	18	.50	.67	.79
	OSN	19	.49	.67	.79
2	G	13	.24	.46	.78
	F	14	.34	.58	.82
	E	15	.29	.61	.83
	D	16	.28	.60	.83
	C	17	.29	.60	.83
	B	18	.46	.62	.83
	OSN	19	.46	.62	.83
3	G	13	.16	.48	.67
	F	14	.31	.51	.68
	E	15	.30	.54	.71
	D	16	.29	.53	.70
	C	17	.29	.52	.71
	B	18	.38	.54	.71
	OSN	19	.37	.53	.70
4	G	13	.24	.65	.90
	F	14	.50	.69	.88
	E	15	.53	.72	.89
	D	16	.48	.71	.89
	C	17	.48	.71	.89
	B	18	.54	.70	.88
	OSN	19	.58	.72	.88
5	G	13	.37	.63	.80
	F	14	.44	.67	.81
	E	15	.55	.71	.83
	D	16	.58	.70	.79
	C	17	.59	.70	.78
	B	18	.59	.70	.80
	OSN	19	.60	.72	.80
6	G	13	.54	.66	.82
	F	14	.55	.69	.85
	E	15	.59	.73	.88
	D	16	.57	.72	.86
	C	17	.57	.71	.85
	B	18	.57	.71	.85
	OSN	19	.59	.72	.85

Range of s_D (.)	Region: $\begin{cases} -10 \leq x \leq 10 \\ -10 \leq y \leq 10 \end{cases}$		Region: $\begin{cases} 0 \leq x \leq 7 \\ -8 \leq y \leq 8 \end{cases}$	
	OSN	OSN*	OSN	OSN*
$\leq 1/2$	224	223	100	108
$1/2$ to 1	211	205	36	28
1 to 2	6	11	0	0
2 to 4	0	2	0	0

The above results (derived from Figures 9 and 12) clearly indicate that the performance of the OSN* relative to the OSN is substantially poorer over the western portions of the innermost grid; over the urban area, however, the two networks compare favorably.

TABLE 8. SPECIFICATION OF DESIGN POINTS FOR THE OSN AND THE OSN*

Number	OSN		OSN*		
	\underline{x}	\underline{y}	\underline{x}	\underline{y}	
1	-16	0	-20	- 3	City/County 6
2	16	0	18	0	EPA 109
3	0	-16	5	-16	EPA 118
4	0	16	0	16	City/County 8
5	-10	-10	- 9	- 8	EPA 119
6	-10	10	-16	8	EPA 120
7	- 7	0	- 7	2	City/County 9
8	0	-10	0	-10	City/County 2
9	1	- 2	1	- 1	EPA 106
10	5	6	5	7	EPA 102
11	10	-10	10	-10	
12	10	- 4	9	- 2	EPA 104
13	10	10	10	12	EPA 108
14	1	8	0	10	EPA 113
15	- 7	- 7	- 6	- 6	
16	6	- 2	4	- 3	EPA 105
17	5	1	6	1	EPA 101
18	- 7	7	- 4	8	
19	7	- 7	9	- 6	EPA 110

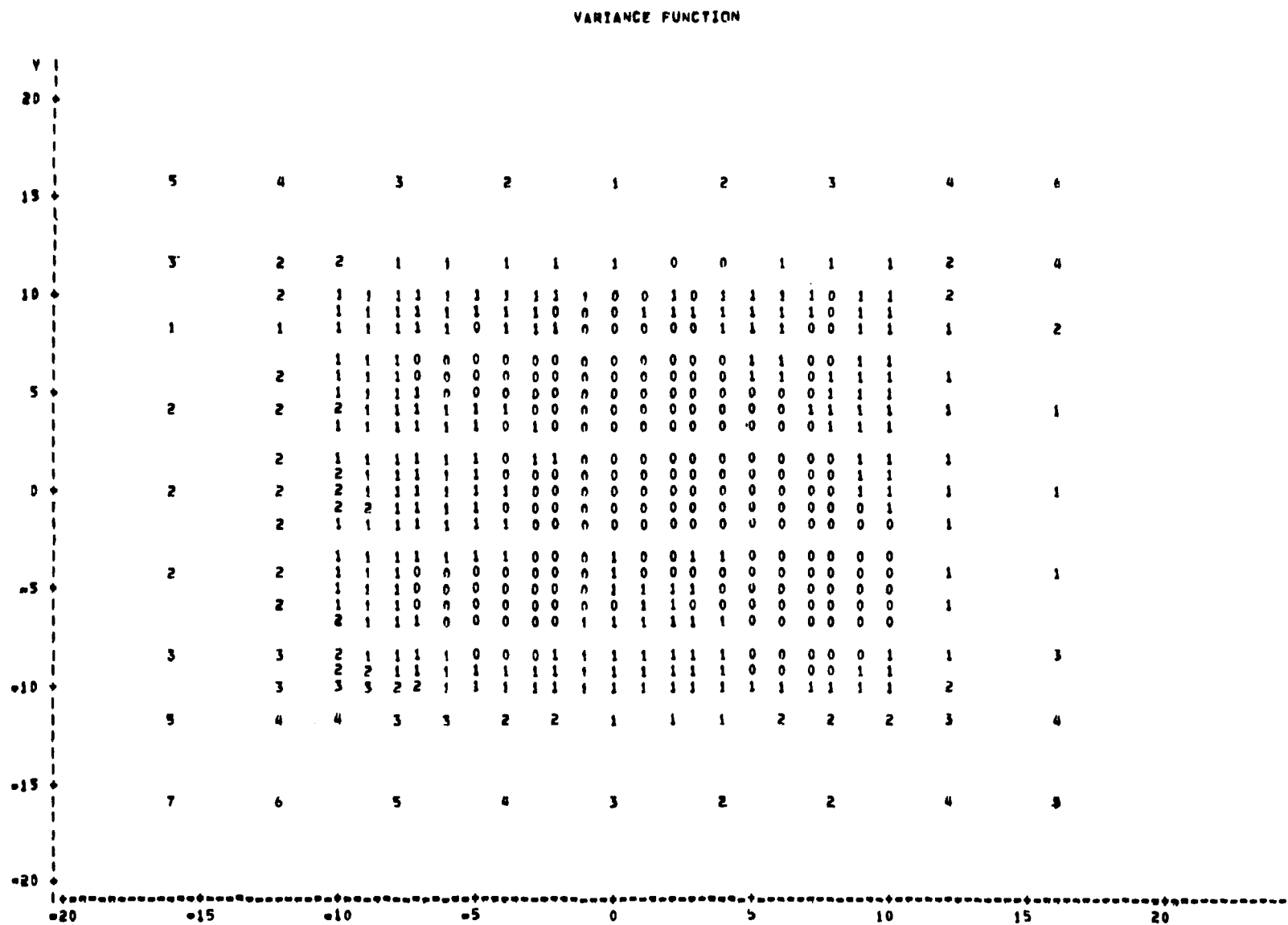


Figure 12. Variance Function^x for the OSN*.

3.3 Objective Variational Analysis Model

The air pollution distribution is obtained using an Objective Variational Analysis Model (OVAM). The model simultaneously minimizes the integrated error variance of the observations from the analysis and the weighted error variance of the analysis from a steady-state solution. In order for the integrated variance to be a minimum, a second-order, Euler-Lagrange equation must be satisfied under specific boundary conditions. The Euler-Lagrange equation is solved by relaxation techniques. The model requires the wind field, the observed pollution concentrations, and the source emissions. This model is generalized so that these parameters can be specified for any urban area.

From an analysis point of view, the distribution of pollution concentrations is primarily dependent upon 1) the distribution of pollutant sources, 2) the mean and turbulent properties of the airflow, 3) measurement locations, and 4) the measured concentrations. The first two of these ingredients are clearly evident in the continuous point source equation:

$$\psi(x,y,z) = \frac{Q}{2\pi\sigma_y\sigma_z\bar{U}} \exp \left\{ -\frac{1}{2}\left(\frac{y}{\sigma_y}\right)^2 + \left(\frac{z}{\sigma_z}\right)^2 \right\} \quad (13)$$

(See Glossary for definition of terms). Equation (13) is a steady-state solution to the mass continuity equation for the pollutant, for constant wind and stability conditions. The distribution of the pollutant concentration can be estimated when the wind, the stability, and the emissions are known. A class of steady-state Gaussian dispersion models such as the Air Quality Display Model (AQDM) (TRW Systems Group, 1969) or the Climatological Dispersion Model (CDM) (Busse and Zimmerman, 1973) estimate the concentrations at given locations under specified conditions. Even more simplified models such as proposed by Gifford and Hanna (1973) are used to estimate concentrations downwind of uniform emission areas. In general, the estimated value will disagree with a measured concentration for the same location because of inappropriate assumptions, poor knowledge of input variables, or both.

Within an urban area, the pattern of pollutant concentrations is not always apparent from a set of concentration measurements at fixed locations.

The presence of sources, the limited number of sampling locations, and the variable wind velocity mask the true distribution from those obtained by conventional subjective or objective analysis.

In conventional objective analysis, the estimated value of a variable at a given location is extrapolated/interpolated from observed values of the variable at specified locations. Cressman (1959) and Barnes (1964) used different distance-dependent weight functions to interpolated within a given radius of an observation. Endlich and Mancuso (1968) used an elliptical weight function oriented along the wind direction and proportional to the wind speed. These techniques smooth the distributions and are incapable of showing maxima or minima where there are no observations. In an urban area with nonuniform sources, it is necessary to have an analysis which accounts for variable distributions of sources and, possibly, locally high or low concentrations where there are no observations.

Sasaki (1958, 1970a, b, c) proposed an analysis technique, first as an initialization procedure for a numerical forecasting scheme, that uses the observed variables at given locations and a model describing the behavior of those variables to produce analysis which is consistent with both the observations and the model. The technique is based on minimizing the weighted error variance of 1) the variable, ϕ , and its observation, $\tilde{\phi}$, and 2) the model equations, $E(\phi)$, over the domain of the integration. The total weighted error variance, EV, is given by

$$EV = \int_{\Omega} \left[\tilde{\alpha}(\phi - \tilde{\phi})^2 + \alpha E^2(\phi) \right] d\Omega .$$

The terms $\tilde{\alpha}$ and α are the weighting functions and are inversely proportional to the typical variance of their respective terms. This formulation is called the "weak constraint" by Sasaki since it is $E^2(\phi)$ which is being minimized rather than $E(\phi)$. The distinction is significant since $E(\phi)$ is normally zero. For example, in some applications the adiabatic equation $\frac{d\theta}{dt} = 0 = E(\phi)$ might be an appropriate constraint. In the weak constraint formalism, θ , the potential temperature is not absolutely conserved over the domain, but its variance while moving a parcel of air is conserved in accordance with the observations.

The distribution of ϕ , which minimizes the integral, EV, is given by the solution to the Euler-Lagrange equations (see Lanczos, 1970). Those equations specify the partial differential equation of ϕ which must be satisfied on the interior of the domain, and specify the boundary conditions which must be met. In most instances, the solution can be obtained by numerical integration.

Sasaki and Lewis (1970) used the technique to analyze three-dimensional mesoscale distributions of wind components, temperature, and moisture associated with severe storms. Stephens (1970) obtained synoptic scale distributions of pressure height fields consistent with the balance equation. All these users have shown that the solution technique acts as a low-pass filter for real or for induced (simulated) errors in the observation field.

Wilkins (1971, 1972) applied the variational objective analysis principles to urban air pollution analyses. He described a method of adjusting a pattern of concentration isopleths using the classical diffusion equation as a constraint, whenever discrepancies in temporal continuity occur between two successive analyses. Errors arising from misanalysis or from a variable wind field were also considered. Using realistic estimates, Wilkins showed that the analysis error of the sequences of an analysis could be reduced to one-tenth the initial error. He also outlined the potential application of the methodology as a part of the continuous urban air monitoring surveillance program.

The approach used in this research project reverts to more basic forms. The differential form of the mass continuity equation for a trace material is used as a constraint instead of an integrated form (Eq. 13). The concentration observations are used where and when they are available. Wilkins' approach could be used to adjust the resulting analyses.

The purpose of the objective analysis is to obtain an estimate of the concentrations where observations are missing. This analysis approach requires that the analysis fit the observed concentrations and the existing emission, transport, and diffusion characteristics throughout the urban area. The "best analysis" is defined as the distribution which minimizes the weighted sum of the error variance a) between the observed and analyzed concentrations, and b) the departure of the results from a steady state.

3.3.1 Description of the Model

Consider a volume having dimensions X (west-east), Y (south-north) and Z (ground-up) which encompasses a flat urban area. The observations of the pollution concentration, ψ , are known for various locations. The ground-level emissions density, $Q(x,y)$ as well as the velocity components, u, v, w (in the x, y and z directions, respectively) are known throughout the volume. The equation of mass conservation of a passive (inert) gas in the atmosphere is written:

$$\frac{\partial \psi}{\partial t} + u \frac{\partial \psi}{\partial x} + v \frac{\partial \psi}{\partial y} + w \frac{\partial \psi}{\partial z} = K_H \left(\frac{\partial^2 \psi}{\partial x^2} + \frac{\partial^2 \psi}{\partial y^2} \right) + \frac{\partial}{\partial z} \left(K_z \frac{\partial \psi}{\partial z} \right) \quad (14)$$

where

- ψ is the concentration ($\mu\text{g}/\text{m}^3$),
- K_H is the eddy diffusivity in the horizontal (m^2/s), and
- K_z is the eddy diffusivity in the vertical (m^2/s).

Since observations are normally made only near the ground, little is actually known about the vertical distribution of the pollutant or about the local vertical velocity, w , from measurements. Therefore, seeking a way to express the concentration within a given volume in terms of its ground-level concentration, the following assumptions are made:

- 1) $\psi(x,y,z) = \psi_0(x,y,0) \exp \left[-\frac{1}{2} (z/S_z)^2 \right]$
- 2) $w \approx 0$ in the layer between $z = 0$ and $z = Z$
- 3) Z is small
- 4) u and v do not vary substantially between their measurement height and Z
- 5) All emissions are from ground-based ($z = 0$) sources. (This is a simplifying assumption, not a model requirement).

Integrating Eq. (14) from $z = 0$ to Z , gives

$$\left. \frac{\partial \psi}{\partial t} + u \frac{\partial \psi}{\partial x} + v \frac{\partial \psi}{\partial y} + w \psi \right|_0^Z = K_H \nabla_H^2 \psi + K_z \left. \frac{\partial \psi}{\partial z} \right|_0^Z \quad (15)$$

where

$$\hat{\psi} = \int_0^Z \psi \, dz$$

and

$$\nabla_H^2 \hat{\psi} = \frac{\partial^2 \hat{\psi}}{\partial x^2} + \frac{\partial^2 \hat{\psi}}{\partial y^2}$$

By Assumption 2,

$$w\psi \Big|_0^Z = 0 \quad . \quad (16)$$

By Assumption 5,

$$K_z \frac{\partial \psi}{\partial z} \Big|_0^Z = K_z(z) \frac{\partial \psi}{\partial z} \Big|_Z + Q(x,y) \cdot \quad (17)$$

Given the functional form of ψ ,

$$\hat{\psi} = \psi_0(x,y) \cdot \int_0^Z \exp -\frac{1}{2} (z/S_z)^2 \, dz$$

or

$$\hat{\psi} = \sqrt{\frac{\pi}{2}} S_z \psi_0(x,y) \operatorname{erf}(z/\sqrt{2} S_z) \quad (18)$$

$$= \gamma(S_z, Z) \cdot \psi_0(x,y)$$

and

$$\begin{aligned} K_z \frac{\partial \psi}{\partial z} \Big|_{z=Z} &= -K(Z) \left(\frac{-Z}{S_z^2} \right) \cdot \psi_0 \exp \left(-\frac{1}{2} (Z/S_z)^2 \right) \\ &= -K(Z) \beta(\sigma_z, Z) \cdot \psi_0 \quad . \end{aligned} \quad (19)$$

Substituting Eqs. (16), (17), (18) and (19) into (15) gives

$$\gamma \left(\frac{\partial \psi_0}{\partial t} + u \frac{\partial \psi_0}{\partial x} + v \frac{\partial \psi_0}{\partial y} \right) - \gamma K_H \nabla_H^2 \psi_0 + K_z(Z) \beta \cdot \psi_0 - Q = 0. \quad (20)$$

Since reported concentrations are averaged over a given time increment or are an instantaneous value during the period, the time variability of the concentration over that interval cannot be accounted for. If the emissions data, Q , and the wind data are appropriate for that time interval, a nearly steady state (i.e. $\frac{\partial \psi}{\partial t} \approx 0$) may be assumed for the time interval. With that assumption, the emissions must be locally balanced by advection and diffusion out of the volume. (The assumption of a steady state is not a requirement of the analysis model. If only one set of observations is available, it is the best assumption. If data for more than one time are available, then the time variability can be included).

A dimensional analysis of the terms of the continuity equation shows the relative contribution of each term and will also aid in computations by reducing truncation errors. Defining characteristic magnitudes of each quantity given

$$\begin{aligned}\psi &= \bar{\psi} \cdot \psi' \\ x, y &= L \cdot (x', y') \\ Q &= \bar{Q} \cdot Q' \\ K &= \bar{K} \cdot K', \quad \text{and} \\ u, v &= \bar{U} (u', v')\end{aligned}$$

where

$\bar{\psi}$ is a characteristic magnitude of ψ_0 , (gm/m^3),
 L is a characteristic length of the urban pollution system (m),
 \bar{Q} is a characteristic surface emission magnitude ($\text{gm}/\text{m}^2 \text{ s}$),
 \bar{U} is a characteristic wind speed (m/s),
and \bar{K} is the characteristic magnitude of K_H or K_z (m^2/s).

Equation (20) becomes

$$\frac{\bar{U}\bar{\psi}\gamma}{L} \left(u' \frac{\partial \psi'}{\partial x'} + v' \frac{\partial \psi'}{\partial y'} \right) - \frac{\gamma \bar{K} \bar{\psi}}{L^2} (K'_H \nabla_H \psi') + \bar{K} \beta \cdot \psi' - \bar{Q} Q' = 0. \quad (21)$$

Dividing Eq. (21) by $\frac{\bar{U}\bar{\psi}\gamma}{L}$, dropping the prime (') from the non-dimensional variables, gives

$$u \frac{\partial \psi}{\partial x} + v \frac{\partial \psi}{\partial y} - R(K_H \nabla_H^2 \psi) + \xi \psi - \eta Q = 0 \quad (22)$$

where

$$\begin{aligned} R &= \bar{K}/\bar{U}L \\ \eta &= L\bar{Q}/\gamma\bar{U}\bar{\psi} \\ \xi &= \bar{K}\beta L/\gamma\bar{U}. \end{aligned}$$

The advection terms, $u \frac{\partial \psi}{\partial x}$, are on the order of unity and the other terms are scaled by the non-dimensional coefficients.

In the atmosphere, K , may take on a wide range of values, depending upon stability conditions. In this study, the conditions are classified by the Pasquill stability categories (Turner, 1969) and the value of the vertical diffusion coefficient, σ_z , for that category. The two terms are related through the Fickian solution to the steady-state diffusion equation which gives

$$\sigma_z^2 = 2Kt \quad .$$

Letting Σ be the characteristic value of σ_z and $T = L/\bar{U}$ be the characteristic travel time gives

$$\bar{K} = \Sigma^2 U/2L \quad . \quad (23)$$

Choosing $\Sigma \sim \sigma_z(x = 1 \text{ km})$, the minimum value of σ_z was encountered. That value is related to the characteristic values of S_z and γ , the coefficient of ψ and η , the coefficient of Q .

The magnitude of the coefficients determines the relevance of the respective terms as compared to the advective term. The simple dimensional terms like L , $\bar{\psi}$, \bar{U} and \bar{Q} can be defined. The terms ξ and η are, however, functions of the standard deviation of the local vertical profile of the concentrations (S_z) which is a function of the local source. S_z is

dependent upon but not identical to σ_z , the vertical standard deviation of a point source of material. S_z reflects the upwind emissions, transport, diffusion, and "background" so that

$$\psi(x,y,z)/\psi(x,y,0) = \exp \left[-\frac{1}{2}(z/S_z)^2 \right]$$

or

$$S_z = z / \sqrt{2 \ln \psi_0 / \psi_z} .$$

At any location, the ψ_0 and ψ_z , will be dependent upon the vertical diffusion of the atmosphere and upwind sources. Σ tends to maximize the coefficients of ψ and Q . This definition permits \bar{K} to adjust with changes in stability classification.

The β term can be written as

$$\beta(x) = \frac{1}{z} \left(z/S_z \right)^2 \exp \left[-\frac{1}{2} (z/S_z)^2 \right] . \quad (24)$$

The maximum value of β occurs for $(z/S_z)^2 \sim 2.0$. If β is evaluated there ($\sim 0.75/z$), the term in Eq. 21 representing vertical flux through the top of the volume will be maximized, and other characteristic values can be evaluated. Choosing $z = \sqrt{2} S_z$ gives a characteristic value, $\bar{\gamma}$, for γ ,

$$\bar{\gamma} = 0.68 \sqrt{\pi/2} S_z ,$$

or

$$\bar{\gamma} = 0.68 \sqrt{\pi/4} z .$$

The characteristic value of ξ , $\bar{\xi}$, is given by

$$\bar{\xi} = \bar{K} L \bar{\beta} / \bar{U} \bar{\gamma} .$$

When $(z/S_z)^2 \sim 2.0$, $\bar{\xi} \approx 0.62 \Sigma^2 / z^2$. If $\Sigma^2 \sim \sigma_z^2 \sim S_z^2$, then

$$\bar{\xi} \approx 0.31 .$$

The characteristic value of η , $\bar{\eta}$, is given by

$$\bar{\eta} = \bar{Q} L / \bar{\psi} \bar{U} \bar{\gamma}$$

Choosing

$$Q = 10^{-8} \text{ gm/m}^2 \text{ s}$$

$$L = 4 \text{ km}$$

$$\bar{\psi} = 10^{-6} \text{ g/m}^3$$

$$\bar{U} = 3 \text{ m/s}$$

$$\gamma = 0.6 \text{ Z}$$

and

$$Z = 10^2 \text{ m}$$

gives

$$\bar{\eta} = 0.22 \text{ .}$$

With those assumed values, and Eq. 22, R is given by

$$R = \Sigma^2 / 2L^2 \\ \approx 1.56 \times 10^{-4} \text{ .}$$

The horizontal diffusion term, therefore, is negligible with respect to the other terms in the analysis as Wilkins also showed.

3.3.2 Analysis Technique

The approach to the analysis techniques taken here was first implemented by Sasaki (1957). Following the hypothesis that the best analysis is one which minimizes the error variance of the observations and the continuity equation through the domain (X by Y), the error variance integral, EV, is formed, i.e.,

$$EV = \int_x \int_y \left[\tilde{\alpha}(\psi - \tilde{\psi})^2 + \alpha A^2 \right] dy dx \quad (26)$$

$$A = u \frac{\partial \psi}{\partial x} + v \frac{\partial \psi}{\partial y} + \xi \psi - \eta Q = 0 \quad (26a)$$

where $\tilde{\psi}$ is the non-dimensional value of the observations,
 ψ is the non-dimensional value of the analysis,
 $\tilde{\alpha}$ is a weight function inversely proportional to the
variance of $\tilde{\psi}$,
and α is a weight function inversely proportional to the
variance of A.

The distribution of ψ which minimizes the integral is given as the solution to the Euler-Lagrange equation (See Stephens, 1970). For the integral in Eq. (26) that equation is

$$\tilde{\alpha} (\psi - \tilde{\psi}) + \alpha (\xi A - \frac{\partial u A}{\partial x} - \frac{\partial v A}{\partial y}) = 0 \quad (27)$$

subject to the boundary conditions that ψ is invariant on the boundary ($\delta\psi = 0$) or the normal gradient of ψ is invariant ($\delta (\frac{\partial\psi}{\partial n}) = 0$).

Considering the simple case of one-dimensional case of uniform flow, $u = 1$, $v = 0$, and constant coefficients ξ and η . The Euler-Lagrange equation reduces to

$$\tilde{\alpha} (\psi - \tilde{\psi}) + \alpha (\xi A - \frac{\partial A}{\partial x}) = 0 \quad (28)$$

where

$$A = \xi \psi + \frac{\partial \psi}{\partial x} - \eta Q \quad (29)$$

Substituting Eq. (29) into Eq. (28) and simplifying gives

$$\alpha \frac{\partial^2 \psi}{\partial x^2} - (\alpha \xi^2 + \tilde{\alpha}) \psi = \alpha (\eta \frac{\partial Q}{\partial x} - \eta \xi Q) - \tilde{\alpha} \tilde{\psi} = H(x) \quad (30)$$

which is a one-dimensional Helmholtz equation of the form

$$\frac{\partial^2 \psi}{\partial x^2} - \mu^2 \psi = H(x) \quad .$$

The forcing function, H , is governed by the weighted observations, the emissions, and the emissions gradient. The magnitude of α and $\tilde{\alpha}$ also influence the solution. If $\tilde{\alpha}/\alpha$ is large (~ 10), Eq. (28) reduces to $\psi = \tilde{\psi}$. If $\tilde{\alpha}/\alpha$ is small (~ 0.1), the observations have far less weight and the distribution of sources governs the solution, e.g.,

$$\frac{\partial^2 \psi}{\partial x^2} - \xi^2 \psi = \eta \frac{\partial Q}{\partial x} - \eta \xi Q \quad . \quad (31)$$

This is exactly the analysis objective--use the observations where they are known and use the emissions and meteorology where the observations are missing to determine the distribution of ψ over the area.

Since $(\alpha\xi + \tilde{\alpha})/\alpha > 0$, Eq. (30) is an elliptic partial differential equation with constant coefficients and is amenable to solution by numerical relaxation. Similar numerical techniques should be valid for integrating Eq. (26) to obtain a solution when the coefficients are variable.

3.3.3 Numerical Solutions

A finite difference grid ($I \times J$) with uniform grid spacing in the x and y directions is assumed to encompass the urban area. At each grid point (i,j) the wind components (u,v) are known; the emission for the area bounded by unit increases of i and j is assigned to that point and is assumed constant over the unit area; the measured (observed) and estimated concentrations are also assigned. The measurements do not necessarily occur at the location, but we assume they have been interpolated to the grid point.

A first guess to the concentration distribution is made at $z = 0$ and at $z = Z$, assuming that a steady-state condition with a constant wind, the given emissions, and a representative atmospheric stability exists. A background concentration, ψ_B , is added to give ψ_0 and $0.999 \psi_B$ is added at $z = Z$ to give ψ_Z , so that S_z will be defined at locations upwind of any source. Although a CDM estimate at the two altitudes might be used, a more rigorous integration has been chosen than the virtual point source approach used in the CDM (see Appendix B). The estimates of ψ at $z = 0$, and Z are analyses used to estimate S_z , γ , η and ξ for each grid point.

With these data, a solution to the analysis equation is obtained using the point-by-point Richardson relaxation procedure (Thompson, 1961). Schemes with more rapid convergence might be used, but may present some problems when the coefficients are variable. If the Richardson procedure will not give a solution, neither will any of the others.

At the v th iteration, A_{ij}^v is computed with existing grid-point estimates of ψ , (ψ_{ij}^v) , using the finite difference analog of Eq. (26a), i.e.

$$A_{ij}^v = \xi_{ij} \psi_{ij}^v + r u_{ij} (\psi_{i+1,j}^v - \psi_{i-1,j}^v) + r v_{ij} (\psi_{i,j+1}^v - \psi_{i,j-1}^v) - \eta_{ij} \dot{Q}_{ij} ;$$

where $r = L/2\Delta x$

and $\dot{Q} = (Q_{i-1,j-1} + Q_{i-1,j} + Q_{i,j-1} + Q_{i,j}) / 4.0$

is the mean value of the area emission adjacent to the point (i,j) . At the south and west edges of the grid, \dot{Q} is estimated by linear extrapolation outward from interior grid points. Along the boundaries, the normal gradient of ψ is computed using the current values of ψ at the boundary and the first interior row or column of the grid. It is advantageous to compute A since the value of the integrand EV of Eq. (26) is evaluated at each iteration.

The residual, R_{ij}^v , at each interior grid is given by the finite difference analog of the analysis equation, (Eq. 27), i.e.,

$$R_{i,j}^v = \alpha \left\{ (\xi A)_{i,j}^v - r \left[(uA)_{i+1,j}^v - (uA)_{i-1,j}^v + (vA)_{i,j+1}^v - (vA)_{i,j-1}^v \right] \right\} + \tilde{\alpha} (\psi_{i,j}^v - \tilde{\psi}_{i,j}) .$$

The improved estimate of $\psi_{i,j}^v$, $\psi_{i,j}^{v+1}$, is given by

$$\psi_{i,j}^{v+1} = \psi_{i,j}^v - R_{i,j}^v / \Omega_{i,j}$$

where

$$\Omega_{ij} = \alpha \left[\xi_{ij}^2 - 2r^2 (u_{ij} + v_{ij}) \right] + \tilde{\alpha} .$$

Successively applied, the recursion formulas lead to convergence of the solution in the constant coefficient case. The solution is obtained when

$$\left| \psi_{ij}^{v+1} - \psi_{ij}^v \right| < 0.01 \quad (32)$$

at every point in the interior of the grid.

This criteria is quite stringent, indicating that the solution is known to one percent or less at every point in the area. Realistically, even in the best conditions, errors of concentration are 5- to 10-times larger. In some instances, $v = 90$ also served as a cutoff value. The trend of the solution is well established by that iteration and convergence with more iterations is assured.

3.3.4 Weighting Factors

The weighting factors, like the other terms of the analysis equation are non-dimensional. They are inversely proportioned to the variance of ψ and $\frac{\partial \psi}{\partial t}$ about the domain of interest. Their relative value (i.e., the ratio $\tilde{\alpha}/\alpha$) is more important to the resulting analysis than is the absolute magnitude of either factor.

The non-dimensional value of A at any point increases in proportion to the ratio L/U (η , ξ , and the advection derivative depend upon L/U). The non-dimensional variance of A is, therefore, proportional to $(L/U)^2$. The dimensional form of $\frac{\partial \psi}{\partial t}$ may be written as $(\bar{\psi}/T)A$. Therefore, the variance of dimensional form $\frac{\partial \psi}{\partial t}$ is proportional to $(\bar{\psi}L/UT)^2$. The variance of $\bar{\psi}$ is proportional to $\bar{\psi}^2$, so that the ratio of $\tilde{\alpha}/\alpha$ is given by

$$\tilde{\alpha}/\alpha \propto (L/UT)^2 .$$

This ratio was taken as unity in developing Eq. (23) and is so taken here. That choice means that the time scale of variability and of sampling is proportional to the transport time. Typical values of L ($=4$ km) and U ($=3$ m/s) gives $T \sim 20$ minutes. If the sampling rate is greater than the transport rate, then T should be proportional to the sampling rate. If the analysis is being used to update the pollution distribution based on recent measurements, the choice of T should depend upon the update frequency.

In practice, however, $\tilde{\alpha}/\alpha$ should be large where there are observations since there is no substitute for a good observation; yet, it should not be so large as to force an observation which is inconsistent with other observations or with the dynamical considerations into the analysis. Where there are no observations, $\tilde{\alpha}/\alpha$ should be small, thereby relying on the dynamics of the system to determine the concentrations.

3.3.5 Test Results

There are many assumptions and interpretations left to the user which have a differing influence on the solution to the analysis equation. Either boundary condition is acceptable and will give a minimum, but not necessarily equal, error variance for the integral. The solution will be different in each case. The choice of space scales, L and Z , may be important to the solution as they affect the characteristic numbers η and ξ . The magnitude of the weighting terms $\tilde{\alpha}$ and α , while left to the user, should be representative of the situation being modeled. The distribution of sources affects the "measured" concentrations, the error integral, and the magnitude of the characteristic numbers. The atmospheric stability assumption also governs the magnitude and distribution of η and ξ . The choices are interdependent.

A series of test cases were developed to verify that the solution can be obtained to determine the effects of different assumptions or parameter choices upon the solutions, and finally, to examine the applicability of the model in a simulated urban area where there are a limited number of observations which contain some error. In these tests, ψ^* , is the concentration of the steady-state numerical solution obtained for $\psi(x,y,0)$, $\tilde{\psi}$ will be the "observed" concentrations throughout the area which may be wholly or partially dependent upon ψ^* , and ψ will denote the concentration given by the solution of the Euler-Lagrange equation. The urban area modeled is 9 km (south-north) by 20 km (west-east). The center of the area source is at $x = 7.5$ km, $y = 4.5$ km. The basic source configuration (Appendix B) was chosen so that the effects of gradients in the emissions patterns can be investigated. Emissions do not occur out of the grid area.

The distribution of concentrations for a basic source configuration in a neutrally stable atmosphere (the Pasquill-Turner D stability) and a background concentration $\psi_B = \psi$ is shown in Figure 13. Since the distribution is symmetrical about the downwind centerline (i.e., $y = 4.5$ km), cross sections along the $y = 5$ km axis will characterize the solutions which are obtained. The distributions of S_z, γ^{-1} , and ξ along $y = 5$ km determined from that distribution when $L = 50$ m are given in Figure 14. Upwind of any source contribution to concentrations at $z = Z$, background relationships prevail and $S_z = 22.35 Z$.

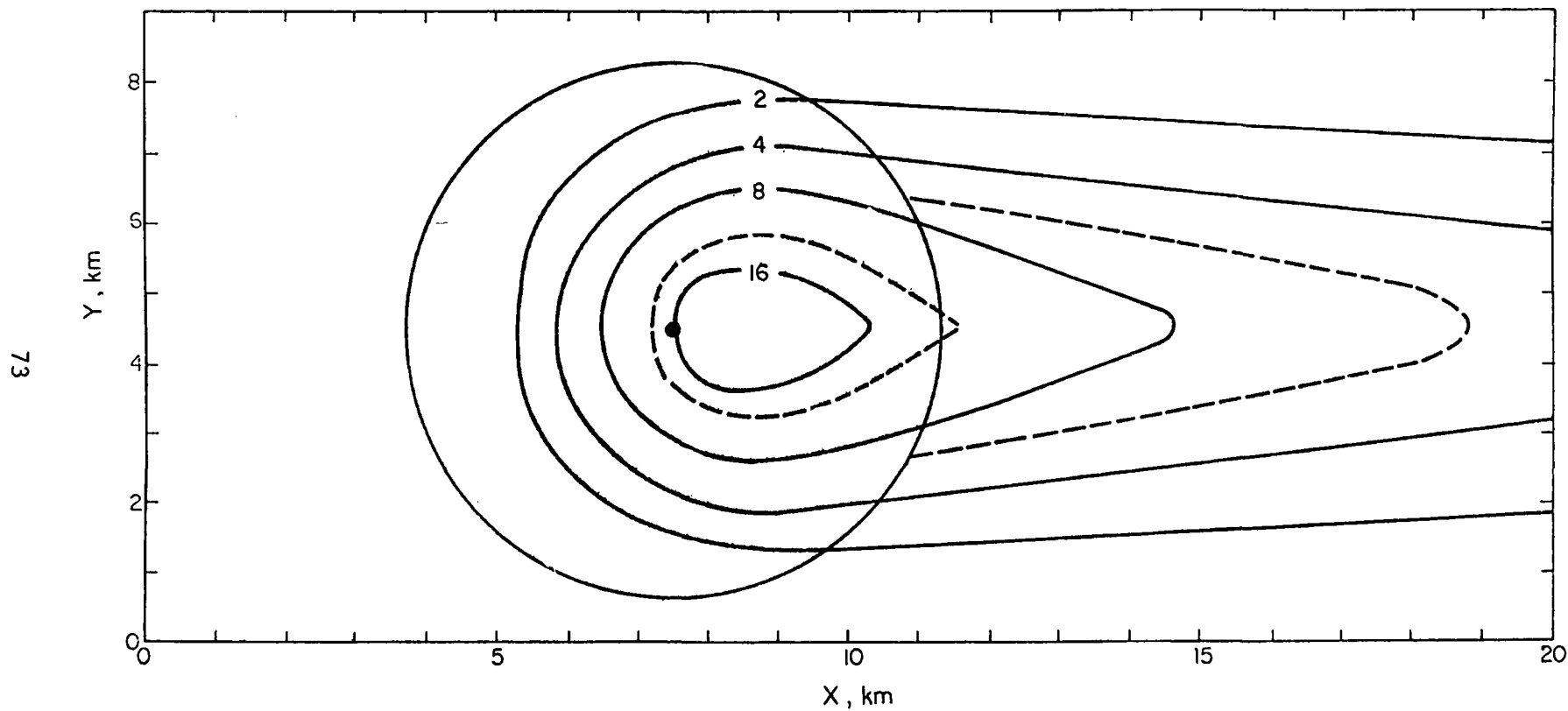


Figure 13. Concentration isopleths ($\mu\text{g}/\text{m}^3$) at ground level from emissions (10 gm/s) normally distributed within the shaded area, at neutral stability and a constant wind, U , of 3 m/s.

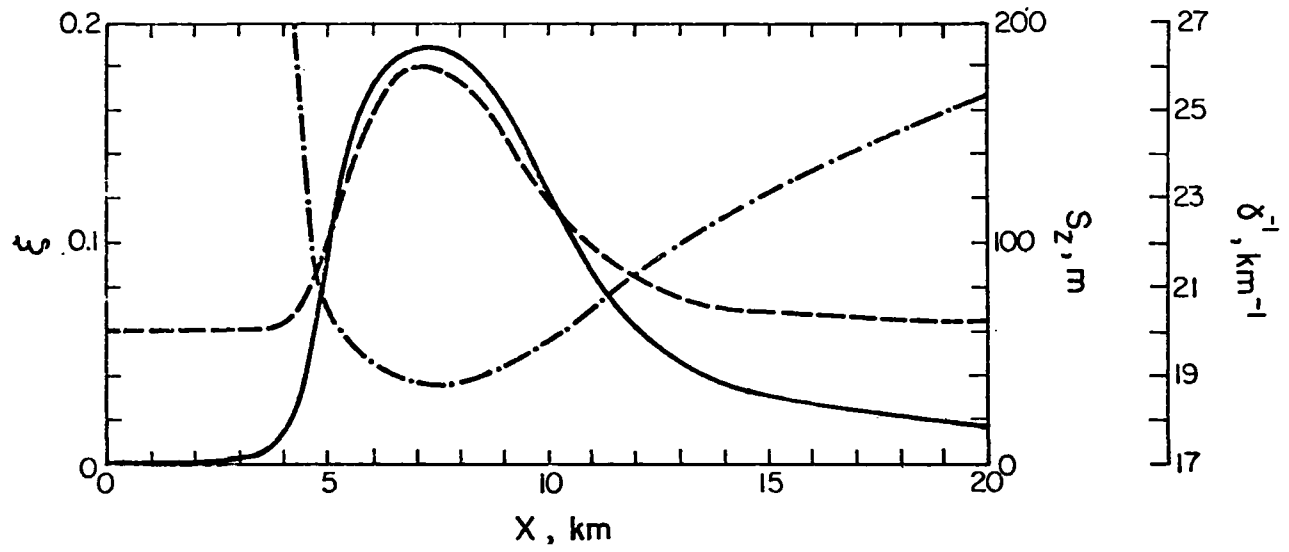


Figure 14. Horizontal distribution of ξ (—), S_z (— · — ·), and γ^{-1} (— — —) along $y = 5\text{km}$ for Case I.

The details and results of the sensitivity analyses for the effects of $\tilde{\alpha}/\alpha$, L , source size, boundary conditions, Z , and observational errors are given in Appendix C. Table C-1 of Appendix C summarizes the input data. A brief description of each case study follows:

Case I: $\tilde{\alpha}/\alpha$ When $\tilde{\alpha}/\alpha = 10$, the analytic solution was returned. As $\tilde{\alpha}/\alpha$ decreases, the influence of the observations decrease so the difference between the observed and the solution increases. The maximum value of the analysis is displaced slightly downwind from the analytic solution, so the analysis predicts lower concentrations upwind of the source and predicts higher concentrations downwind of the source. Total mass is approximately conserved.

Case II: L The effects of the constraint equation were studied by choosing $\tilde{\alpha}/\alpha = 0.01$. Under these conditions, the analysis reduces to a one-dimensional Poisson equation whose solution depends upon the choice of L . When $L = 1$ km, the solution was achieved in fewer iterations, but differed only slightly with the solutions when $L = 4$ or 10 km.

Case III: (a) Source Configuration:

The total amount of emissions was kept constant but was distributed over larger areas by increasing the standard deviation, q_x , of the Gaussian-shaped emission pattern from 1.25 to 2.50 to 5.0 km. As the emissions became more uniform, i.e., q_x increased, the concentration estimates of the analysis equation ($\tilde{\alpha}/\alpha = 0.01$) approached the analytical solution for that emission pattern.

Case III: (b) Boundary Conditions:

The boundary conditions were changed from invariant ($\psi = \text{constant}$) to constant flux conditions across the boundaries, and the same source-dependent experiments were rerun. The greatest error and error variance

occurred in the $q = 1.25$ case when a negative concentration was analyzed at the upwind boundary. That was caused by the lack of emissions there. At the downwind boundary, maintaining the gradient required that the concentrations there were overestimated by 1.67 times the observed. As the emissions became more dispersed ($q = 2.5$), the analysis approached the analysis with constant boundary conditions and the analytic solution. For $q = 5.0$, the analyses with different boundary conditions were indistinguishable.

Case IV:

Effects of Z

The effects of choosing different values of Z , the height of the urban volume upon the analysis equation ($\tilde{\alpha}/\alpha = 0.01$) were investigated using $Z = 100$ m, 200 m, and 31.5 m ($= S_z$) and comparing the resulting analyses with solutions when $Z = 50$ m ($\sim \sqrt{2} S_z$). As Z increases, the analysis progressively and substantially underestimates the maximum concentration and displaces it further downwind. When $Z = 200$ m, the analysis underestimated the true concentration at every point. The smaller value of Z showed good agreement upwind of the source area but consistently overestimated the concentration downwind of the peak concentration. The choice of $Z \sim \sqrt{2} S_z$ gives the best overall agreement, minimum error variance, of all of the values used.

Case V:

Observational Errors

Random errors were drawn from a normal distribution with zero mean and ψ_B standard deviation and were added to the analytic solution at each point forming the "observed" distribution. The analysis, with $\tilde{\alpha}/\alpha = 1.0$, reduced the magnitude of the perturbations and the analysis approached the analysis of an unperturbed field. Thus, the OVAM filters the high frequency perturbation.

The results of the sensitivity analyses and tests clearly show that the OVAM works well with a well-defined initial distribution of concentration, i.e., when there are good estimates at every point. However, in practice, only a few observations are known in the urban area. To test the technique more realistically, observations ($\tilde{\psi} = \psi^*$) were selected and retained at 20 randomly selected grid points. The weight ratio, $\tilde{\alpha}/\alpha$, at those points was assigned a value of 1.0. "New observations" were obtained at the remaining boundary and interior grid points by interpolation from the retained observations using a $1/R^2$ weight function, e.g.,

$$\tilde{\psi}_{i,j} = \sum \tilde{\psi}_{\ell,m} R^{-2}(i,j,\ell,m) / \sum R^{-2}$$

where

$$R^2 = (i-\ell)^2 + (j-m)^2 \quad (\neq 0)$$

$\tilde{\psi}(\ell,m)$ are the retained values of ψ and the summation is over all retained variables. For these "new" observations $\tilde{\alpha}/\alpha = 0.1$.

In this manner, the solution for ψ is initially estimated, based solely on the observations. Where there are observations, greater weight is accorded than where there are interpolated values. The relaxation coefficient, Ω , changes accordingly at each point of the interior. An analytical test to guarantee a convergent solution with a variable, Ω , was not performed. The experience of Cases I-V suggested that the relaxation would converge to a solution even if $\tilde{\alpha} \rightarrow 0$.

The initial distribution of the "observed" concentrations, $\tilde{\psi}$, and the location of the retained observation is shown in Figure 15. The analytic solution, ψ^* , for the same conditions is shown in Figure 13. Obviously, $\tilde{\psi}$ is a poor representation of ψ^* , especially in the areas near the source. This clearly points out the potential problems of using a straightforward interpolation scheme to obtain concentration estimates in an urban area.

The solution concentration along $y = 5$ is shown with the analytic solution, the initial distribution, and the results obtained in Case II in Figure 16. The solution is an obvious improvement to the observations in

Figure 15. Concentration distribution ($\mu\text{g}/\text{m}^3$) with x as determined using R^{-2} interpolation of randomly selected observations (*) from the distribution of Figure 12.

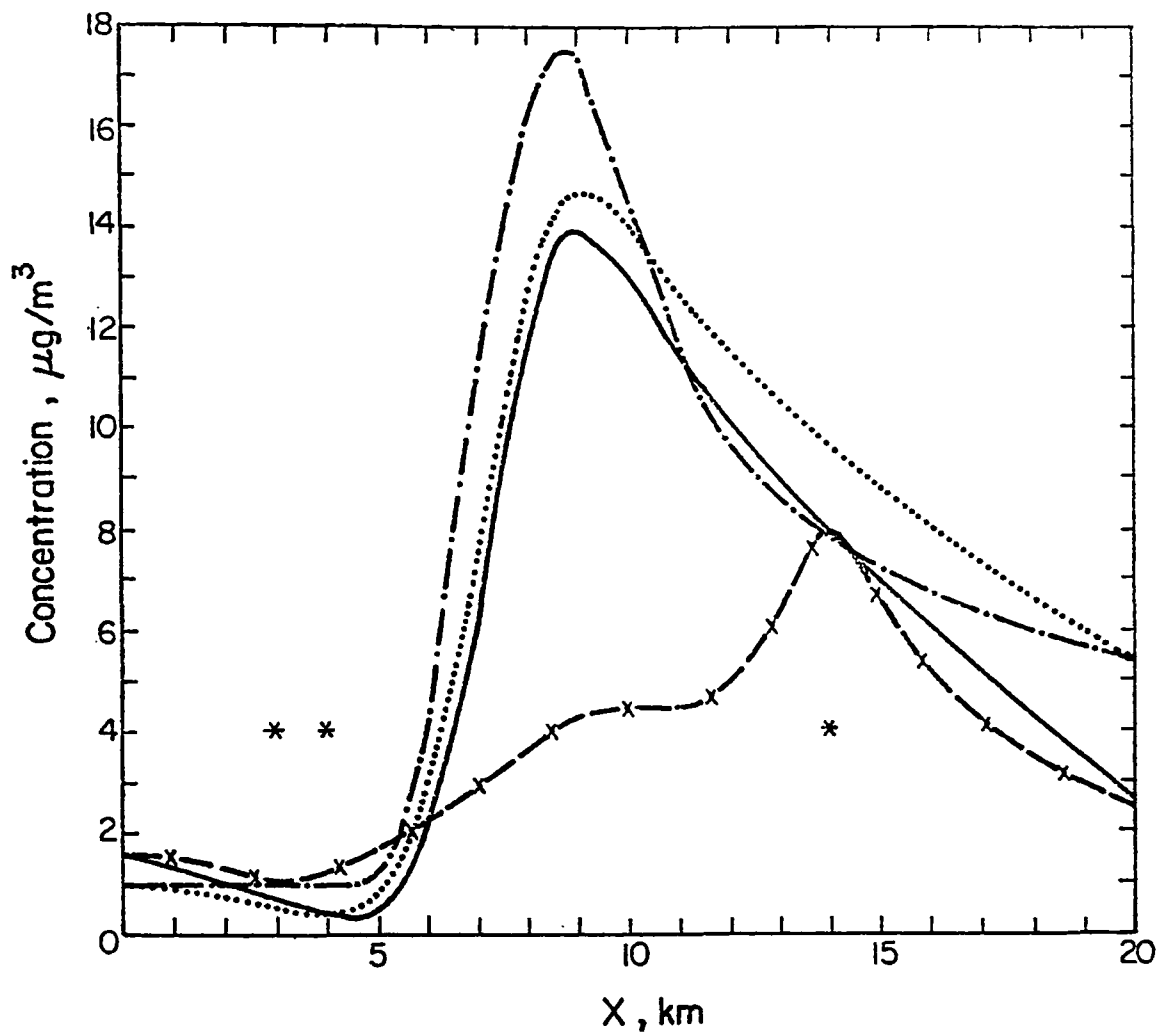


Figure 16. Concentration distribution ($\mu\text{g}/\text{m}^3$) with x for Case VI showing ψ^* (— · —), $\psi(x)$ (— — x), ψ from Case II (····)* along $y = 5$ km. Asterisks (*) indicate locations of observations on the y axis.

the domain. In this case, 3 of the 15 retained observations lie along the $y = 5$ km axis, at $x = 3, 4$ and 14 km. At 14 km, the solution ($8.006 \mu\text{g}/\text{m}^3$) is nearly identical to the observed value ($7.928 \mu\text{g}/\text{m}^3$) and off by about $0.5 \mu\text{g}/\text{m}^3$ at the other two locations. In general, this solution behaves much the same as those cases when $\tilde{\alpha}/\alpha = 0.01$. The different boundary values and the observation at $x = 14$ km seem to anchor the solution, letting the constraint equation fill in the remainder of the distribution.

The expression $p_{i,j} = (\psi_{ij} - \psi^*_{ij})/\psi^*_{ij}$ was used to measure the error of the analysis relative to the analytic solution. The initial error average showed a mean of 0.265 and a standard deviation of 0.743 . The solution had a mean error of 0.169 and standard deviation of 0.450 . The weighted mean square error of the analysis, i.e., the numerical value of the integral, EV, decreased to 10.8 percent of its original value, as shown in Figure 17.

A different set of observations were picked from ψ^* , and the procedures used were used to get new observations. Those data were then perturbed (as in Case V) as a final simulation of a case using field data to give the distribution of Figure 18. The observations, an approximate solution, and the analytic solution are shown in Figure 19.

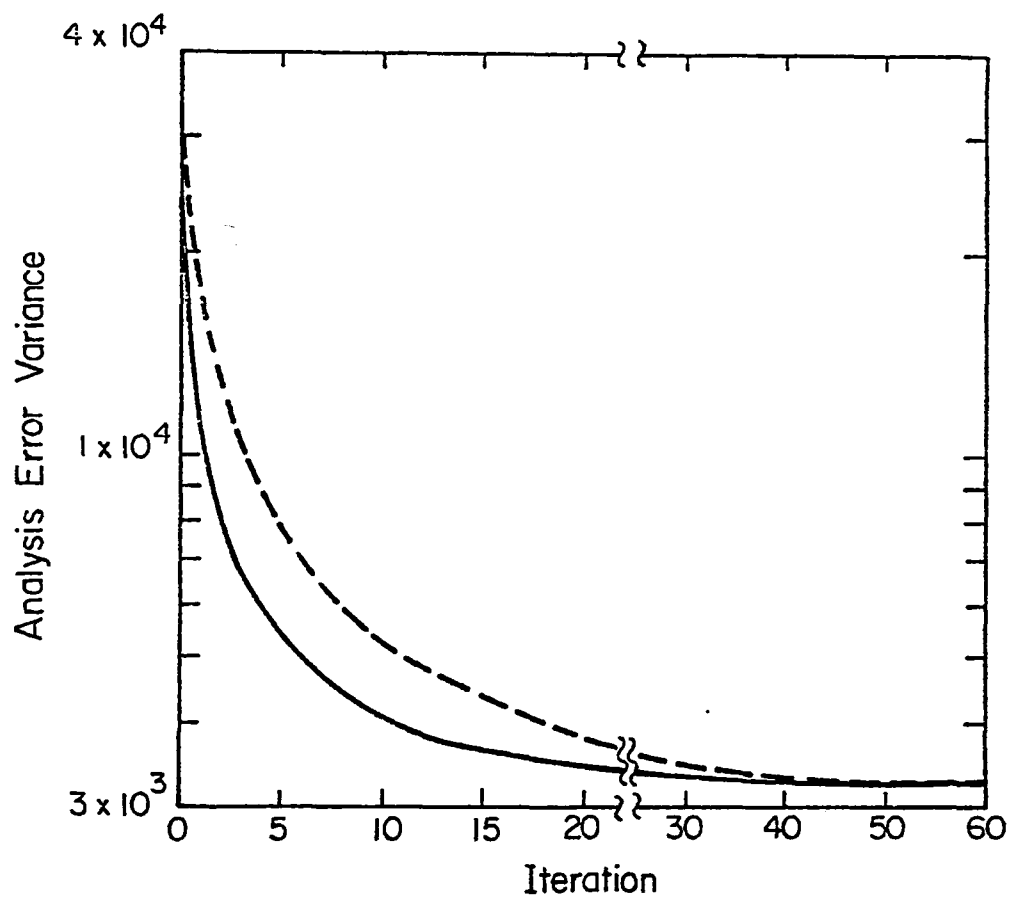


Figure 17. Analysis error variance versus iteration in Case VI (—) and Case VII (---).

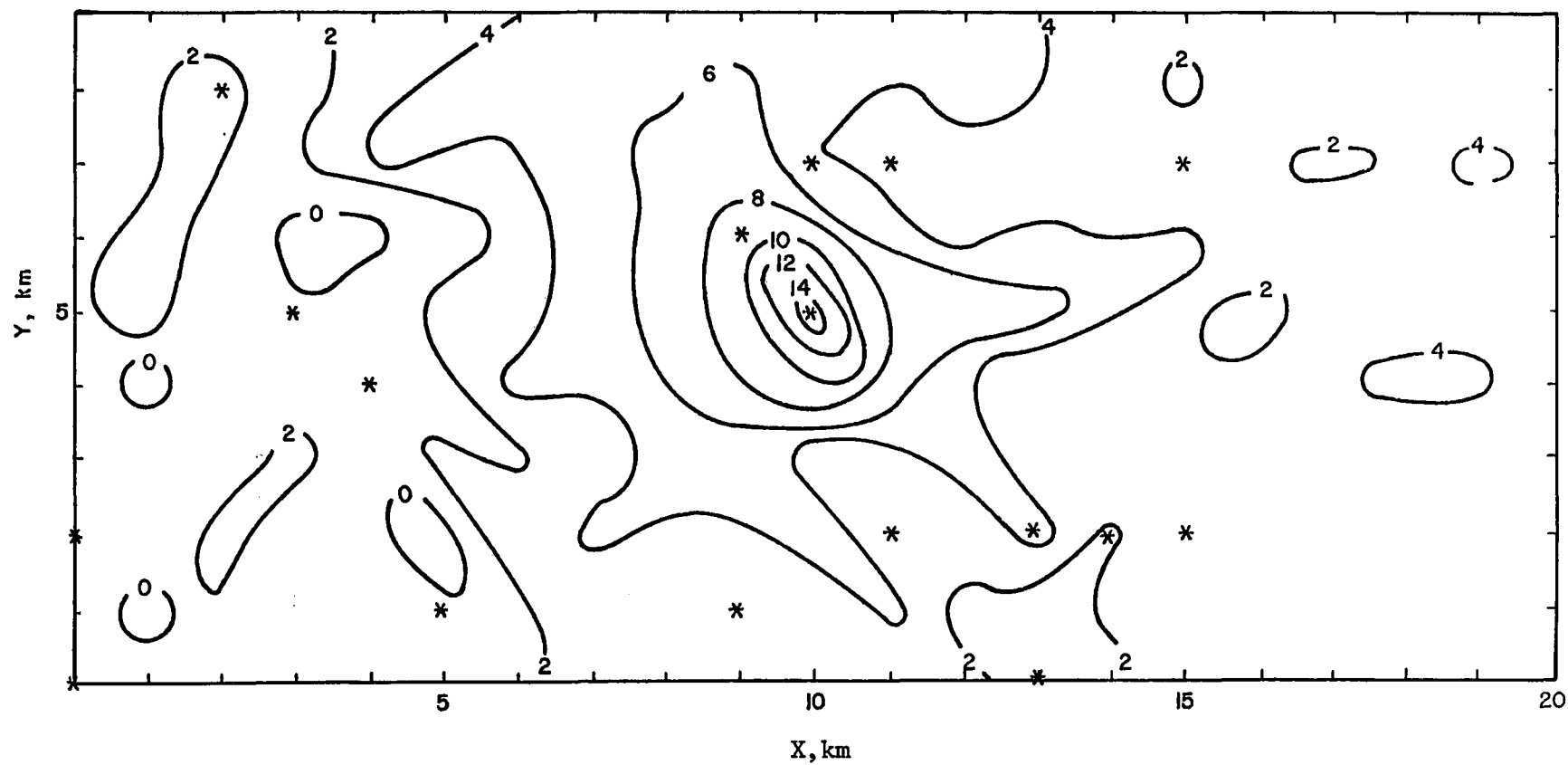


Figure 18. Concentration isopleths ($\mu\text{g}/\text{m}^3$) determined from an R^{-2} interpolation of perturbed observations at randomly selected data points (*) of the distribution of Figure 25.

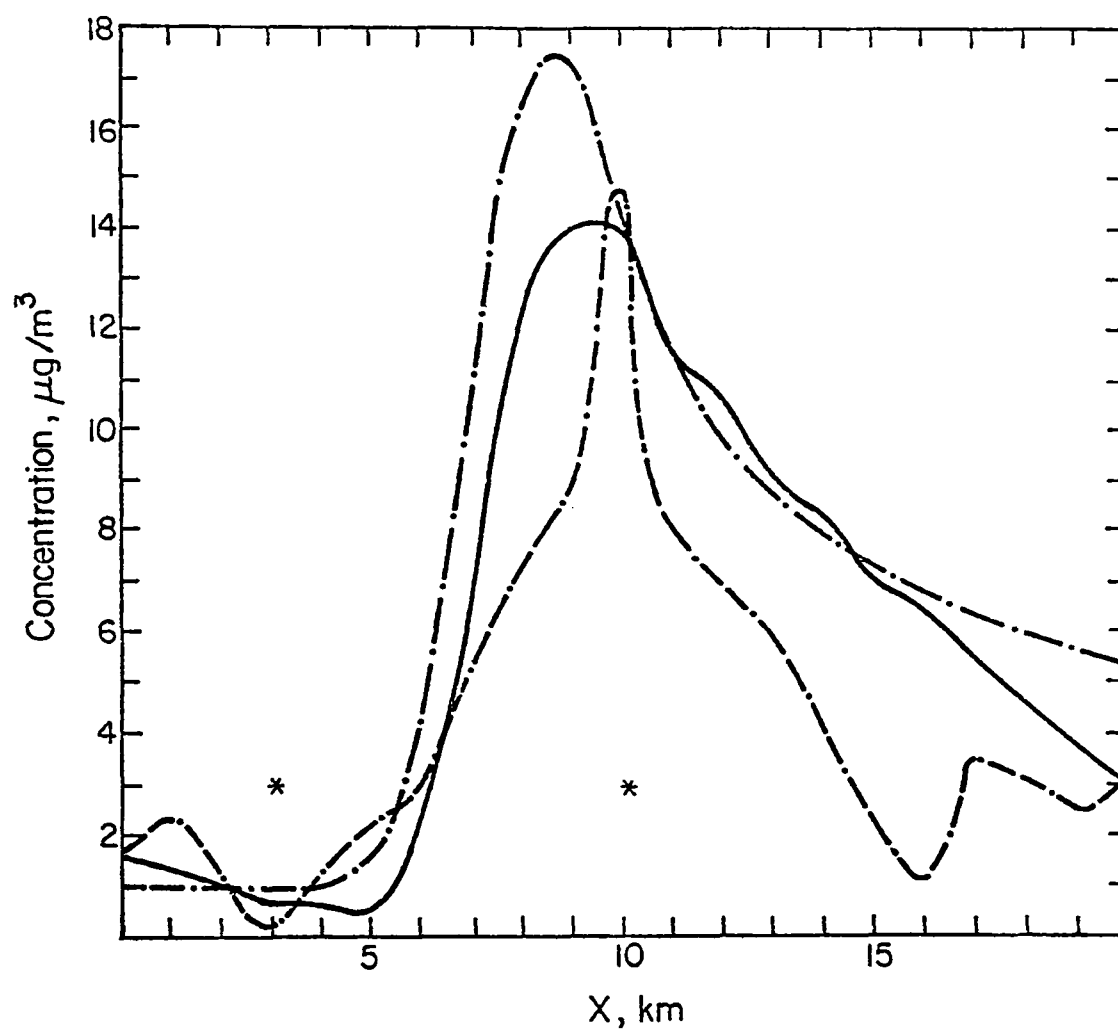


Figure 19. Concentration distributions with x for Case VII showing ψ^* (— · — ·), ψ (— — —) and ψ (—) along $y = 5$ km. Asterisks (*) indicate locations of observations on the $y = 5$ km axis.

4.0 TEST AND EVALUATION

4.1 Operational Optimum Network

It was economically unfeasible for RTI to set up a 19-station network in St. Louis. To reduce the cost of the field program required to validate these results, it was decided to use stations in either the RAPS or city/county air pollution network (see Figure 20) when there was overlap or near overlap. This tractable version of the OSN is designated the OSN*, and the station plot is given in Figure 21. Once again, the numbers next to the stations are used to designate stations which are to be deleted if less than optimum subclasses are desired. The analysis of the OSN* was discussed in Section 3.2.7.

It should be noted that one of the most important aspects of the entire technique was the selection of the regression model to describe the airflow. The 13 term model was selected because 1) the 13-term model was considered the smallest model which would yield reasonably good results, 2) most urban areas could not suffer the economic burden that would be required to establish an OSN using a regression model with many more terms than 13 and 3) models with as many as 10 more terms did not yield an extremely significant improvement over the 13-term model.

The sampling network selection technique can be also applied using models with a smaller number of terms in order to establish an initial network with a small number of stations. This might be done because a certain city may only be able to initially afford R number of stations, but the minimum regression model which gives adequate results may have S number of terms where $S < R$. So, for economic reasons, a regression model with less terms than S must be used. This approach is very limited because a point will be reached rather quickly when, no matter how many stations are added at some later time, the cost of the stations will over-balance the improvement; i.e., a base error exists due to the missing terms in the model which cannot be reduced by improving the estimate of the coefficients in the model (adding stations) but only by adding the required terms. Unfortunately, if the terms are added as the network is enlarged, the OSN obtained from the inadequate model may not be optimum for the improved model.

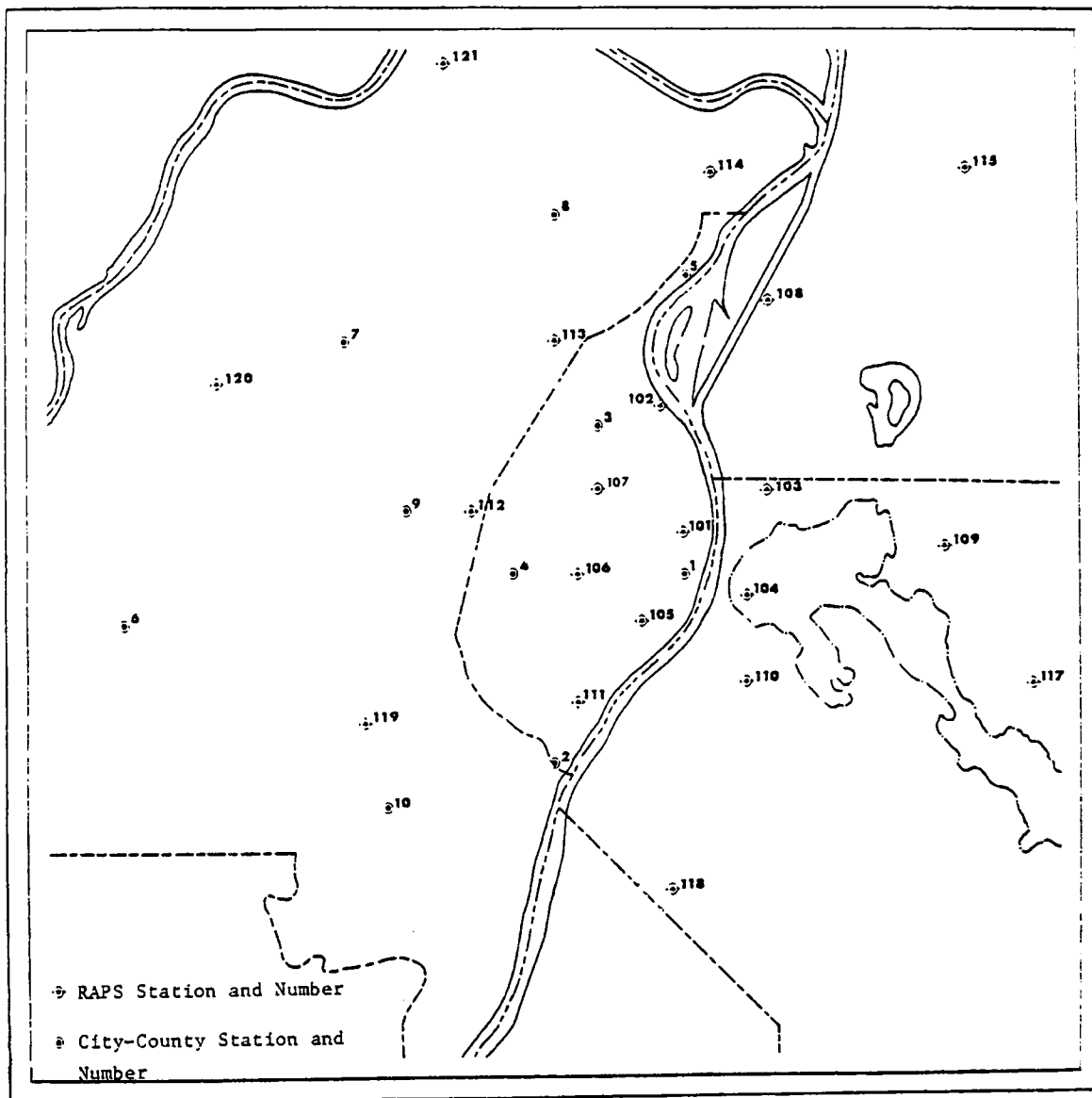


Figure 20. Station array in the RAPS network and in the City/County Network in St. Louis, Missouri.

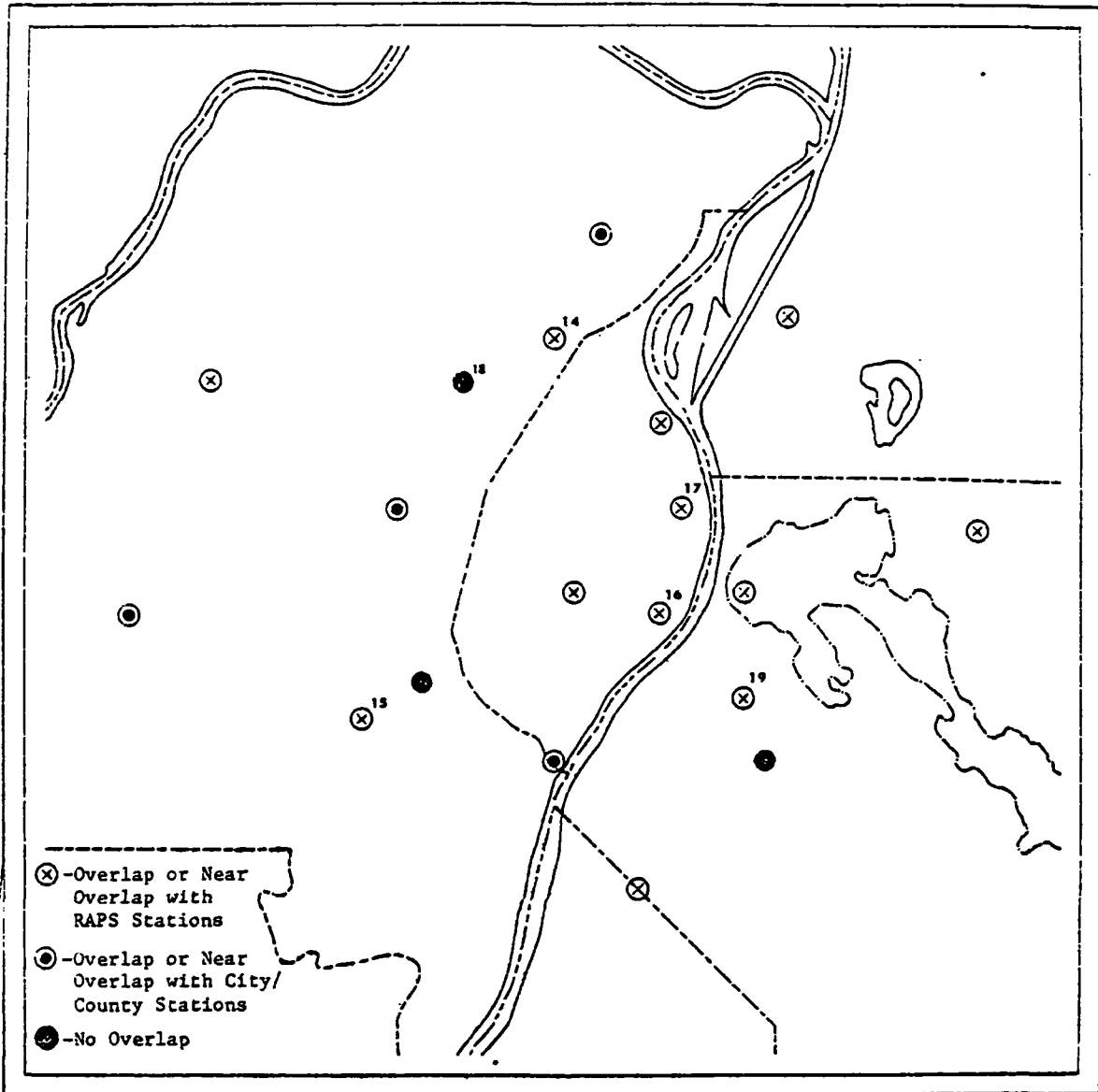


Figure 21. Stations in the OSN* for St. Louis, Missouri.

4.2 Field Programs

The major emphasis of the second phase of this research project involved the preparation and execution of a summer and winter field program in St. Louis. These field programs were held during the period when EPA was performing an intensive study in St. Louis (July and August 1975 and February and March 1976). During this time, there was a concerted effort to maintain a high level of performance of the RAPS stations.

As indicated in Figure 19, three stations did not overlap with either a RAPS station or a city/county air pollution station. It was necessary for RTI to establish its own stations in these locations. Sampling stations were located on the grounds of Incarnate Word Academy in northwest St. Louis county; on the grounds of Kenrick Seminary in southwest St. Louis county; and on the grounds of the East Side Sanitary District's South Pumping Station in East St. Louis, Illinois. Figure 22 shows the location of these stations (the black dots).

The facility on the grounds of Incarnate Word Academy consisted of the RTI Mobile Ambient Air Monitoring Laboratory which is a 31-foot motorized laboratory equipped for ambient air monitoring. A Beckman 6800 was used to measure THC, CH₄ and CO at this and all other locations maintained by RTI. The Beckman 6800 was chosen to conform with the instrumentation in the RAMS stations and, thus, avoids a possible bias due to different instruments. Outputs of the respective instruments were recorded in analog and digital form in the mobile laboratory. An onboard mini-computer provides for real time data processing and display of selected parameters in terms of their 5-minute values as well as computed hourly averages. The facility contains a 10-meter crank-up tower for the wind system. Wind speed and direction was recorded in analog (strip chart recorder) and digital form. The facility was located at the southwest end of the baseball field on the campus of Incarnate Word Academy. There were no obstructions to the wind flow to the north and east for more than a mile. The school complex was located to the west approximately 100 m from the van. To the south was a housing project.

The facilities at both the South Pumping Station and on the grounds of Kenrick Seminary were similar. These consisted of an 8-foot by 7-foot metal house and a 10-m tower. The metal house contained facilities for both

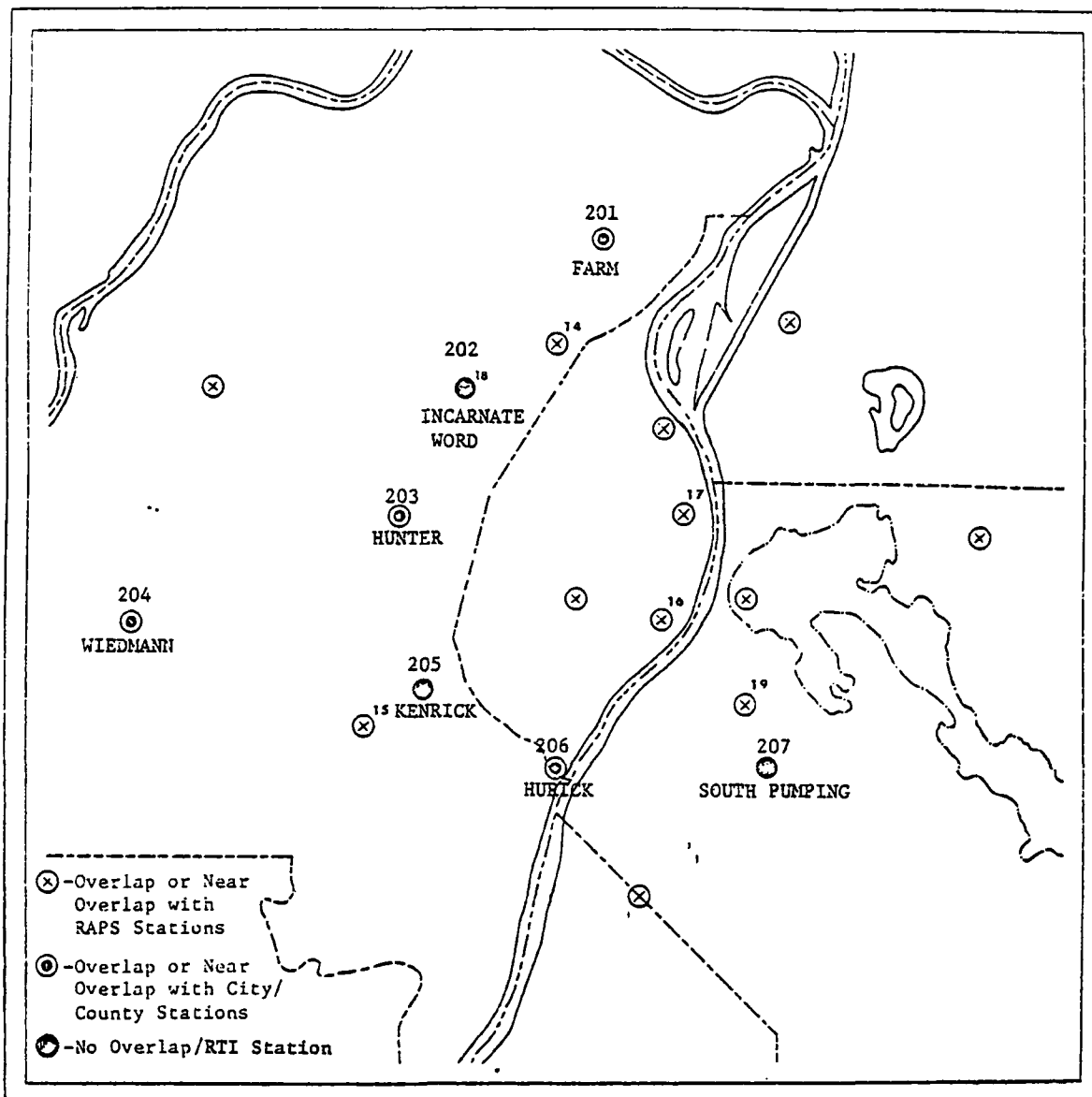


Figure 22. Location, name and number of stations maintained by RTI.

heating and cooling, and housed the Beckman 6800 and the strip chart recorders. The air intake for the Beckman 6800 and the wind system were placed at the 10-m level of the tower.

The facility at Kenrick Seminary was located in a wooded portion of the campus, approximately 100 m southwest of the seminary complex and about 100 m north of the heat plant for the seminary. The South Pumping Station is located in the rural portion of Cohokia, Illinois. The RTI station was located near the top of a flood control levee about 100 m southeast of the pumping station, the only obstruction to the flow in the general area.

Through the cooperation of the St. Louis City/County Air Pollution Agencies, Beckman 6800's were also placed in each of the city/county stations which overlap with the OSN. As in the case of Kenrick Seminary and the South Pumping Station, the data were recorded on strip chart records. Wind data were collected at these stations by systems already on site and maintained by the city/county agencies. The exposures at these stations were generally good.

Dynamic calibration techniques were used to calibrate each Beckman 6800 air quality chromatograph at specific intervals. The Beckman analyzers at each of the seven stations manned by RTI were calibrated every two days. The calibration consisted of a dynamic zero and an upscale calibration at 80 percent of the instrument's range. These instruments were also calibrated by EPA. The calibration data were used to update the transfer equations for converting strip chart readings to physical units.

A dynamic calibration procedure was also used by EPA to calibrate their Beckman 6800's. The EPA Beckman 6800's were calibrated daily to obtain updated transfer equations. Their daily calibration consisted of a dynamic zero and an upscale calibration of the instrument's range. Multi-point calibrations were accomplished weekly.

4.3 Analysis of Data

To date, all data from the winter and summer field programs have been reduced. The analysis described below is in progress. Results of these analyses will be presented in later reports.

- 1) The data from the field programs will be used to estimate wind speeds and directions over the domain of the network by fitting the regression model to data from the OSN*.
- 2) These predicted winds will be statistically compared to actual data from stations not in the OSN*.
- 3) Emissions inventory obtained for St. Louis, the wind distribution obtained using the data from the OSN*, and the air pollution data from the OSN* will be combined with the objective variational analysis model to yield the air pollution distribution over the domain of the network.
- 4) Air pollution concentrations established using the objective variational analysis model will be compared with observed data at locations where air pollution data are available but are not stations of the OSN*.

APPENDIX A

A THEORETICAL STUDY OF THE ST. LOUIS HEAT ISLAND: THE WIND AND TEMPERATURE DISTRIBUTION

Reprinted from the Journal of Applied Meteorology,
Vol. 15, p. 417-440, by permission of the American
Meteorological Society.

A Theoretical Study of the St. Louis Heat Island: The Wind and Temperature Distribution

FRED M. VUKOVICH, J. W. DUNN III AND BOBBY W. CRISSMAN

Research Triangle Institute, Research Triangle Park, N. C. 27709

(Manuscript received 21 July 1975, in revised form 26 January 1976)

ABSTRACT

A three-dimensional primitive equation model was used to study the St. Louis heat island. In this paper, the influence of synoptic wind speed and wind direction on the heat island is presented. With respect to the synoptic wind speed, it was found that the temperature and wind distribution associated with the St. Louis heat island changed markedly as the wind speed increased. When the synoptic wind speed was small, the intensity of the heat island was independent of the wind direction. However, for large synoptic wind speeds, the intensity of the heat island changed, and the change was dependent on the wind direction. These changes were due to the influence of the local topography.

1. Introduction

It has been shown that an urban complex acts as a heat reservoir producing the so-called urban heat island (Landsberg, 1956; Chandler, 1964, 1965, 1967; Woollum, 1964; Lowry, 1967; Mitchell, 1961; Clarke, 1969). Some rather generalized theoretical studies have shown that the urban heat island should create a solenoidal circulation (Delage and Taylor, 1970; Vukovich, 1971, 1973, 1975; Bornstein, 1972); i.e., the differential heating between the urban region and the surrounding suburbs and rural region sets up a mass and thermal contrast which results in the conversion of available potential energy into kinetic energy through convective circulation. These results are generalized because they do not apply to any specific urban heat island. Furthermore, the results treat a two-dimensional heat island, and are therefore limited in application.

This paper gives some of the results of a three-dimensional numerical simulation of the heat island circulation in St. Louis, Mo. The numerical model incorporates the basic forcing functions characterizing St. Louis; i.e., the topography, the building heights, the roughness variations, and the temperature perturbations describing the heat island. St. Louis was chosen for study because the verification of the various models developed in the research program in which these numerical simulations were performed, will be performed using data from the Regional Air Pollution Study (RAPS) which has begun in St. Louis.

2. The model

The basic equations governing the dynamics and thermodynamics for dry convection in the model are

as follows:

$$\frac{\partial u}{\partial t} + u \frac{\partial u}{\partial x} + v \frac{\partial u}{\partial y} + w \frac{\partial u}{\partial z} = -\frac{R\theta}{p} \left(\frac{p}{p_0} \right)^{\kappa} \frac{\partial p}{\partial x} + f_v + A_z \frac{\partial^2 u}{\partial x^2} + A_y \frac{\partial^2 u}{\partial y^2} + A_{xz} \frac{\partial^2 u}{\partial z^2} \quad (1)$$

$$\frac{\partial v}{\partial t} + u \frac{\partial v}{\partial x} + v \frac{\partial v}{\partial y} + w \frac{\partial v}{\partial z} = -\frac{R\theta}{p} \left(\frac{p}{p_0} \right)^{\kappa} \frac{\partial p}{\partial y} - f_u + A_z \frac{\partial^2 v}{\partial x^2} + A_y \frac{\partial^2 v}{\partial y^2} + A_{yz} \frac{\partial^2 v}{\partial z^2} \quad (2)$$

$$\frac{\partial \theta}{\partial t} + u \frac{\partial \theta}{\partial x} + v \frac{\partial \theta}{\partial y} + w \frac{\partial \theta}{\partial z} = A_z \frac{\partial^2 \theta}{\partial x^2} + A_y \frac{\partial^2 \theta}{\partial y^2} + A_{Hz} \frac{\partial^2 \theta}{\partial z^2} \quad (3)$$

$$\rho \frac{\partial w}{\partial z^2} + 2 \frac{\partial \rho}{\partial z} \frac{\partial w}{\partial z} + w \frac{\partial^2 \rho}{\partial z^2} = -\frac{\partial}{\partial z} \left[\frac{\partial(\rho u)}{\partial x} + \frac{\partial(\rho v)}{\partial y} \right] \quad (4)$$

$$\frac{\partial p}{\partial z} = -\frac{p g}{R\theta} \left(\frac{p_0}{p} \right)^{\kappa} \quad (5)$$

The symbols used are the conventional ones used in meteorology. In the above equations, the horizontal diffusion coefficients for momentum and heat were considered identical. The local rate of density change was set to zero ($\partial \rho / \partial t = 0$), an assumption which yielded Eq. (4) for the vertical velocity. The most important approximation used in the model is the hydrostatic assumption through which the pressure field was derived. The use of this assumption was justified since we dealt with a relatively shallow

atmosphere, i.e., the top of the atmosphere is 4.0 km in the model. Furthermore, the vertical accelerations produced by the forcing functions in the urban area are less than $10^{-5} g$ which suggests that the hydrostatic approximation is reasonable in any case.

Perturbation principles were applied to the above equation. In the perturbation analysis, variables designated by the overbar (\bar{p} , for instance) are used to represent the synoptic state which is assumed to be both in geostrophic and hydrostatic equilibrium. Primed variables are used to represent the perturbations produced by the available forcing functions in the city area.

The horizontal dimensions of the grid on which the model is structured are 144 km by 144 km which more than adequately covers the urban and suburban regions of St. Louis. A nested grid is employed in which the central region (20×20 grid points centered over the city) has a grid spacing of 1 km. Outside the central region, the grid spacing increases in both x and y according to the expression, 2^i [km], where $i=1, 2, 3, 4$ until the grid spacing equals 16 km. At this point, the grid spacing is held constant for three more grid points. Fig. 1 shows a portion of the total grid.

In regions where grid spacing is constant, centered difference formulas are used for first- and second-order space derivatives. In the region of changing grid spacing, upstream differencing is employed to give first-order space derivatives, and non-centered differencing is used to determined second-order space derivatives.

At the horizontal boundaries, mass, momentum and heat are allowed to flow out except at the upstream boundary; i.e.,

at $x = -72$ km (upstream boundary)

$$u' = v' = \theta' = p' = 0,$$

at $x = +72$ km (downstream boundary)

$$\frac{\partial u}{\partial x} = \frac{\partial v}{\partial x} = \frac{\partial \theta}{\partial x} = \frac{\partial p}{\partial x} = 0,$$

at $y = \pm 72$ km (lateral boundaries)

$$\frac{\partial u}{\partial y} = \frac{\partial v}{\partial y} = \frac{\partial \theta}{\partial y} = \frac{\partial p}{\partial y} = 0.$$

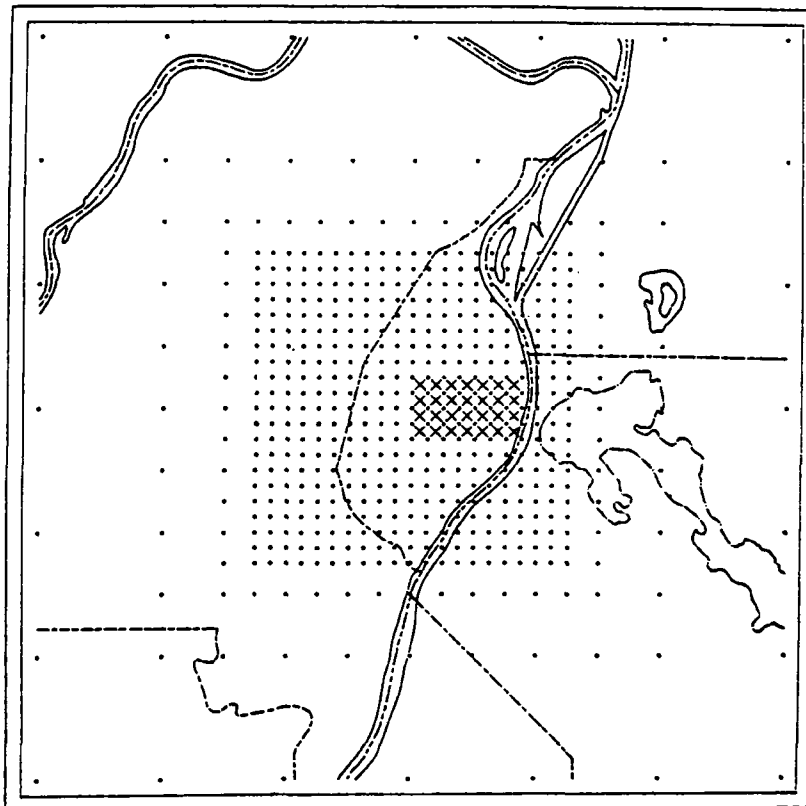


FIG. 1. Horizontal grid. The grid spacing in the center, uniformly spaced area is 1 km. For the first outer set of grid points, the grid spacing is 2 km; for the second outer set, 4 km; and for the third outer set, 8 km. The hatched region indicates the area of increased roughness in the city of St. Louis.

There are eight vertical levels including the lower boundary and the upper boundary. The vertical levels are $z=0, 100, 300, 600, 1000, 1500, 2500$ and 4000 m. These are based on a definition of the $z=0$ plane for the local area. This will be discussed later. Upstream differencing is used exclusively in the vertical. The upper boundary conditions are:

$$\left. \begin{aligned} w' &= v' = u' = \theta' = p' = 0 \\ u &= \bar{u}, \quad p = \bar{p}, \quad \theta = \bar{\theta} \end{aligned} \right\} z = 4 \text{ km.}$$

The lower boundary conditions will be discussed in detail later.

The primary forcing functions in urban areas are heating and local terrain effects. In order to describe the effect of terrain, the topography is parameterized for the model. The average height of the local terrain and the average building heights were computed in areas about each grid point. The building heights were determined from Sanborn Maps, courtesy of the St. Louis City Planning Office. The size of the area depends on the grid spacing; i.e., for a 1 km grid spacing, the area about the grid point is 1 km^2 , and for a 2 km grid spacing, it is 4 km^2 , etc. The minimum averaged terrain height was determined from the set of average values, and this value was subtracted from each terrain height before the average building height was added. The result, after adding in the average building height, is the reference height $H(x, y)$ for the area around each grid square. The $z=0$ plane is defined where $H(x, y)=0$ which was located over the Mississippi River in St. Louis. Fig. 2 gives the distribution of $H(x, y)$ used in the model. At $z=H(x, y)$ and at the side walls of an obstacle that may be higher than the first grid point above $z=0$ where the prediction equations are integrated, the following boundary conditions are used for the wind:

$$u = v = w = 0.$$

If $z^* - H(x, y) < 15$ m, where z^* is the height of the first grid point above H , the prediction equations became unstable for the time increment used in integration. Therefore, values of $H(x, y)$ which did not satisfy this criteria were reduced to $H(x, y) = z^* - 15$. For St. Louis, all values of $H(x, y)$ are less than 100 m; which is the height of the first level above the $z=0$ plane in the model. About six $H(x, y)$ values exceed the stability criteria and were reduced.

In order to characterize the effects of an urban heat island, a field of potential temperature departures, $\delta\theta(x, y)$, defined at $z=H(x, y)$, were used. For St. Louis, this field was obtained from data presented in a Stanford University report (1953) and from available surface weather data for the region. The resultant field of $\delta\theta(x, y)$ determined from these data are average values and are given in Fig. 2. The negative values of $\delta\theta(x, y)$ to the west, north and south

are due to radiational processes in Forest Park, in the combined areas of Bellefontaine Cemetery, Calvary Cemetery and O'Fallon Park, and in Tower Grove Park. The urban heat island represented by the $\delta\theta(x, y)$ values was allowed to develop gradually with time by letting

$$\Delta\theta(x, y) = \delta\theta(x, y) [1 - \exp(-\gamma t)],$$

where γ is the rate constant and for this study is such that $\Delta\theta(x, y) \approx \delta\theta(x, y)$ in 3 h.

The boundary condition for the potential temperature distribution at $z=H(x, y)$ is

$$\theta(x, y, H) = \bar{\theta}(y, 0) + \Delta\theta(x, y).$$

If an obstacle was higher than one or more grid levels, then at $z=H(x, y)$ and at the side walls of the obstacle

$$\theta(x, y, H) = \bar{\theta}(y, H) + \Delta\theta(x, y).$$

The initial synoptic field represented by the overbar was determined as if the terrain were not present.

The heat and momentum fluxes at $z=H(x, y)$ were determined through simultaneous solution of the boundary layer profile equations for the friction velocities u_* and v_* and the scale temperature T^* . These parameters are proportional to the momentum and heat fluxes, respectively, at the surface. The profile equations used were

$$\begin{aligned} u &= \frac{u_*}{k} \left[\ln \left(\frac{z-H}{z_0} \right) + \frac{\alpha T^* k [g(z-H)]^{1/4}}{\theta U^*} \right], \\ v &= \frac{v_*}{k} \left[\ln \left(\frac{z-H}{z_0} \right) + \frac{\alpha T^* k [g(z-H)]^{1/4}}{\theta U^*} \right], \\ \theta &= \theta(H) + \frac{T^*}{k} \left[\ln \left(\frac{z-H}{z_0} \right) + \frac{\alpha T^* k [g(z-H)]^{1/4}}{\theta U^*} \right], \end{aligned}$$

where $U^* = (u_*^2 + v_*^2)^{1/2}$ and $\alpha = 18$.

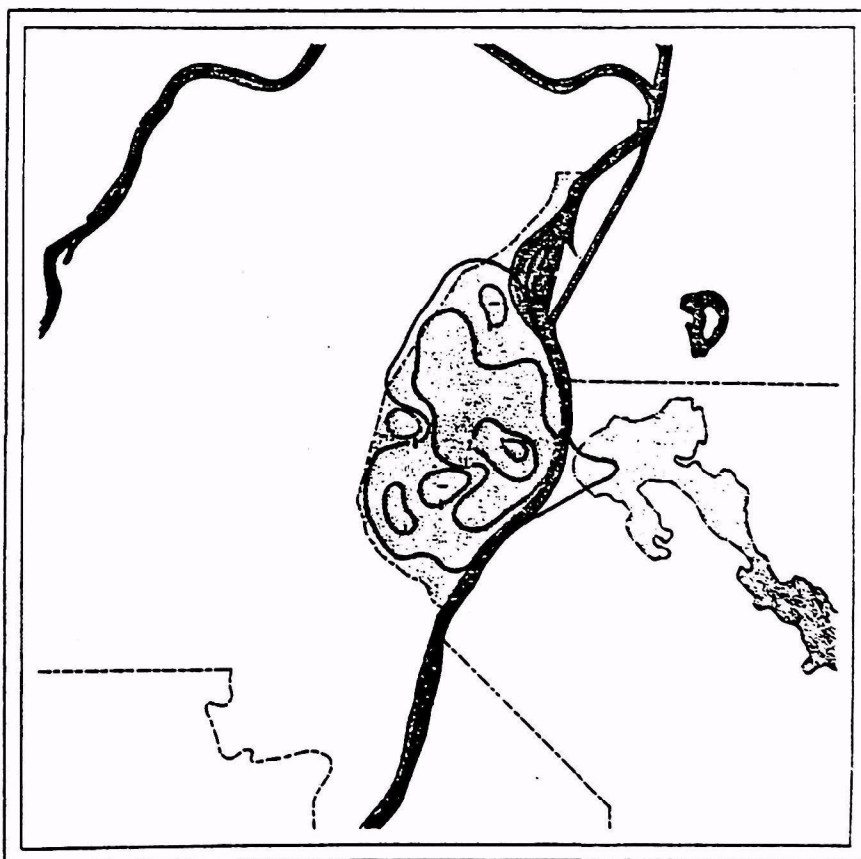
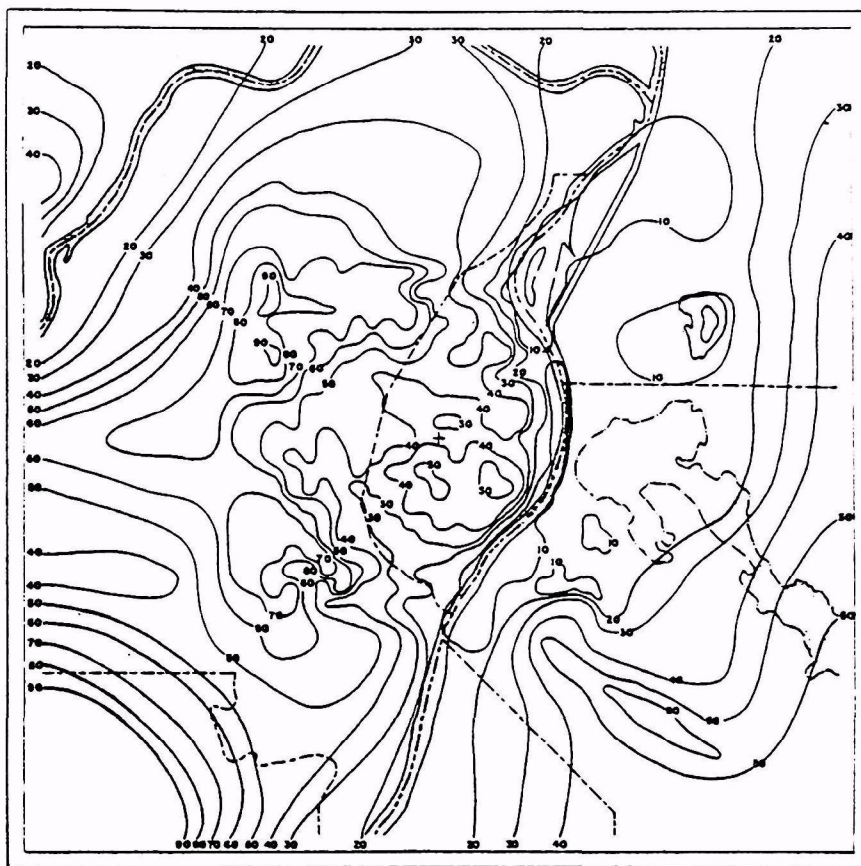
The roughness length z_0 was allowed to vary in the following manner. In regions outside the city

$$z_0 = 0.0015 H(x, y).$$

Using the above expressions and for the given values of $H(x, y)$ in the St. Louis area other than in the built-up sections, $1 \text{ cm} \leq z_0 \leq 13 \text{ cm}$. In the built-up sections

$$z_0 = 0.02 H(x, y),$$

which yielded values of z_0 as large as 1 m. This technique is an adaptation of one suggested by Lettau (1969). In the model only one major built-up section was designated. This region was bounded by Forest Park to the west, the Mississippi River to the east, approximately St. Louis Avenue to the north, and Russell Avenue to the south (see shaded area, Fig. 1).



The formulas for the vertical eddy diffusion coefficients are

$$\left. \begin{aligned} A_{zz} &= l^2 \left| \frac{du}{dz} \right| \\ A_{yz} &= l^2 \left| \frac{dv}{dz} \right| \\ A_{Hx} &= l_H^2 \left| \frac{dV}{dz} \right| \end{aligned} \right\},$$

where $V^2 = u^2 + v^2$. The mixing lengths are given by

$$\left. \begin{aligned} l &= k(z-H)(1-\alpha_1 \text{Ri})^{\frac{1}{2}} \\ l_H &= l(1-\alpha_1 \text{Ri})^{\frac{1}{2}} \end{aligned} \right\} \frac{\partial \theta}{\partial z} \leq 0,$$

$$\left. \begin{aligned} l &= k(z-H)(1+\alpha_2 \text{Ri})^{-\frac{1}{2}} \\ l_H &= l(1+\alpha_2 \text{Ri})^{-\frac{1}{2}} \end{aligned} \right\} \frac{\partial \theta}{\partial z} > 0,$$

where $\alpha_1 = 18$, $\alpha_2 = 11$, and Ri is the Richardson number.

Since the magnitude of diffusion brought about by subgrid-scale motion is dependent, among other things, on eddy size, and since larger grid spacings incorporate larger subgrid-scale eddies, the horizontal diffusion coefficients are directly proportional to the square root of the local mean grid spacing. The constant of proportionality depends mainly on the boundary layer stability.

The initial wind field is assumed to have a wind direction parallel to the x axis and a speed which varies in z alone. The initial potential temperature distribution is given at $x = -72$ km and $y = -72$ km. Since the synoptic state (initial conditions) was assumed in geostrophic and hydrostatic equilibrium, the necessary initial pressure and potential temperature fields were derived through integration of the geostrophic and hydrostatic equations.

The initial conditions are represented by two categories of stability and five different wind profiles. Fig. 3 shows the vertical distribution of potential temperature. Profile 1 describes an atmosphere with a shallow, near-isothermal layer from the surface to the 100 m level. Above the 100 m level, the atmosphere is stable with a lapse rate equivalent to the Standard Atmosphere lapse rate. Profile 2 describes an atmosphere in which the first 600 m has an adia-

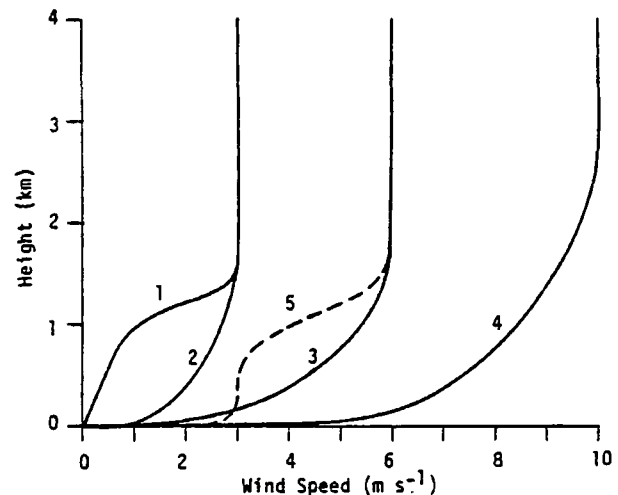
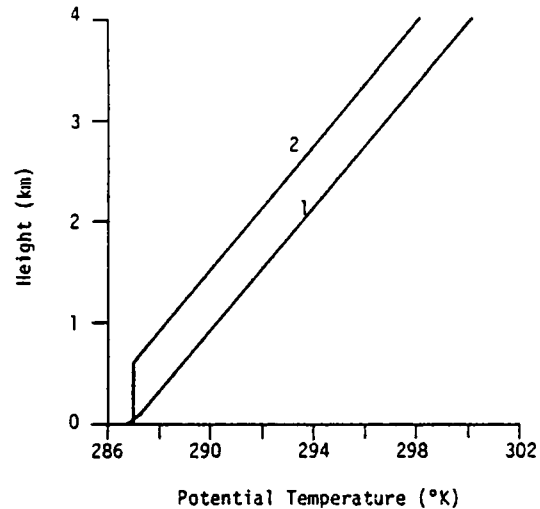


FIG. 3. The vertical distributions of the initial potential temperature (upper) and the initial wind speed (lower) used to integrate the equations of motion.

batic lapse rate. Above 600 m, the lapse rate is again equivalent to the Standard Atmosphere lapse rate. Profile 1 may be considered an evening sounding and Profile 2 a noon sounding.

The initial wind profiles used are also shown in Fig. 3. Since the urban heat island normally develops in the late afternoon and is most intense in the evening when the boundary layer is stable, the results to be presented here will employ the potential temperature Profile 1 combined with wind Profiles 1-4. In a future paper, the influence of an adiabatic boundary layer

FIG. 2. Upper: The distribution of topography heights (m) above the $z=0$ plane in the St. Louis region. The values of topography include both natural topography and area-averaged building heights.

Lower: The distribution of surface temperature ($^{\circ}\text{C}$) used to generate the urban heat island in St. Louis.

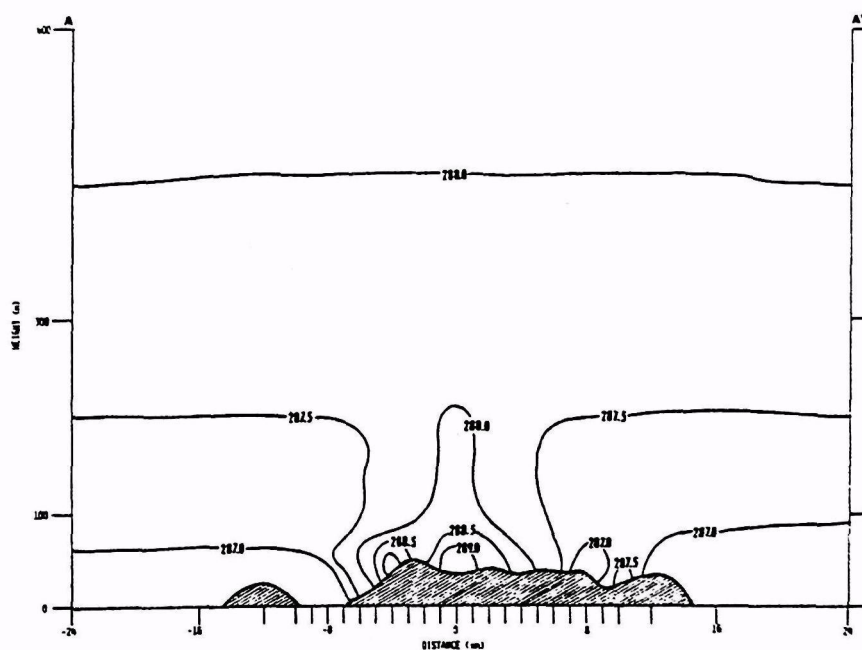
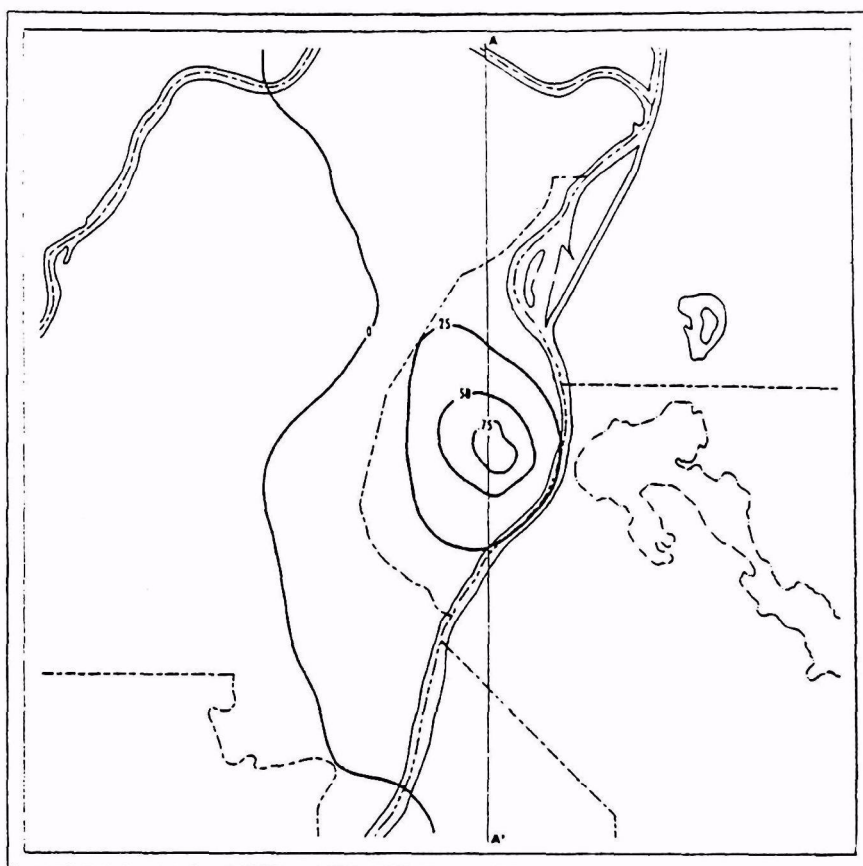


FIG. 4. Upper: The horizontal distribution of the quasi-steady-state, perturbation potential temperature (K) at the 100 m level for the northwind case. The initial conditions were $P(1,1)$.

Lower: The vertical cross section of potential temperature (K) along the line AA'.

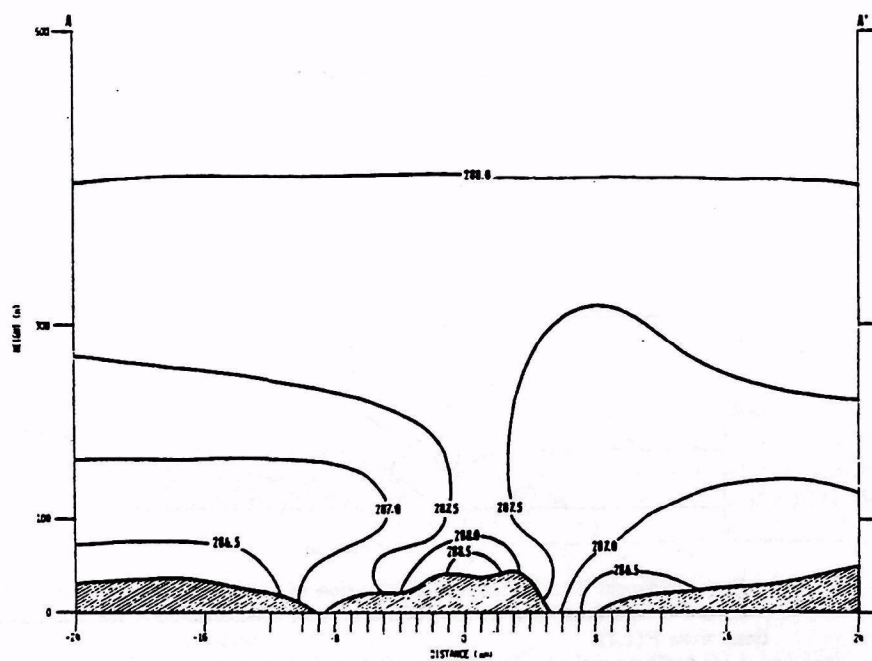
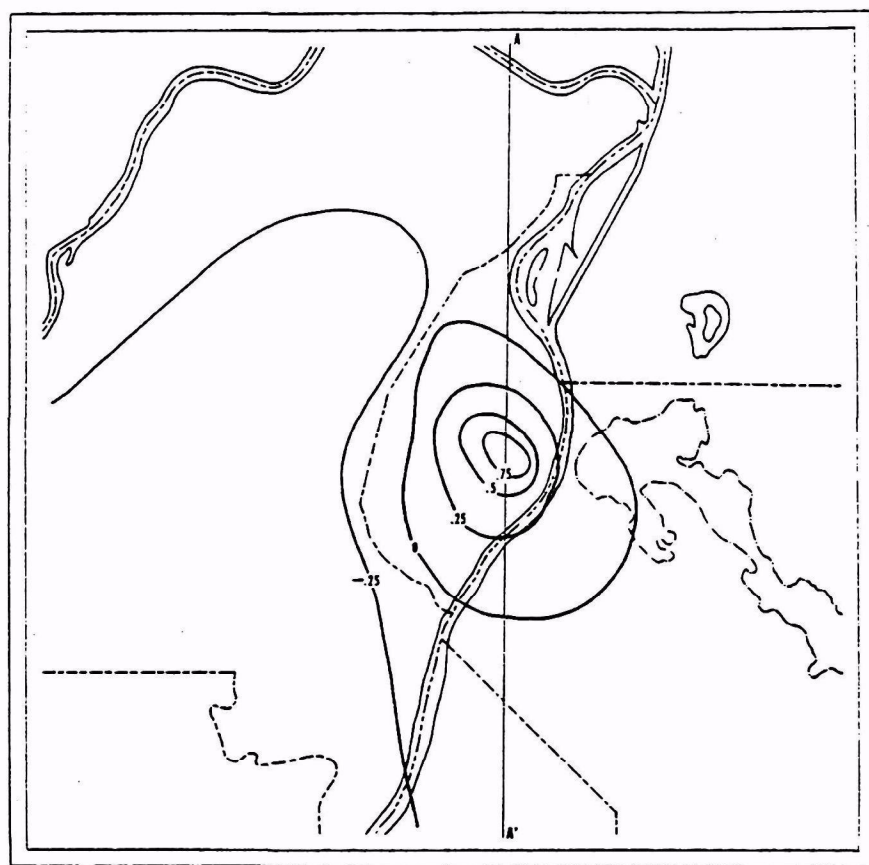


FIG. 5. As in Fig. 4 except for initial conditions $P(2,1)$.

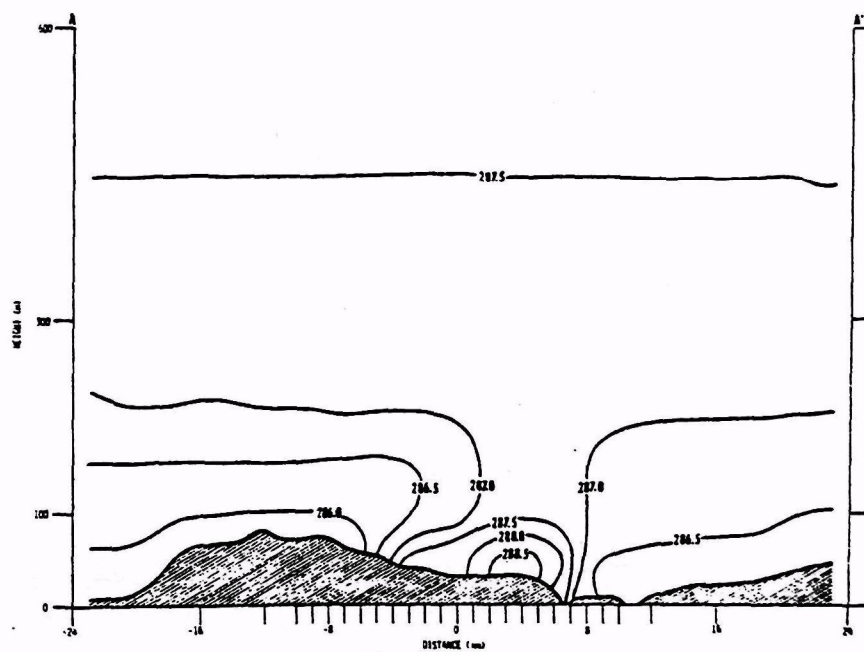
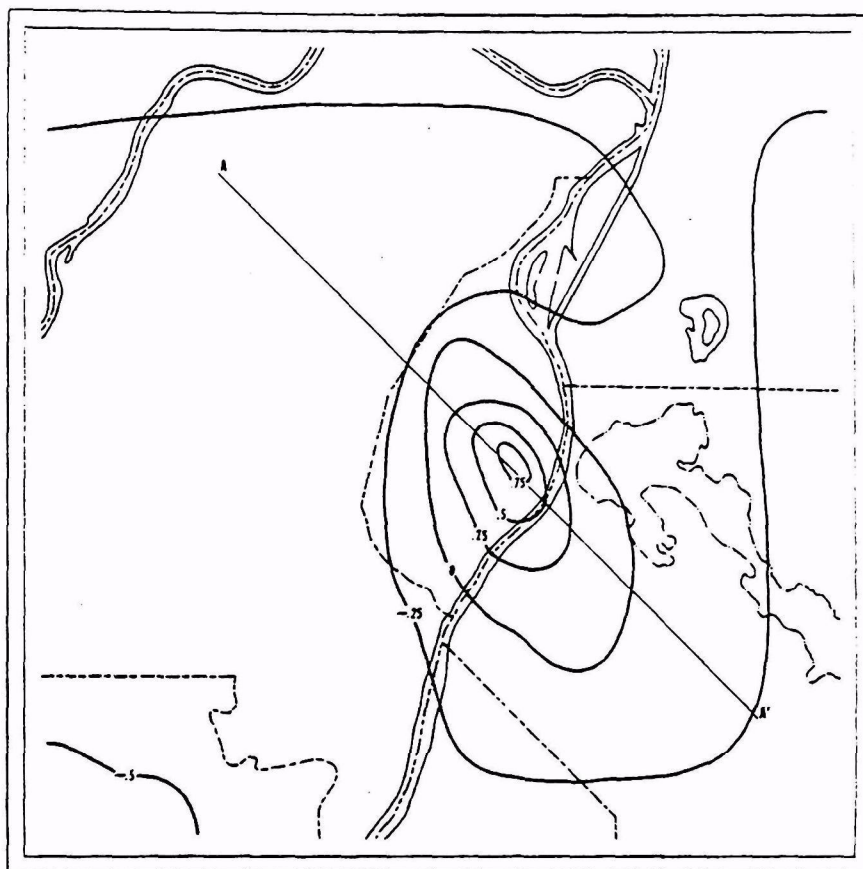


FIG. 6. As in Fig. 4 except for initial conditions $P(3,1)$.

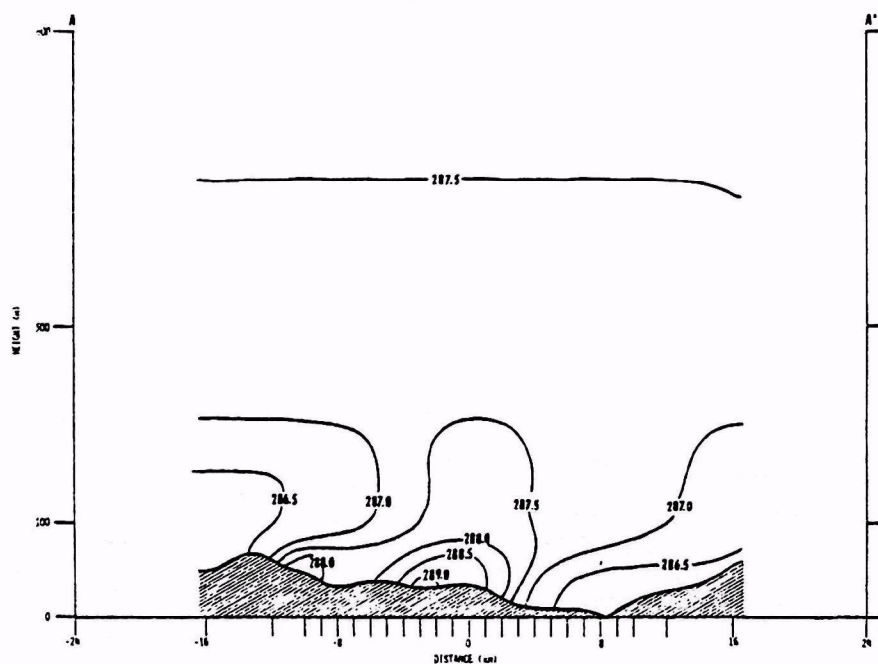
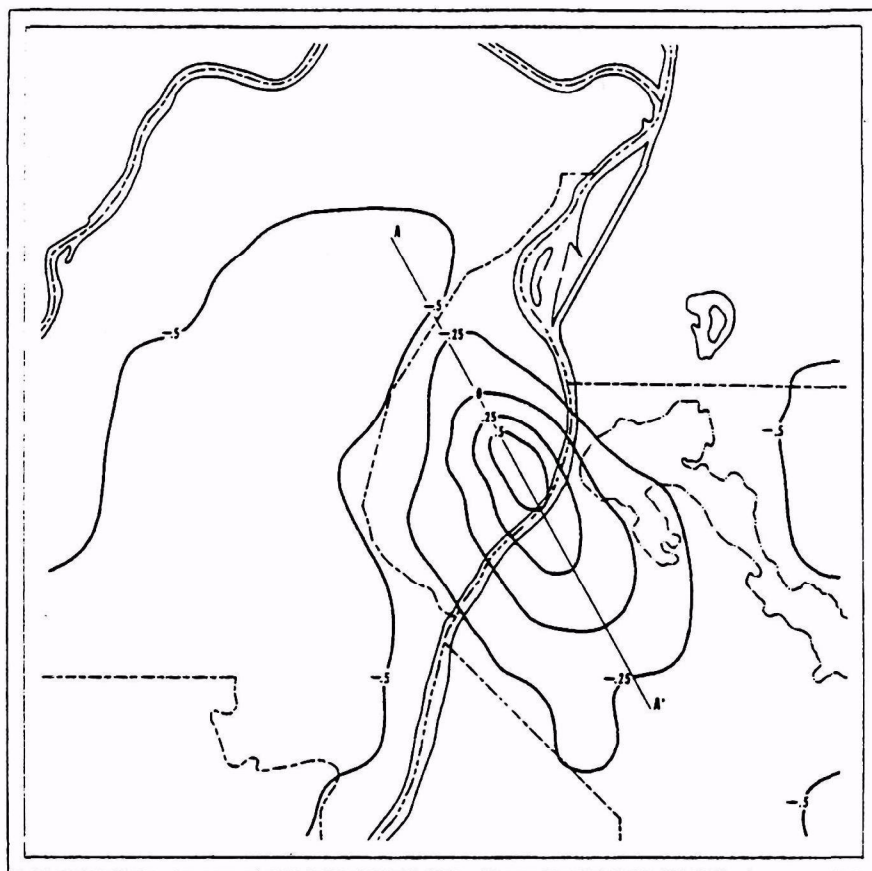
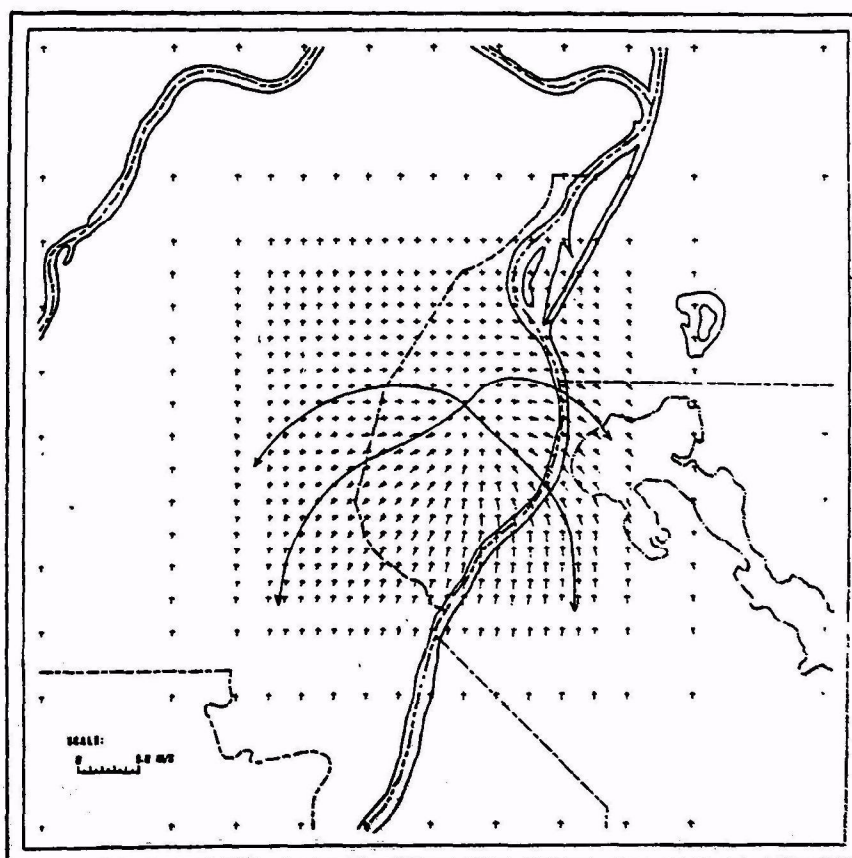
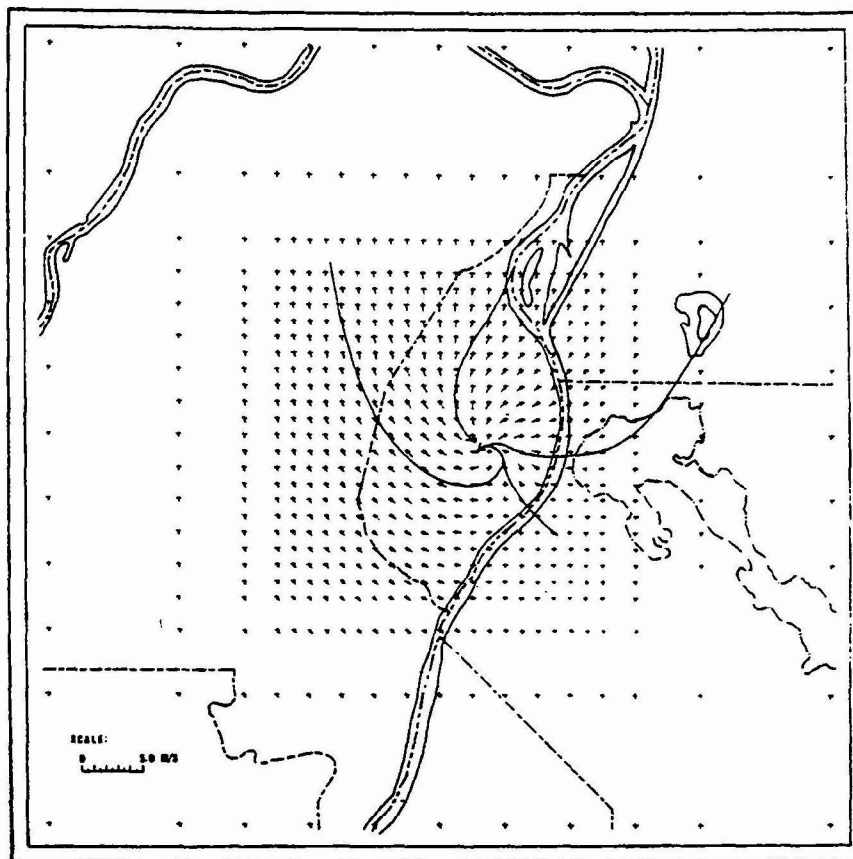


FIG. 7. As in Fig. 4 except for initial conditions P(4,1).



will be presented. In the text, the notation $P(2,1)$ will be used to specify the initial wind and temperature profiles, i.e., wind Profile 2 and potential temperature Profile 1 in this example.

In order to study flow in the city for various wind directions, the $H(x,y)$ and $\delta\theta(x,y)$ fields which define the city area were rotated to effectively yield a new angle for the wind. Eight wind directions were used, representing an eight-point compass rose. For the time integration, forward time differencing was combined with the leapfrog method to control the divergence of the solution at even and odd time steps. For the purposes of this paper, the quasi-steady-state solution will be presented. In future papers, the time evolution of the heat island circulation will be presented. Steady state was achieved in 5 h or more. This varies some from case to case.

3. The thermal distribution

The following describes the results of integrating the equations of motion using the initial conditions $P(1,1)$ through $P(4,1)$; i.e., the boundary layer was stable from case to case, and only the wind speed and shear changed. The initial (geostrophic) wind direction is from the north in the initial cases. However, later in this section, the influence of wind direction will be discussed. The horizontal diffusion coefficients are of the order $10^3 \text{ m}^2 \text{ s}^{-1}$ in each case.

Fig. 4 shows the perturbation potential temperature distribution at the 100 m level associated with the St. Louis heat island for initial conditions $P(1,1)$. The temperature perturbation is concentrated in the city limits since there is little thermal advection. The central temperature perturbation is 0.92 K. Fig. 4 also shows the vertical distribution of potential temperature along the line AA'. Potential temperature data were acquired at grid points nearest to the line. The heat island is depicted as a region having an unstable boundary layer surrounded by a stable boundary layer in the suburbs and rural regions. The top of the heat island is found over the center of the city. In this case, it has been determined from detailed analysis that the top of the heat island is slightly higher than the 300 m level. The higher penetration of the heating in the center of the city is thought to be a combined effect of increased roughness and the larger $\delta\theta$ values.

For initial conditions $P(2,1)$, the thermal plume at 100 m (Fig. 5) is oriented north-northwest and south-southeast, and extends about 10 km southeast of the center of St. Louis, due to the increased thermal advection. It is believed, however, that the actual

downstream extent of the heat plume in this case and in the preceding case should be greater since advection is hampered by the dampening produced both by using upstream differencing and by expanding the grid. The central perturbation temperature in this case is 0.85 K, a decrease of 0.07 K from the previous case. The vertical cross section (Fig. 5, lower) along AA' shows that the layer between the 100 and 300 m levels is less stable downstream of the heat island than upstream. This is due to the thermal advection and is identical to the effect described by Clarke (1969) in the Cincinnati boundary layer. Strong stability developed near the surface immediately downstream of the heat island due to the upper level heat transport. The maximum vertical extent of the heat island (~ 300 m) was located in the central regions of the city where there was increased roughness and large values of $\delta\theta$.

As the initial wind speed and shear is increased further, the heat plume from the St. Louis island is displaced further downstream [Fig. 6 gives the results for $P(3,1)$]. The displacement is about 15 km. The maximum positive temperature perturbation is 0.83 K, which is about a 0.02 K decrease from the previous case [$P(2,1)$]. The vertical cross section along AA' again demonstrates that the stability in the layer between 100 and 300 m is stronger upwind of the heat island than downwind. The strong near-surface stability found in the previous analysis downwind of the heat island and produced by the upper level heat transport is not present in this analysis. This may be a result of the orientation of the cross section used. The top of the heat island is at about the 250 m level.

In the case when initial conditions $P(4,1)$ are used, the heat plume is displaced 22 km downwind of the center of St. Louis (Fig. 7). The maximum positive temperature perturbation in this case is 0.80 K. The general decline of the temperature perturbation from case to case is directly related to the increased wind speed and shear (Vukovich, 1975). The vertical cross section indicates weaker stability downstream of the heat island between 100 and 300 m as before. A strong near-surface stable layer, produced by the upper level advection of heat, extends 10 km downstream from the outer fringes of the city. The top of the heat island is at approximately the 200 m level. It is suggested that the decrease in the vertical extent of the heat island from case to case is due to the increase in wind speed. In general, the top of the heat island found using this model agrees well with that determined using the data given in the Stanford University report (1953).

FIG. 8. Upper: The horizontal distribution of the quasi-steady-state horizontal wind vector at the 100 m level for the north wind case. The initial conditions were $P(1,1)$. Lower: The horizontal distribution of the quasi-steady-state wind vector at the 300-m level for the north wind case. The initial conditions were $P(1,1)$.

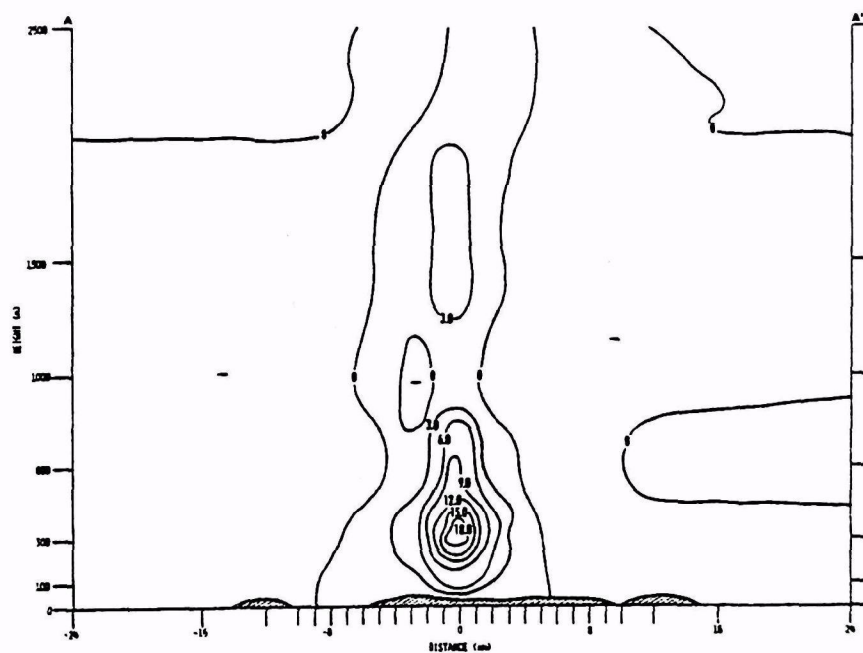
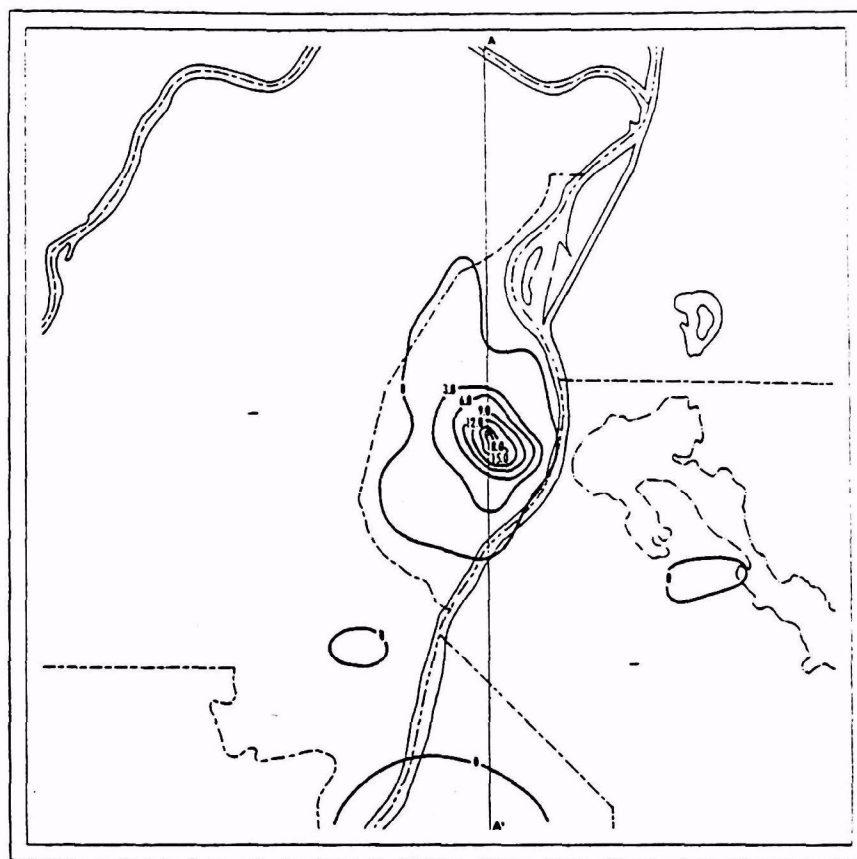


FIG. 9. Upper: The horizontal distribution of the vertical velocity (cm s^{-1}) at the 300 m level for the north wind case. The initial conditions were P(1,1). Positive values indicate upward vertical motions.

Lower: The vertical cross section of vertical velocity (cm s^{-1}) along line AA'. Positive values indicate upward vertical motions.

Changes in wind direction have little effect on the development of the heat island when initial conditions P(1,1) or P(2,1) are used, i.e., the heat island is confined mainly to the city limits with only slight downwind displacement. When the wind speeds increase, as in initial conditions P(3,1) and P(4,1), the downwind transport of the heat plume and other factors describing the thermal distribution are generally the same for the other wind directions with the exception of (geostrophic) winds from the east and southeast. In those cases, the maximum positive temperature perturbation was smaller (~ 0.60 K), and the heat plume was displaced downstream ~ 6 km less than for the other cases. The downwind region between the 100 and 300 m levels of relatively less stable air than the upwind region did not extend as far downstream in this case as in the other cases. The downwind stability in that layer became equivalent to the upwind stability about 12 km from the heat island center. The top of the heat island was at the 250 m level. The differences were attributed to the combined effects of increased friction and adiabatic cooling produced by flow over the hills west of the city. The topography also affected the wind field. This will be discussed in the next section.

4. Wind distribution

The cases demonstrating the wind distribution associated with the St. Louis heat island circulation will show the results of integrating the equations of motion for the same initial conditions used for the thermal distribution when just the effect of wind shear and speed are of interest. Fig. 8 shows the distribution of the horizontal wind velocity at the 100 m level for the initial conditions P(1,1). Various streamlines are drawn in the figure to help in the analysis of the flow. Due to the weak initial wind field, a rather pronounced zone of convergence and strong cyclonic curvature in the flow are established in the central region of the city. The strongest winds are found upwind (north) of the city's central region and are a result of relatively large pressure gradient accelerations. The weakest winds are found southeast of the city's center and, for the most part, are a result of pressure gradient accelerations opposite to the direction of the synoptic flow. The 300 m level is characterized by divergence (Fig. 8, lower). The strongest winds at this level are found downwind (south) of the city whereas the weakest winds are north of the city. The horizontal distribution of the vertical velocity at the 300 m level (Fig. 9) shows

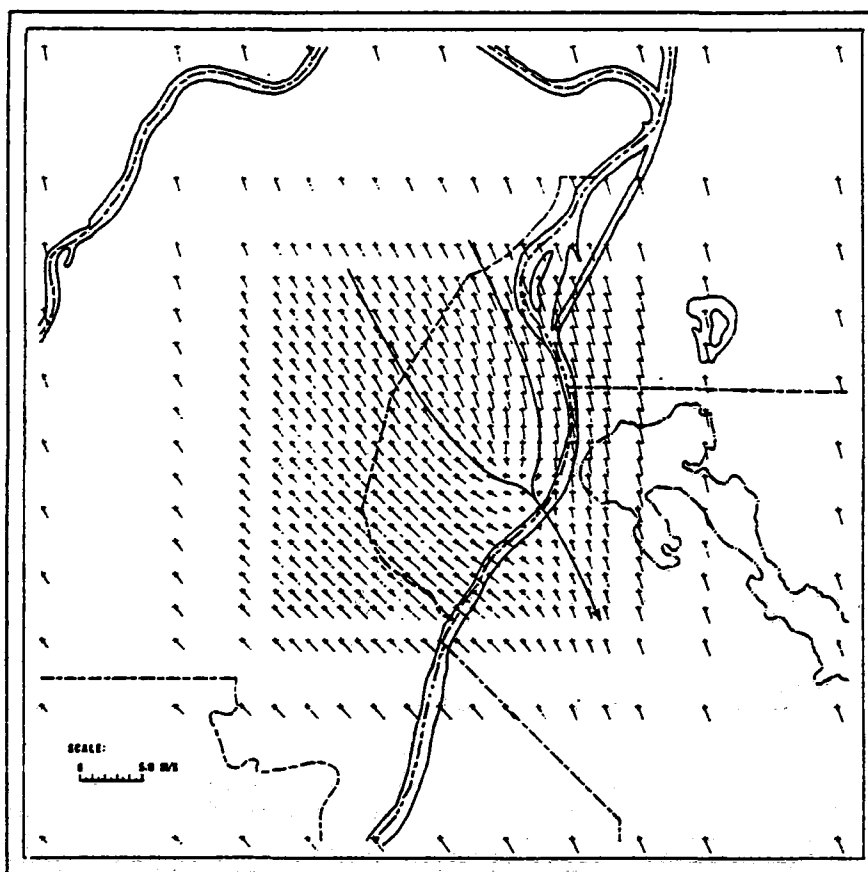


FIG. 10a. As in Fig. 8 (upper) except for initial conditions P(2,1).

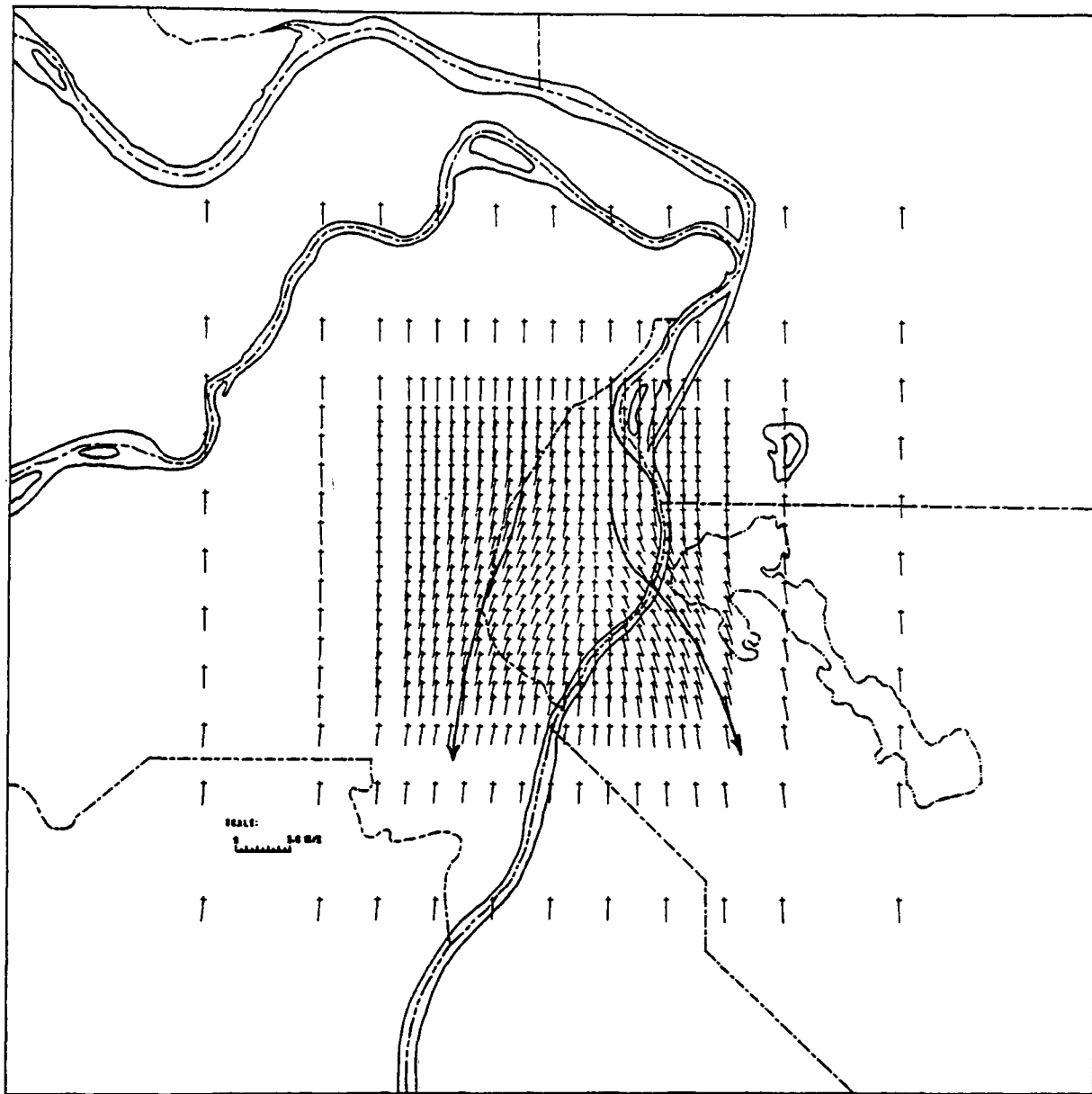


FIG. 10b. As in Fig. 8 (lower) except for initial conditions P(2,1).

a concentrated region of upward vertical motion over the city's central region. The maximum upward velocity is 19 cm s^{-1} . The vertical cross section of the vertical velocity along line AA' (also shown in Fig. 9) suggests that the upper boundary of the St. Louis heat island circulation in this case is at about the 1 km level (where the vertical velocity is zero).

The horizontal wind field at the 100 m level for initial conditions P(2,1) given in Fig. 10a shows a zone of convergence in the central regions of the city, but the strong cyclonic curvature in the flow, obvious in the previous case, is not prevalent in this case. The strongest winds are again found upwind

(north) of the city, but the weakest winds are located in the center of the city. The relative difference in wind speed upstream and downstream is again due to pressure gradient accelerations. The pressure gradient acceleration opposes the increased frictional effect in the urban boundary layer due to the thermal instability, and apparently dominates the flow. At the 300 m level (Fig. 10b) divergence prevails, but there is no obvious difference between upstream and downstream wind speeds. The initial wind speeds in this particular case are similar to those observed by Ackerman (1972) in a case study of flow over St. Louis at night; however, the wind direction was from

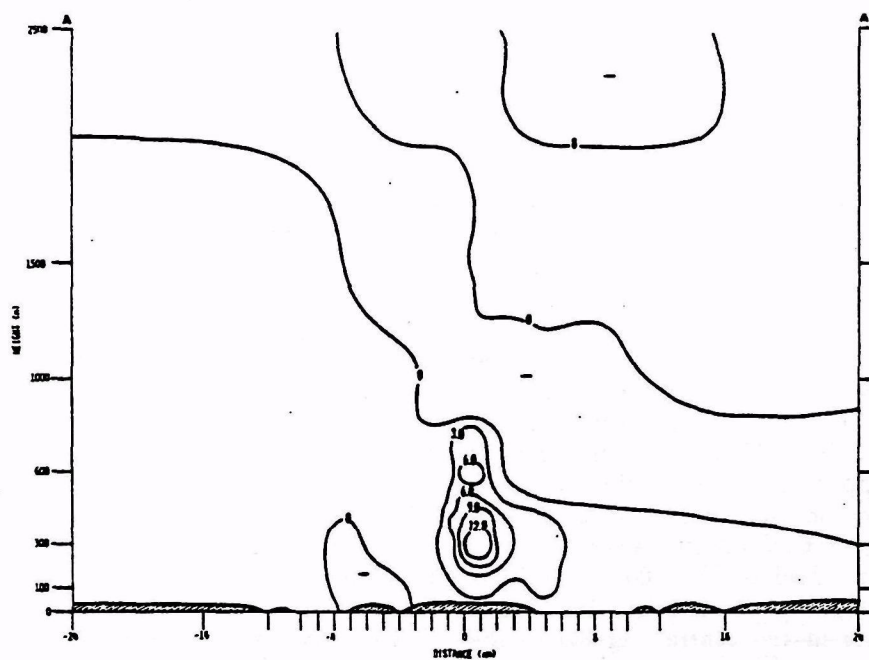
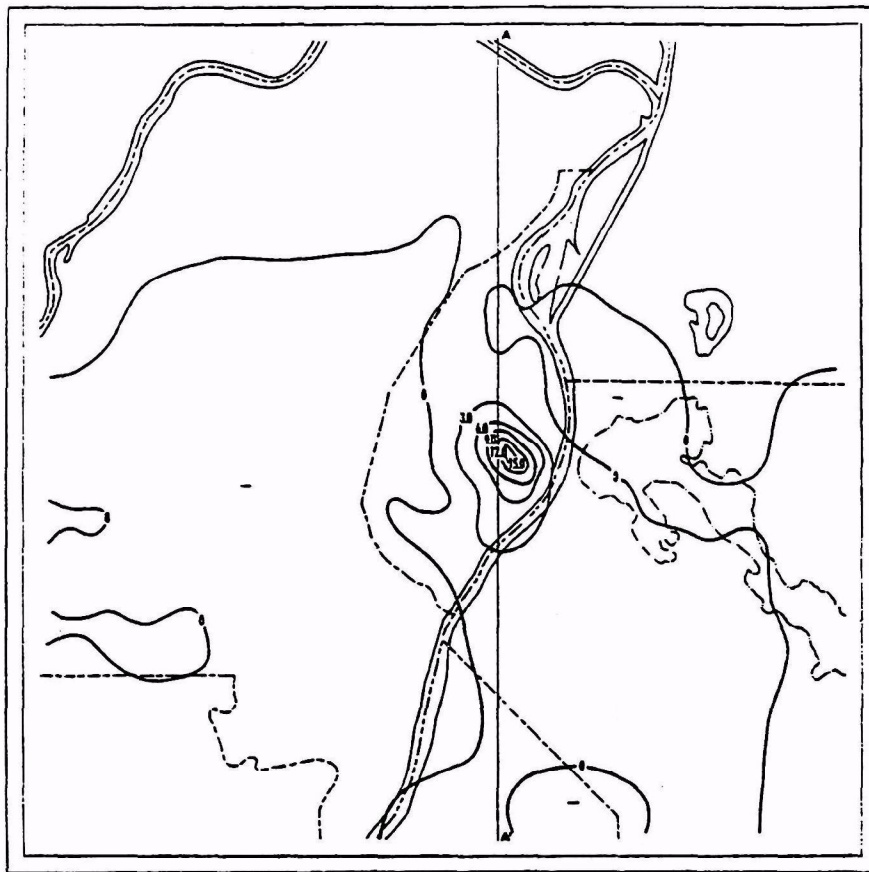


FIG. 11. As in Fig. 9 except for initial conditions $P(2,1)$.

the east-northeast in her case. She observed convergence over the city at the 100 m level and divergence at the 350 m level.

The vertical velocity distribution at 300 m (Fig. 11) shows a concentration of upward vertical motion in the central regions of the city, with some slight downwind displacement. In this case, the maximum upward speed is 16 cm s^{-1} . The suburban and rural regions west and south of the city are characterized by weak downward motion ($\sim -3.0 \text{ cm s}^{-1}$) at 300 m, as is the case in East St. Louis and Belleville, Ill. The vertical cross section along AA' suggests that the top of the urban heat island circulation is found at about the 900 m level. Upward vertical motions, for the most part, characterize the boundary layer below the 300 m level north and south of the city.

As the wind speed and shear increase further, as in the case of initial conditions P(3,1), the inflow at 100 m, present in the previous cases, is replaced by a line of convergence which is displaced downstream of the city's center (Fig. 12a). The strongest horizontal wind speeds are found immediately upwind of the city's center. The weakest wind speeds are found in the southwest corner of the figure, and are a result of increased frictional effects due to the bluffs in that region. The wind speeds immediately downwind

(southeast) of the city's center are weaker than those immediately north, east or west of the city. At 300 m (Fig. 12b), the horizontal divergence is still obvious, but upstream and downstream wind speed differences are not immediately discernable.

The vertical velocity distribution over the city (Fig. 13) shows some downstream displacement, but for the most part the region of upward vertical motion is concentrated over the city. The maximum updraft velocity is 12 cm s^{-1} . Minor centers of downward motion are located immediately southwest of the center of upward motion and downstream of the region of upward motion over the city. According to the vertical cross section along AA', the top of the heat island circulation is at about the 1400 m level. Regions of relatively strong downward motion are developed aloft due to the imposition of the strong initial wind speeds and wind shear.

When initial conditions P(4,1) are employed, the horizontal wind field at the 100 m level (Fig. 14a) indicates that the line of convergence is displaced farther downstream than in the previous case [P(3,1)]. The horizontal velocities immediately upstream of the central regions of the city are still somewhat larger than those immediately downstream. At 300 m (Fig. 14b), the divergence found at this level in the pre-

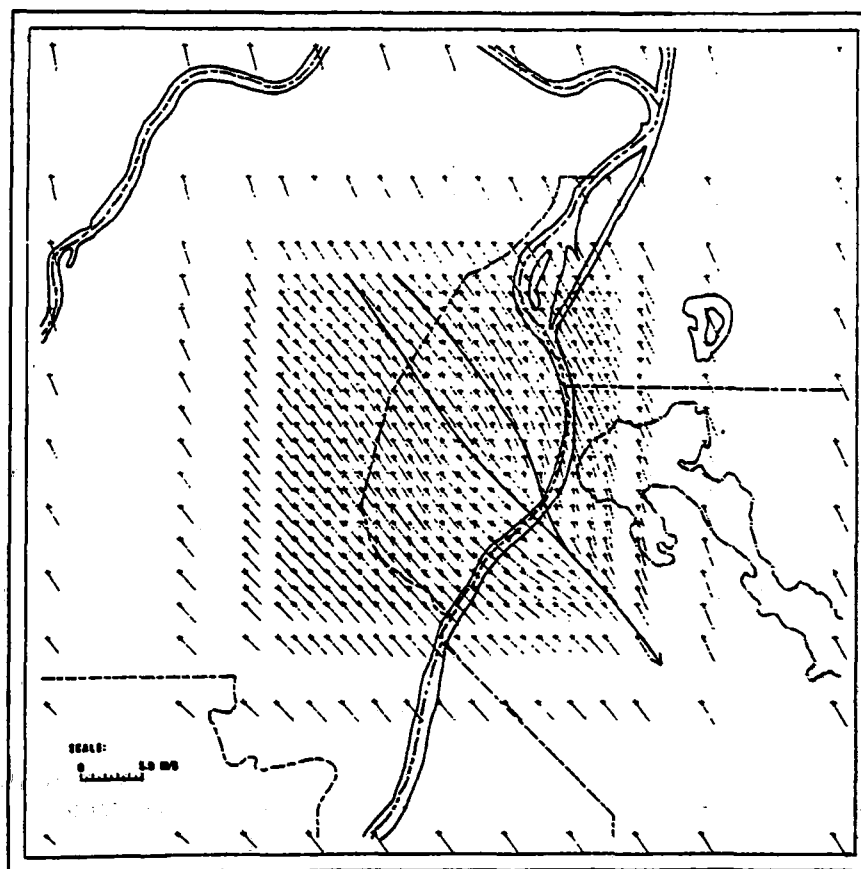


FIG. 12a. As in Fig. 8 (upper) except for initial conditions P(3,1).

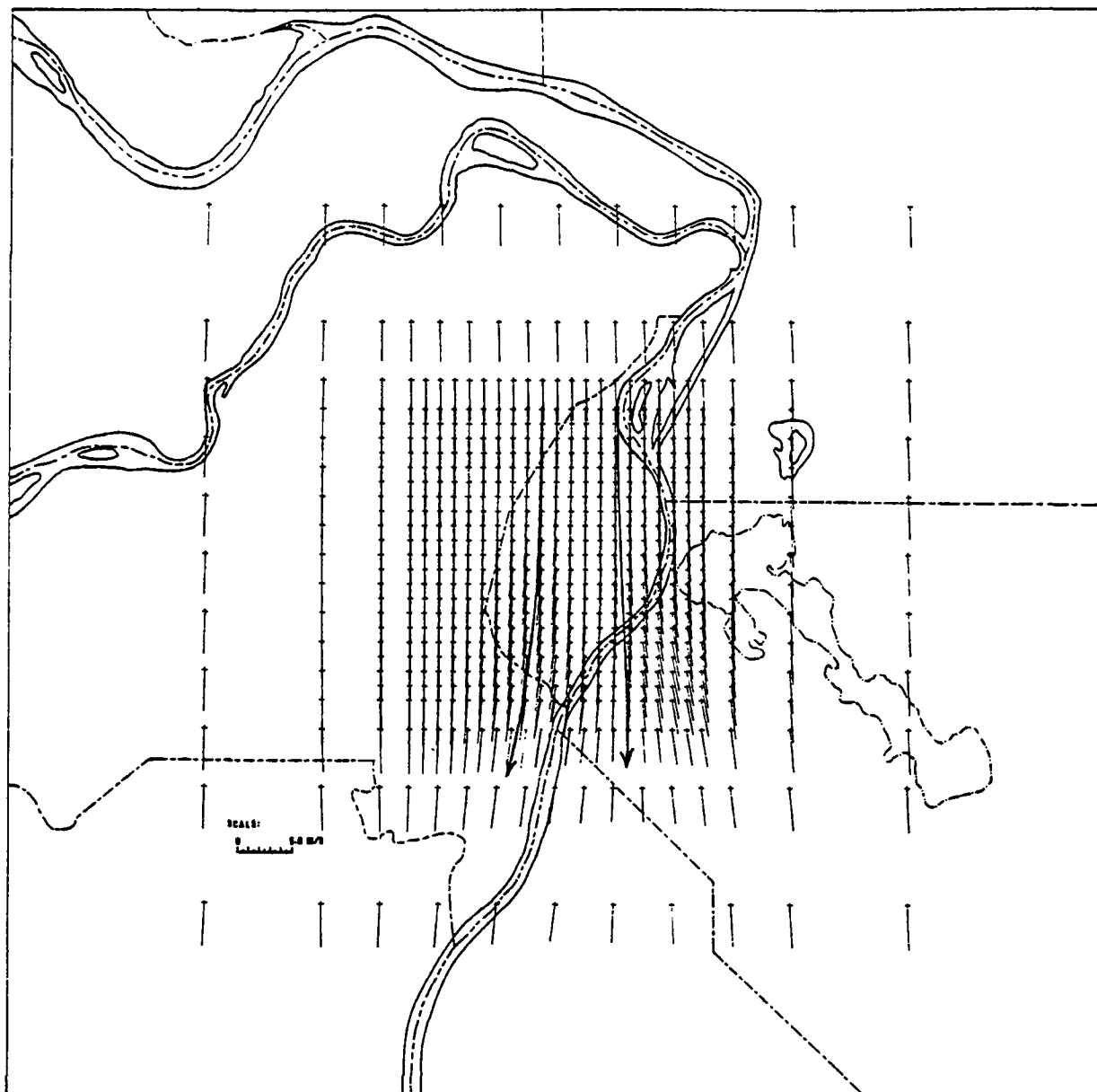


FIG. 12b. As in Fig. 8 (lower) except for initial conditions P(3,1).

vious cases appears to be located on the east side of the city.

The vertical velocity distribution (Fig. 15) is characterized by an elongated region of upward vertical motion extending from the center of the city downstream about 20 km and containing three centers of maximum updraft. The largest updraft velocity is located in the center farthest downstream of the city and is 11 cm s^{-1} . The increased vertical velocity downstream of the city may be a result of the interaction of flow over a barrier, since it appears that the downstream center is located upwind of the bluffs southeast of St. Louis, and of the heat island circulation. The marked downstream displacement of both the zone of convergence and the updraft vertical

velocity distribution in the case of strong initial winds was predicted by Vukovich (1971); however, his model predicted downward motion over the center of the city which does not occur in this case. Relatively strong downdrafts are found immediately southwest of the elongated region of updraft, and weaker downdrafts are found to the northeast. The pattern of an elongated region of upward motion with downward motion on either side almost coincides with the pattern detected by Angell *et al.* (1973) over Oklahoma City in the evening with strong horizontal winds. During the day they found the strongest updraft velocities immediately upwind of the city with a secondary maximum downwind. They attributed the upward motion during the day to the barrier effect

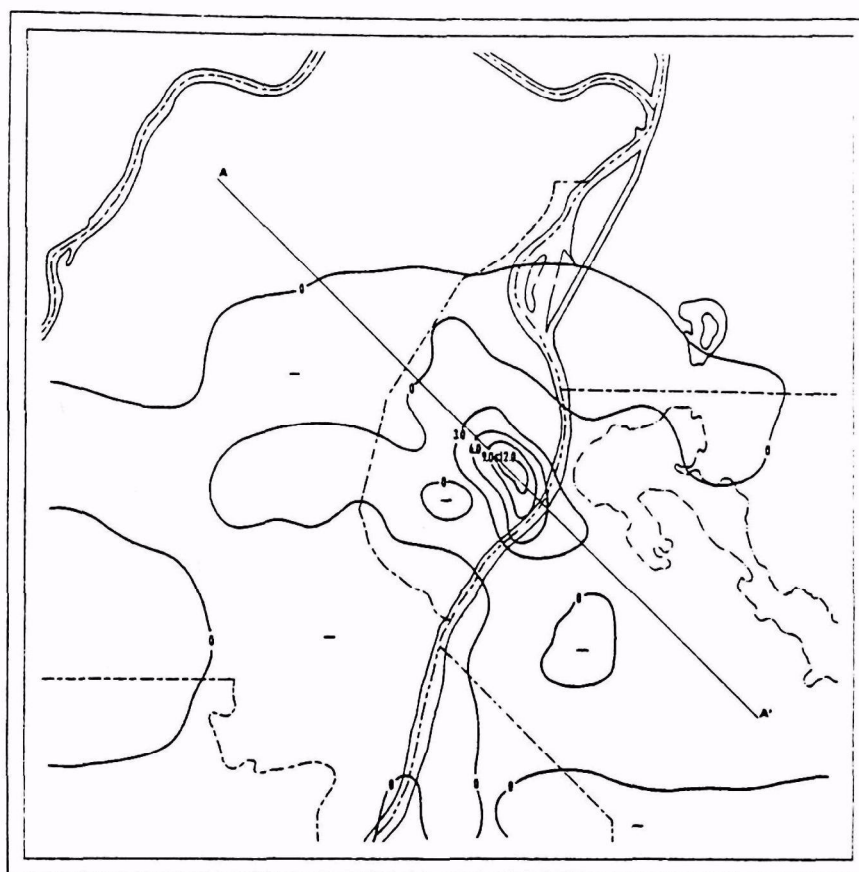


FIG. 13. As in Fig. 9 except for initial conditions P(3,1).

of the city rather than to a thermal effect of the city; but during the evening, they indicated the possible influence of the urban heat island.

The vertical cross section along AA' (Fig. 15, lower) suggests that the top of the circulation induced by the heat island is 1500 m over the city, but somewhat less downstream. The height of the top of the perturbation has increased as the initial wind speed and wind shear increased. Vukovich (1975) has shown that such an increase is to be expected when the characteristic Richardson number decreases; this is brought about in this case by increasing the initial wind shear. Furthermore, the magnitude of the updraft velocity generally decreased, which may also be attributed to the increase in the wind shear (Vukovich, 1975).

Changes in wind direction did not significantly affect the momentum perturbation produced by the St. Louis heat island except when initial condition P(4,1) was employed. The effects of changes of wind direction are best shown using the vertical velocity distribution. The most intense upward vertical velocities, among all cases in which initial conditions P(4,1) were used, were found when the initial wind was from the northeast (Fig. 16). The tongue of upward

vertical motion extended to a point 30 km downstream of the city's central region. Two updraft centers existed, with the downstream center, located about 17 km from the city's central regions, having the largest updraft velocity (14 cm s^{-1}). A secondary maximum was found immediately upstream of the center of the city ($\sim 6.0 \text{ cm s}^{-1}$). Weak updrafts were also found over the city to the north and northwest. Weak downdrafts existed immediately east and west of the tongue of upward motion. In this particular case, it is suggested that the line of convergence produced by the urban heat island was intensified by topographically induced convergence as air was channeled southward over the Mississippi River between the bluffs.

The weakest upward motion occurred when the initial wind was from the west (Fig. 16). As in the previous cases, the tongue of updraft velocities extended about 30 km downstream from the city's center. Two relatively weak updraft centers (3.0 cm s^{-1}) were apparent—one located over the center of the city and the other about 8 km from the city's center. Downdraft centers were found to the west, northwest, southeast and southwest of the city's center. The rapid decrease of surface elevation east

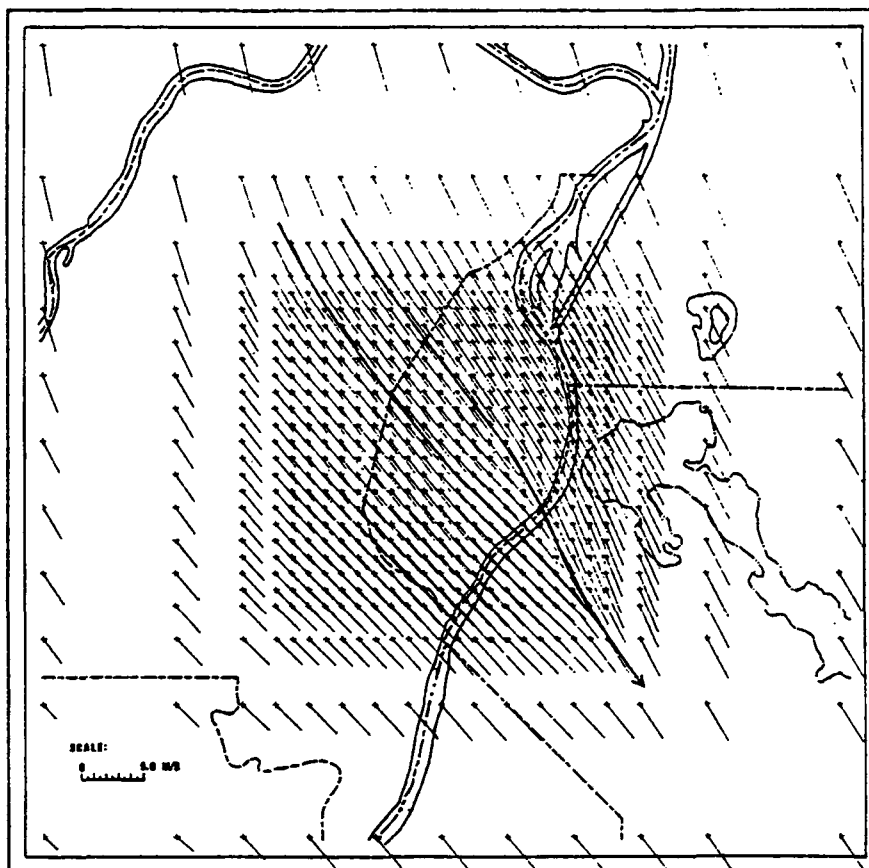


FIG. 14a. As in Fig. 8 (upper) except for initial conditions P(4,1).

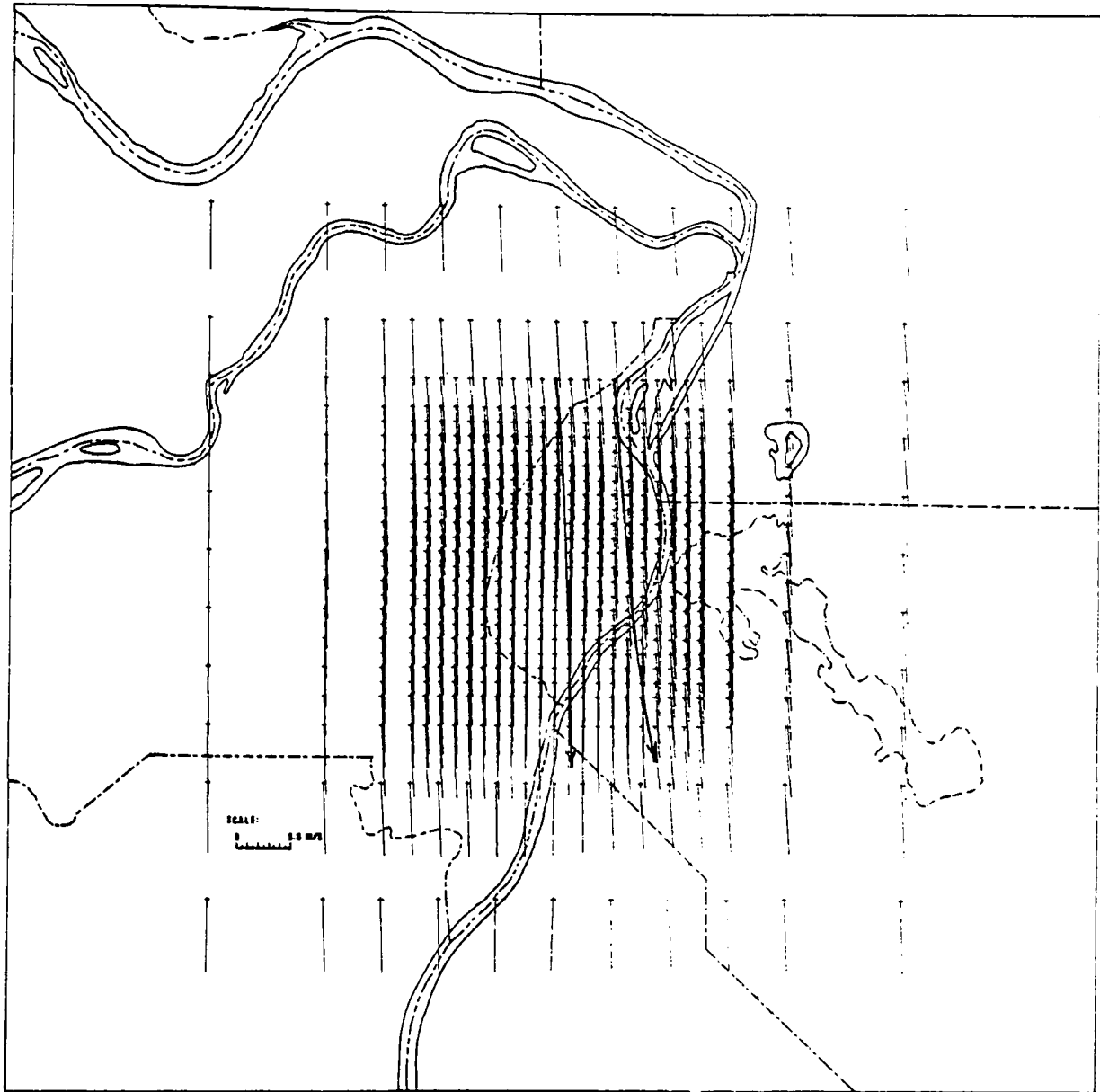


FIG. 14b. As in Fig. 8 (lower) except for initial conditions P(4,1).

of St. Louis due to the river bottom would produce vertical expansion, horizontal divergence, and downward vertical motions in the boundary layer flow. This would act in contrast to the vertical contraction, horizontal convergence, and upward vertical motion produced by the urban heat island, resulting in a reduced heat island effect downstream. Though this effect occurred in both the north and northeast wind cases, it appears that in this case the location of the downstream updraft center is immediately over the region of rapid, surface elevation decrease. This did not occur in the other cases. Furthermore, in the west wind case, general downdrafts would be created over the city due to the general decrease in surface

elevation from the west county region to the Mississippi River, which could account for the reduction of the overall intensity of the heat island in this case.

The most complex pattern of vertical velocity was found when the initial wind was from the east (Fig. 16). The tongue of updraft velocities present in all the previous cases is not well defined in this case. Two updraft centers were evident, but these appeared to be separate entities. The maximum updraft speed in the center over the city's center was about 8 cm s^{-1} , and that in the downstream center was about 7 cm s^{-1} . The downdraft center immediately west-northwest of the city's center, is located over a low topographical region, suggesting either a topographically induced

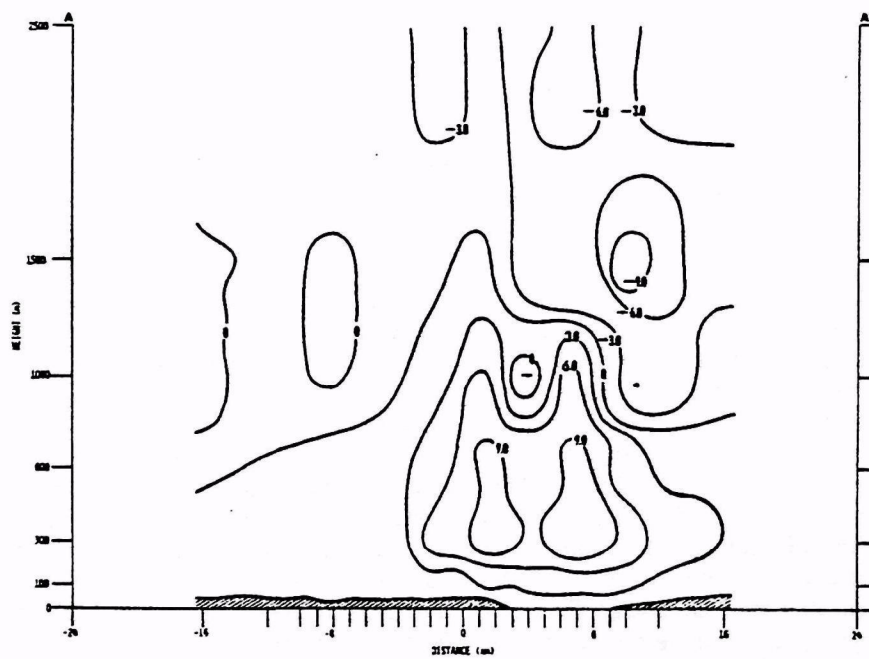
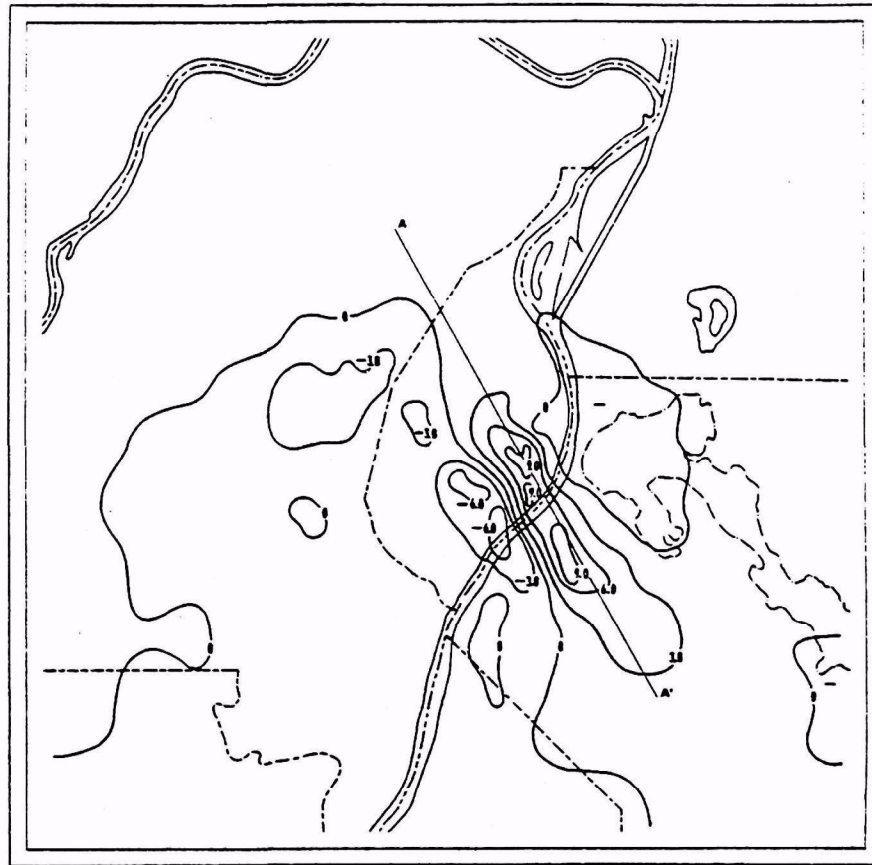


FIG. 15. As in Fig. 9 except for initial conditions $P(4,1)$.

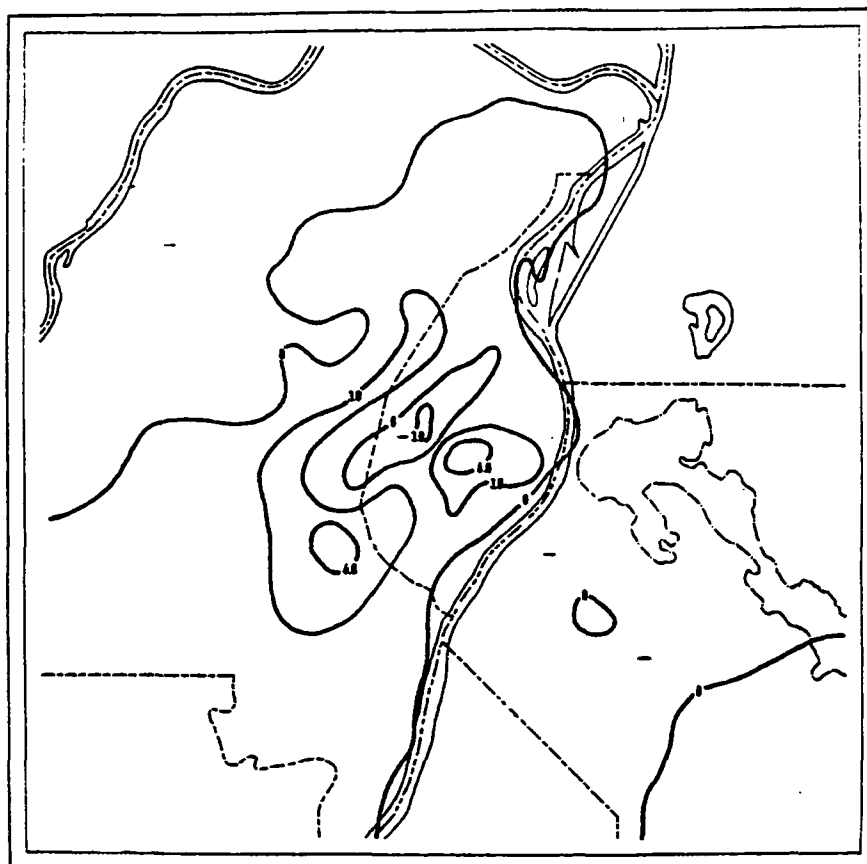


FIG. 16. Upper: The vertical velocity (cm s^{-1}) distribution at the 300 m level for the northeast (upper), west (middle) and east (lower) wind case. The initial conditions were $P(4,1)$. Positive values indicate upward vertical motions.

downdraft or an intensification of a compensating downdraft associated with the heat island perturbation by the topography. The downstream updraft center may be associated with the heat island perturbation or with a topographical perturbation induced by flow over the bluffs to the southwest or with a combination of both effects. The third explanation appears to be the most plausible. The narrow region of upward motion oriented northeast-southwest, found immediately northwest of the downdraft center, is probably a product of the flow over the bluffs found to the west.

5. Conclusions

The influence of synoptic wind speed and direction on the St. Louis heat island have been studied. It is found that, as the wind speed increases, the intensity of the heat island circulation decreases, and the heat plume associated with the heat island extends further downwind. Thus, the heat island circulation changes from a system characterized by cyclonic rotation to one characterized simply by a convergence line. In the case of wind profile 4, the heat plume and the convergence line associated with the urban heat island

extend farther downstream, which is to be expected. However, a tongue of positive vertical motion also extends downstream from the heat island center and contains a number of centers of positive vertical motion. The center containing the largest positive upward motion in the tongue is generally the one farther downstream from the heat island center. It is suggested that this may be a result of topographical effects. In the future, the interaction of topography and the heat island will be examined much more thoroughly.

It is found that when the wind speeds are small, the intensity of the St. Louis heat island is independent of wind direction. However, under strong wind speeds, the intensity of the heat island changes markedly from one wind direction to the next. The most dramatic changes occur when the wind direction is from the west, east and southeast, in comparison to those cases when the wind direction is from the northeast or north. In all cases, the changes are attributed to the influence of local topography on the urban heat island. These effects do not appear until the initial wind speed near the surface reaches a critical value which apparently is greater than or equal to 3 m s^{-1} .

Acknowledgment. This research was supported by NSF/RANN Grant GI-34345.

REFERENCES

- Ackerman, B., 1972: Winds in the Ekman layer over St. Louis. *Preprints Conf. Urban Environment*, Philadelphia, Amer. Meteor. Soc., 22-28.
- Angell, J. K., W. H. Hoecker, C. R. Dickson and D. H. Pack, 1973: Urban influence on a strong daytime air flow as determined from tethered flights. *J. Appl. Meteor.*, 12, 924-936.
- Bornstein, R. D., 1972: Two-dimensional non-steady numerical simulation of nighttime flow of a stable planetary boundary layer over a rough warm city. *Proc. Conf. Urban Environment*, Philadelphia, Amer. Meteor. Soc., 89-94.
- Chandler, T. J., 1964: City growth and urban climates. *Weather*, 19, 170-171.
- , 1965: *The Climate of London*. Hutchinson and Co., 250 pp.
- , 1967: London's heat island. *Biometeorology*, Part II. *Proc. Third Intern. Biometeorological Congress*, Pau, France, 1-7 September 1963, Oxford, Pergamon Press, 589-597.
- Clarke, J. F., 1969: Nocturnal urban boundary layer over Cincinnati, Ohio. *Mon. Wea. Rev.*, 97, 582-589.
- Delage, Y., and T. A. Taylor, 1970: Numerical studies of heat island circulations. *Boundary-Layer Meteor.*, 1, 201-226.
- Landsberg, H. E., 1956: The climate of towns. *Proc. Intern. Symp. Man's Role in Changing the Face of the Earth*. The University of Chicago Press, 584-606.
- Lettau, H., 1969: Note on aerodynamic roughness-parameter estimation on the basis of roughness-element description. *J. Appl. Meteor.*, 8, 822-832.
- Lowry, W. P., 1967: The climate of cities. *Sci. Amer.*, 217, No. 2, 15-32.
- Mitchell, J. M., Jr., 1961: The thermal climate of cities. *Air over Cities*, U. S. Public Health Service Rep. A62-5, Cincinnati, Ohio, 131-145.
- Stanford University Aerosol Laboratory and the Ralph M. Parson's Company, 1953: Behavior of aerosols within cities. Joint Quarterly Reports, Nos. 3, 4, 5 and 6.
- Vukovich, F. M., 1971: Theoretical analysis of the effect of mean wind and stability on a heat island circulation characteristic of an urban complex. *Mon. Wea. Rev.*, 99, 919-926.
- , 1973: A study of the atmospheric response due to a diurnal heating function characteristic of an urban complex. *Mon. Wea. Rev.*, 101, 467-474.
- , 1975: A study of the effect of wind shear on a heat island circulation characteristic of an urban complex. *Mon. Wea. Rev.*, 103, 27-33.
- Woollum, C. A., 1964: Notes from a study of the micrometeorology of the Washington, D. C. area for the winter and spring seasons. *Weatherwise*, 17, 263-271.

APPENDIX B

AREA SOURCES WITH OBJECTIVE VARIATIONAL ANALYSIS MODEL

AREA SOURCES WITH OBJECTIVE VARIATIONAL ANALYSIS MODEL

During the development of the model, an estimate of the area emissions for the test grid was needed. Rather than use an existing emissions inventory, a binormal, Gaussian distribution centered at a prescribed x_o, y_o with a total emission, Q_{int} and standard deviation q_x and q_y was chosen. Thus, at every point (x,y) the emission was given by:

$$Q(x,y) = \frac{Q_{int}}{\sqrt{2\pi} q_x q_y} \exp \left\{ -\frac{1}{2} \left[\left(\frac{x-x_o}{q_x} \right)^2 + \left(\frac{y-y_o}{q_y} \right)^2 \right] \right\} .$$

In this formulation the amount of material emitted, the location of sources and the shape of the distribution can be specified with great versatility. For example, a line source in the y direction can be approximated by choosing $q_y > 10 \Delta x$, and $q_x < \Delta x/2$; a point source by $q_y < \Delta x/2$, $q_x < \Delta x/2$; or large nearly uniform area sources ($q_y, q_x > 5\Delta x$).

RELATIVE DISPERSION OVERLAY

Rather than adopt the approach that area sources can be treated as virtual point sources, such as in the models of the EPA's UNAMAP Library, the concentration at a receptor downwind of an area source was computed as the integrated concentration arising from a set of smaller areas of uniform emissions.

Referring to Figure B-1, the concentration at x,y due to an emitting area centered at x_o, y_o is the integral of the subareas of the larger area. A representative area is located at (\hat{x}, \hat{y}) . Assuming a steady-state Gaussian point source at that point, the concentration at (x,y) , $d\psi(x,y)$, is given by

$$d\psi(x,y) = \frac{Q(\hat{x}, \hat{y})}{2\pi \bar{U} \sigma_z(x-\hat{x}) \sigma_y(x-\hat{x})} \exp \left[-\frac{1}{2} \left(\frac{y-\hat{y}}{\sigma_y(x-\hat{x})} \right)^2 \right] .$$

Letting $\hat{x} = x_o + v$, $\hat{y} = y_o + u$ and integrating gives

$$\psi(x,y) = \int_{-\Delta x/2}^{\Delta x/2} \left\{ \frac{Q(x_o, y_o)}{\pi \bar{U} \sigma_z(x-x_o-v)} \int_{-\Delta y/2}^{\Delta y/2} \exp \left[-\frac{1}{2} \left(\frac{y-y_o-u}{\sigma_y(x-x_o-v)} \right)^2 \right] \left(\frac{du}{\sigma_y(x-x_o-v)} \right) \right\} dv$$

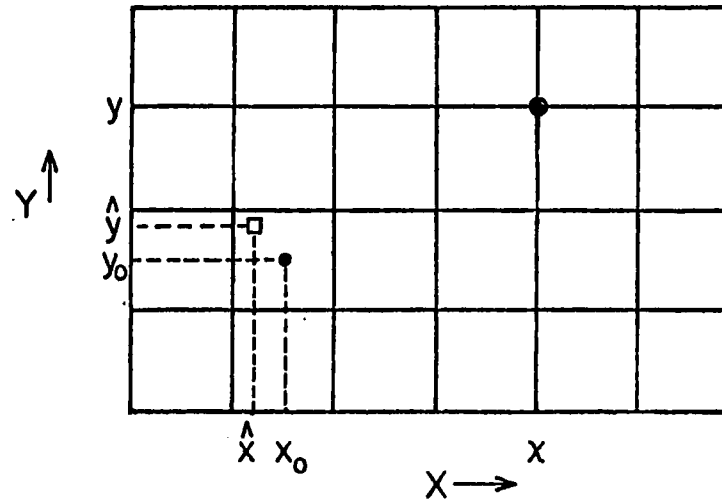


Figure B-1. Coordinates for determining the contribution of emissions from a subarea (\hat{x}, \hat{y}) within the finite difference grid (x_0, y_0) upon a receptor at a general grid point (x, y) .

Evaluating the interior (bracketed) integral, B, gives,

$$B = \sqrt{2\pi} \operatorname{erf} (p(v))$$

when

$$p(v) = \frac{1}{\sqrt{2}} \frac{(y-y_o-\Delta y/2)}{\sigma_y(x-x_o-v)} \quad .$$

The complete integral is

$$\psi = \sqrt{\frac{2}{\pi}} \frac{Q(x_o, y_o)}{U} \int_{-\Delta x/2}^{\Delta x/2} \operatorname{erf} (p(v)) \cdot \frac{dv}{\sigma_z(x-x_o-v)}$$

which is evaluated numerically for specific locations, ℓ , m

$$x = (x_o - \Delta x/2) + \ell \Delta x \quad \ell = 1, 2, 3, \dots, I$$

$$y = (y_o - \Delta x/2) + m \Delta x \quad m = 1, 2, \dots, 5 \quad .$$

For a given atmospheric stability condition, a $\psi(\ell, m)$ can be determined. The total concentration at a given point is the integral of all of the contributions from upwind sources which can be rapidly calculated using the appropriate (ℓ, m) array, emissions and wind.

When the actual wind is not oriented parallel to the x direction, the same array can be oriented along the direction of the v component and that contribution can be computed. If the wind component changes sign between the source and the receptor, it is assumed that the source did not affect that receptor.

ATMOSPHERIC STABILITY

In practice, for models based on the Gaussian distribution, atmospheric stability is accounted for in the magnitude of σ_y and σ_z , the cross wind, and vertical plume spread coefficients. These quantities are expressed, in general, as functions of distance downwind from a source, x, by

$$\begin{aligned} \sigma_y &= a_1 + a_2 x^b \\ \sigma_z &= c_1 + c_2 x^d \quad . \end{aligned}$$

Martin's (1976) values of a_1 , a_2 , b , c_1 , c_2 and d for the six Pasquill Turner stability categories can be used. If the relationship of σ_y and σ_z to the eddy diffusion coefficient is used, then

$$\sigma_y^2 = 2K_y t$$

and

$$\sigma_z^2 = 2K_z t$$

where $t = x/U$ is the travel time from source to receptor.

APPENDIX C

SENSITIVITY ANALYSIS AND TESTING OF THE VARIATIONAL OBJECTIVE ANALYSIS MODEL

SENSITIVITY ANALYSIS AND TESTING OF THE VARIATIONAL OBJECTIVE ANALYSIS MODEL

CASE I - THE ROLE OF $\tilde{\alpha}/\alpha$

The most favorable conditions for obtaining a solution to the analysis in the idealized case occur when errorless observations are made at every grid point, and they are known to satisfy an analytical distribution. In such a case, the solution analysis should be the analytical solution. Departure, therefrom, might indicate weaknesses in the formulation of the analysis technique, the numerical techniques used, or the differences in the solution of the constraint equation and the analytical concentration.

Accordingly, choosing $\tilde{\alpha}/\alpha = 10$ everywhere should make $\psi = \psi = \psi^*$. Using the input variables listed in Table C-1, this solution was confirmed. Decreasing the ratio of 1.0, and then 0.1 progressively, increases the influence of the constraint equation upon the solution. As shown in Figure C-1, ψ continually departs from $\tilde{\psi}$. The maximum value decreases and is displaced further downstream, the upwind concentrations decrease, and the downwind concentrations increase accordingly. The total mass is approximately conserved, but it is redistributed by the analysis. These results show that the constraint equation does influence the solution away from $\psi = \psi^*$. That solutions were obtained as the ψ/ψ^* ratio changes suggest that a solution can be obtained when the ratio is variable; this is verified later.

CASE II - THE ROLE OF THE CONSTRAINT EQUATION

With the assurance of a convergent solution, the role of the constraint equation was examined by letting $\tilde{\alpha}/\alpha = 0.01$; this ratio minimizes the contribution of the observations to the solution and emphasizes the role of the constraint equation. In effect, this case investigates the solution which could be obtained if there were no observations and only emissions, wind and stability were known. Test parameters are given in Table C-1.

The solution, ψ , along $y = 5$ km is shown in Figure C-2 with the analytic concentration, ψ^* . Clearly, ψ underestimates ψ^* as much as 100 percent (10.8 versus 5.2 @ $x = 7$) when $x < 10$ km and overestimates (10.5 versus 8.6 at $x = 13$ km) along the remainder of the axis. The peak value of ψ is about 1 km downwind of the maximum of ψ^* . The integrated deficit of $(\psi - \psi^*)$ is 1.08

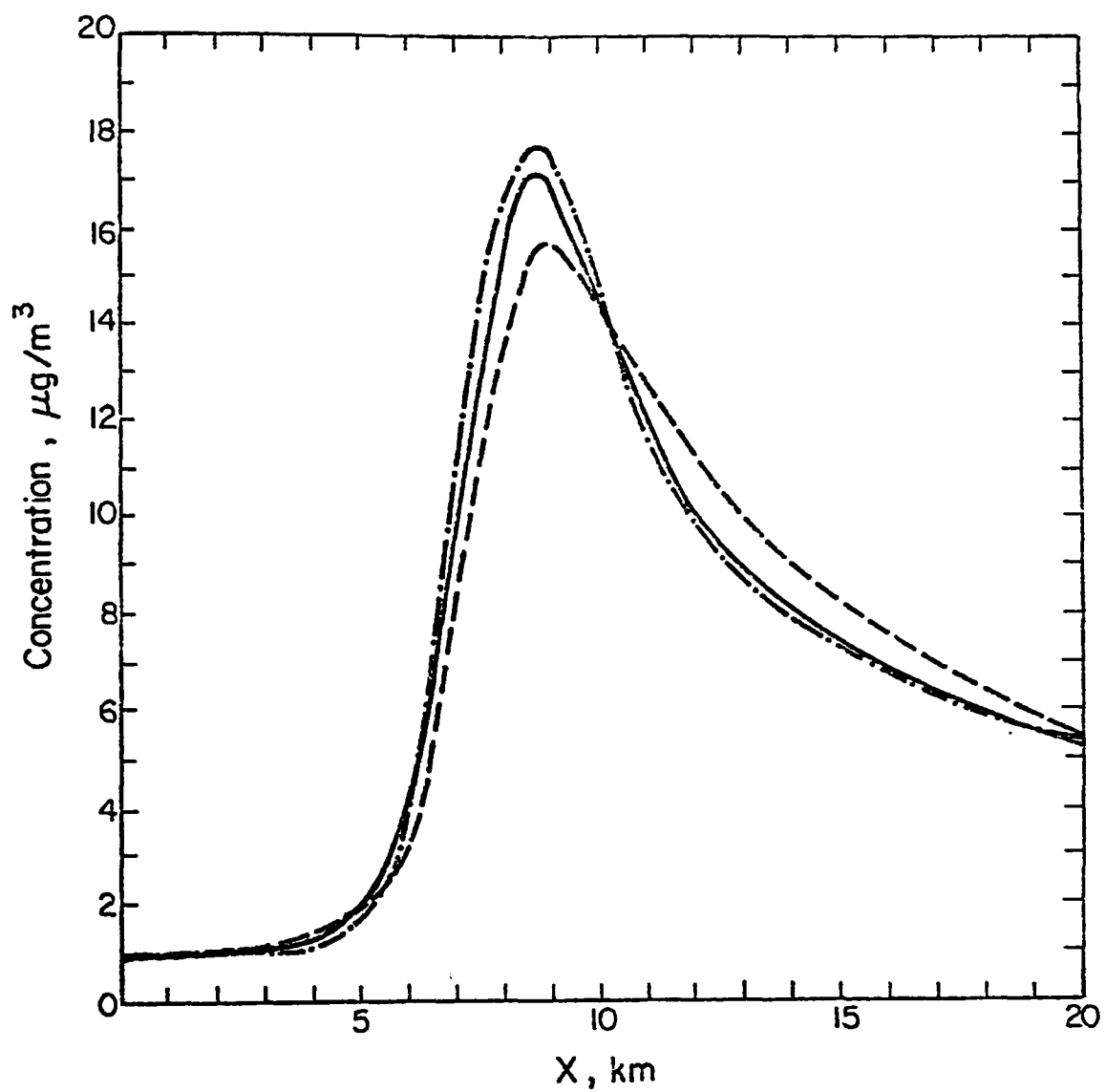


Figure C-1. Concentration distributions with x for Case I, showing ψ^* (— · — ·) and ψ when $\tilde{\alpha}/\alpha = 10$ (— · — ·), $\tilde{\alpha}/\alpha = 1.0$ (————) and $\tilde{\alpha}'/\alpha = 0.1$ (— — —).

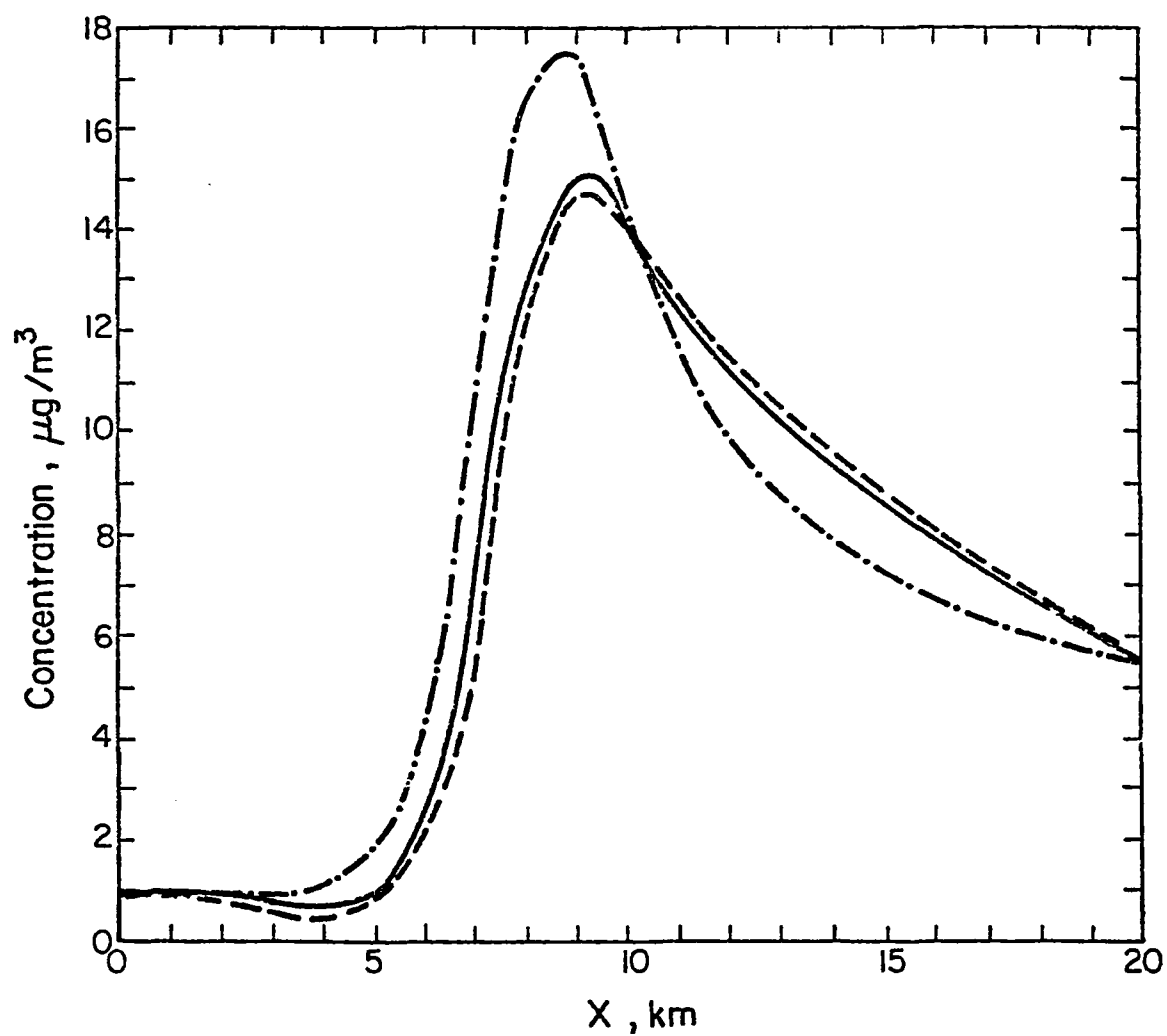


Figure C-2. Concentration distributions with x for Case II showing ψ^* (— · — ·) and ψ when $L = 1$ km, (—) and $L = 4$ or 10 km (— — —) for Case II.

TABLE C-1. PRINCIPAL INPUT VARIABLES AND CHARACTERISTIC NUMBERS

CASE	L (km)	Z (m)	$\tilde{\alpha}/a$	q (km)	BC*	$\bar{\gamma}$	$\bar{\eta}$	ξ_{\max}	COMMENT
Ia b c	1	50	10 1 0.1	1.25	CV	35.0	28.5	.19	Test for Solutions
IIa b c	1 4 10	50	0.01	1.25	CV	35.0	28.5 114.0 285.0	.19 .76 1.89	Basic Experiment Cases II-IV
IIIa b	1	50	0.01	2.50 5.00	CV/CG CV/CG	35.0	28.5	.16 .11	Solutions Dominated by the Constraint Equations
IVa b c	1	31.5 100 200	0.01	1.25	CV	27.0 39.4 39.5	37.1 25.4 25.3	.30 .05 .01	
V	4	50	1.0	1.25	CV	35.0	114.0	.76	Observations Errors
VI	4	50	1.0	1.25	CV	35.0	114.0	.76	Observations Removed See text for $\tilde{\alpha}/a$
VII	4	50	1.0	1.25	CV	35.0	114.0	.76	Observations Removed and Perturbed

Note: In all experiments $\bar{U} = 3$ m/s $Q_{\text{int}} = 10$ g/s, $\bar{\psi} = 1$ $\mu\text{g}/\text{m}^3$, $q_y = q_x$.

*BC - Boundary Conditions, CG - Constant Gradient, CV - Constant Value

Cases VI and VII are discussed in the text (Pages 77 to 84).

times the integrated surplus, indicating that the total mass density of pollutant was nearly conserved in this plane.

The reasons for the solution profile became apparent after examining Eq. (31) which is appropriate for small $\tilde{\alpha}/\alpha$, i.e.,

$$\frac{\partial^2 \psi}{\partial x^2} - \xi^2 \psi = \eta \frac{\partial Q}{\partial x} - \eta \xi Q$$

For $\xi < 0.2$ and the parameters of this test, the $\xi^2 \psi$ term is much smaller than the remaining terms and the solution is dominated by the curvature term of ψ . For the source configuration used, $\frac{\partial Q}{\partial x} = - \left(\frac{x-x_0}{q_x^2} \right) Q$, so the equation reduces to

$$\frac{\partial^2 \psi}{\partial x^2} \approx - \eta Q \left(\frac{x-x_0}{q_x^2} + \xi \right)$$

Therefore, for $(x-x_0 + \xi q_x^2) > 0$, the curvature of ψ is positive and ψ is concave upward. In this case, $(x-x_0 + \xi q_x^2) < 0$ for $x < 7.1$ km. Beyond that point, the curvature remains negative for as long as Q makes a contribution; e.g., $x-x_0 > 3 q_x$ ($x > 12.5$ km). After that point, Q is very small, the curvature of ψ is near zero. As evident in the solution, the slope of ψ is nearly constant for $x > 13$ km.

When the curvature is a minimum, the function should be a maximum. The curvature is an extreme when

$$\frac{\partial}{\partial x} \left[- \eta Q \left(\frac{x-x_0}{q_x^2} + \xi \right) \right] = 0$$

which, with the Gaussian source distribution, constant η and ξ , occurs when

$$2 \left(\frac{x-x_0}{q_x^2} \right) = \left(- \xi \pm \sqrt{\xi^2 + 4/q_x^2} \right)$$

For small values of ξ (~ 0.1) and small values of q_x (< 2), maxima and minima of ψ should occur when

$$x - x_0 \approx \pm q_x \quad . \quad (C-1)$$

The numerical solution of ψ agrees with this result near the maximum concentration. The disagreement about the location of the expected minimum concentration of ψ , i.e., a minimum @ $x-x_0 = -q_x$ and the computed minimum (near $x = 3.5$) probably arises from not including gradients of ψ and η in the development. Near $x = 3.5$, the gradients of ξ and η are large (Figure 14) and should be considered.

The magnitude of ξ can be increased by increasing L . However, this proportionally increases the coefficient of all of the terms of the finite difference equation so that the solution is generally unaffected. Test cases with $L = 4$ km and 10 km showed only a slight difference in the numerical solution (Figure C-2).

The convergence criteria was met after 67 iterations in the $L = 1$ km case. After 90 iterations, the solution criteria was not achieved at 26 points when $L = 4$ km. At that point, the constraint field, A , was approximately 10 times larger, residuals were 10 times larger, Ω was 100 times larger so the changes of ψ were a tenth of those made in the $L = 1$ km case. Thus, convergence was slower. The trend toward convergence left no doubt that a solution would have been attained with further iterations. A different, faster relaxation procedure would have helped reduce the number of iterations needed to obtain a solution.

CASE III - SOURCE DISTRIBUTION/BOUNDARY CONDITIONS

The analysis of Case II is continued by examining the influence of the source shape upon the distribution. The total emission was held constant but the distribution parameters q_x and q_y were increased to 2.5 km and then to 5.0 km. The analytic concentration ψ^* and the solution concentrations, ψ , along the $y = 5$ km axis when $\tilde{\alpha}/\alpha = 0.01$ are shown in Figure 29 for both constant value ($\delta\psi = 0$) and constant gradient [$\delta(\frac{\partial\psi}{\partial n}) = 0$] boundary conditions. The solution indicated by $\delta\psi = 0$ in Figure C-3a was discussed in Case II. Changing the boundary conditions changes the solutions, especially in areas where the emissions are very small. Upwind of the source, the effects of "background"

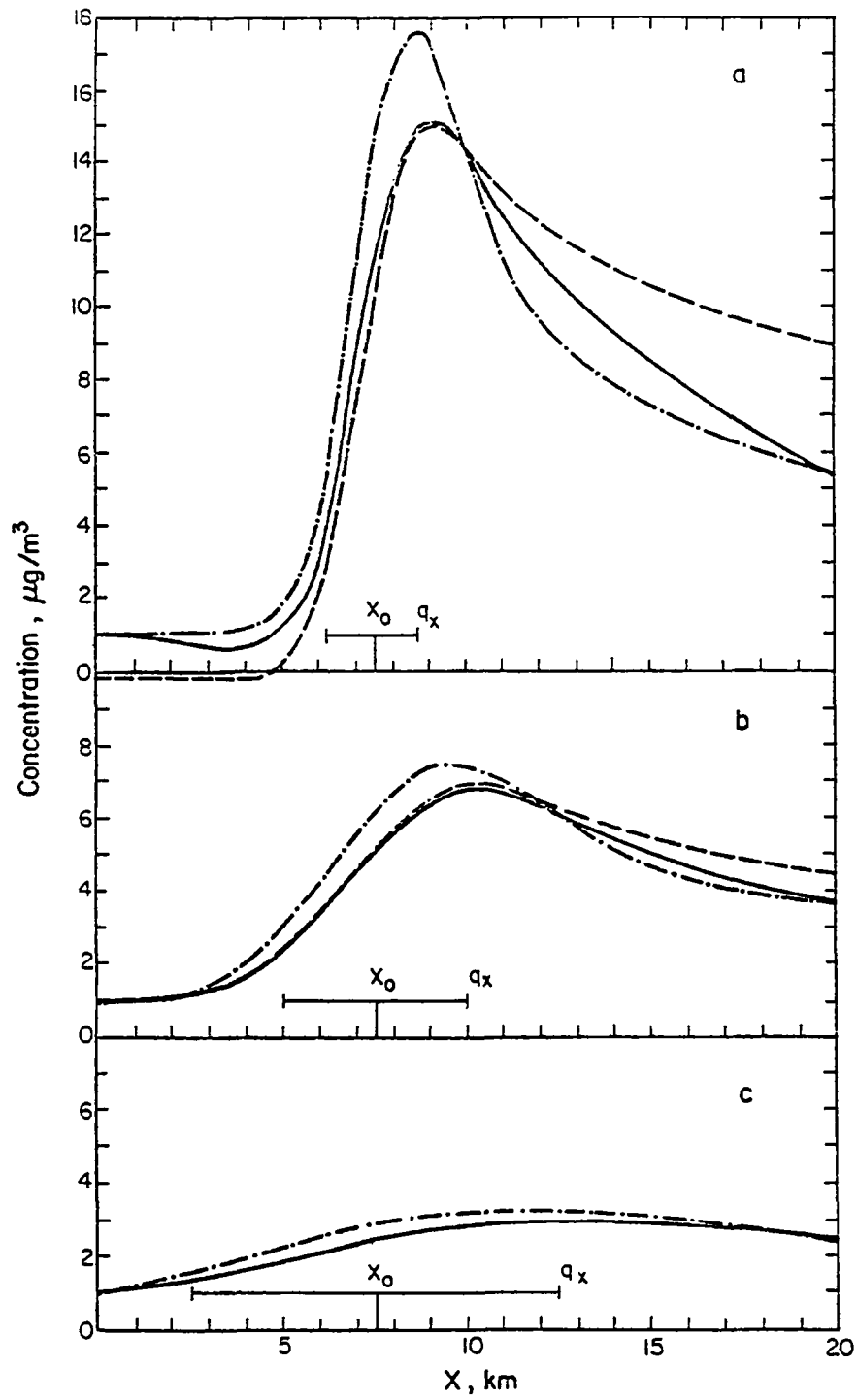


Figure C-3. Concentration distribution of ψ^* (— · —) and ψ with constant boundary conditions (—) and constant flux boundary condition (— — —) for the Case III with a) $q_x = 1.25$ km, b) $q_x = 2.50$ km and c) $q_x = 5.00$ km.

are lost to the analysis. Downwind the constraint equation overestimates the concentration by a large amount. Between $x_0 - 2q_x$ and $x_0 + 2q_x$, distribution of emissions rather than the boundary conditions control the solution.

When the emissions are more uniformly distributed $q_x = q_y = 2.5$ km, ψ (Figure C-3b) becomes more like ψ^* , and the boundary conditions have less effect upon the solution. The maximum ψ is displaced about 1.5 km further downwind of the maximum ψ^* (~ 1.5 km) as Eq. (C-1) predicts, but the maximum values differ only slightly. Further spreading of the emissions ($q_x = q_y = 5.0$) further brings the analytic and constraint solutions closer together. The boundary conditions showed no substantial effect on the solution since emissions were effective at the upwind and downwind boundary of the grid. Clearly, the constraint equation gives a better reproduction of the actual distribution of concentration when the source is uniformly distributed, regardless of the boundary conditions.

CASE IV - EFFECTS OF Z

In the development of the constraint equation, $\gamma(x)$ was nearly maximized by choosing $Z \sim \sqrt{2} S_z$. The choice of Z affects the values of γ , η and ξ and hence, the solution. Furthermore, the background concentration of ψ at Z is arbitrarily given as 0.999 times the background at $z = 0$ to give a finite value of S at points upwind of the sources. Increasing Z effectively makes the background even more uniform with height. The effects of assuming different values of Z on the constraint equation solution ($\tilde{\alpha}/\alpha = 0.01$) were investigated numerically. The experimental data are given in Table C-1. Although the convergence criteria had not been met after 90 iterations, when Z was increased, the distribution of ψ along the $y = 5$ km axis shown in Figure C-4 indicate the trend of the solution. As Z increases, the solution progressively underestimates ψ^* , and the maximum ψ is displaced progressively further downwind.

A reduction of Z ($z = S(\Delta x)$) reproduces the magnitude and location of the maximum ψ^* quite well but overestimates the downwind concentrations. The error variance, initially 36.6, is reduced to 13.5 in contrast to the $Z = 50$ m case when the error variance begins at 46.0 and reduces to 8.3. By that measure, the overall solution has not been improved using the smaller Z.

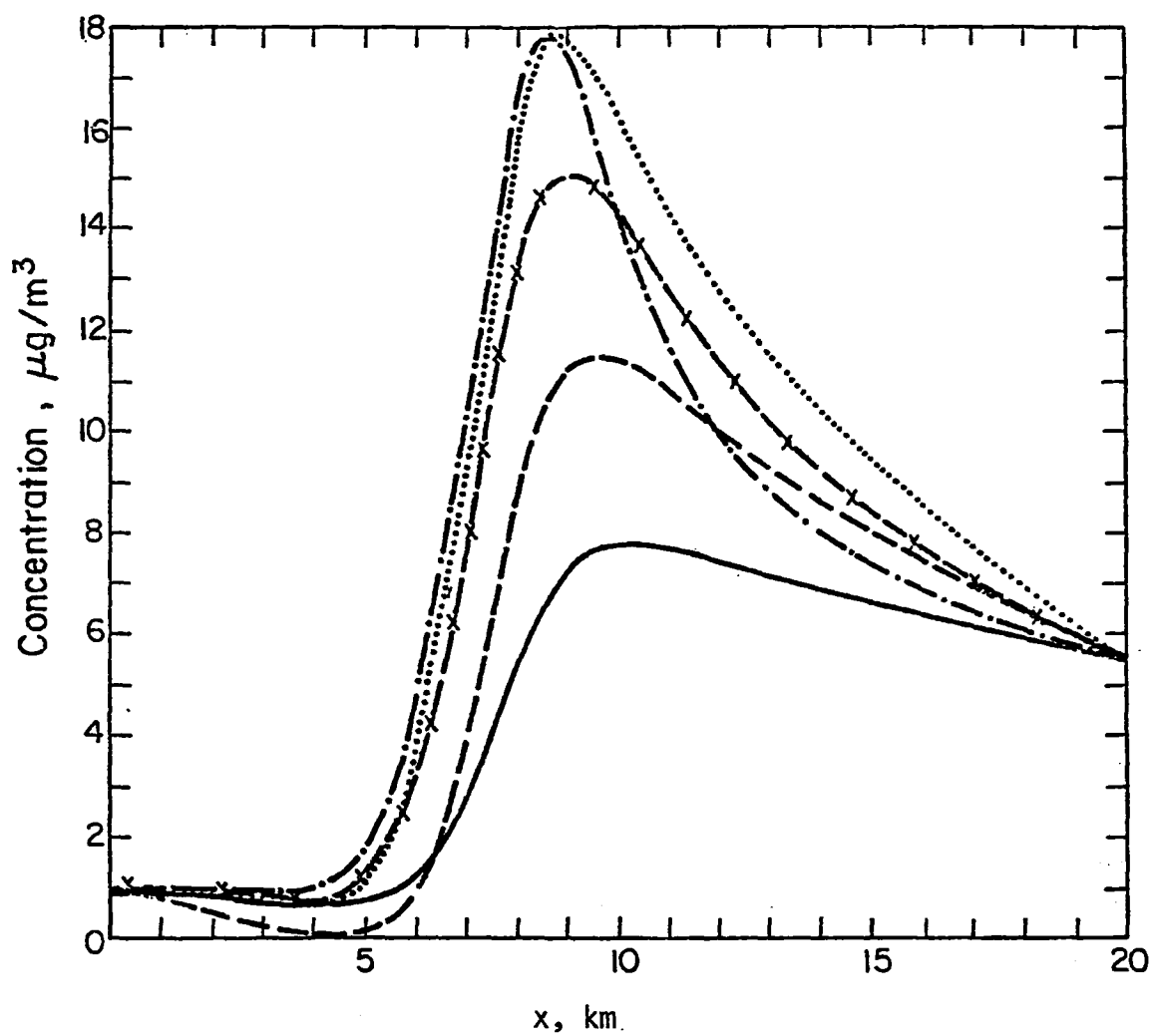


Figure C-4. Concentration distributions with x for Case IV, showing ψ^* (— · — ·), and ψ when $Z = 200$ m (—), $Z = 100$ m (— — —), $Z = 50$ m (x — — x) and $Z = 31.5$ m (····).

The solutions for variable Z clearly show that the choice of Z and the background value of Z strongly influence the resulting concentrations. This does not present a major problem when the impact of area sources upon ground level air quality is considered. However, elevated sources will require careful consideration and possibly some revision of the analysis approach.

CASE V - OBSERVATIONAL ERRORS

A certain amount of error exists in each measurement of a pollutant concentration. In an effort to simulate a more realistic situation and the performance of the analysis technique in that situation, the observations, $\tilde{\psi}$, were redefined so that at all interior points,

$$\tilde{\psi}_{i,j} = \psi_{i,j}^* + E_{ij}(0, \psi_B)$$

where E_{ij} is a number drawn from a normal (Gaussian) population having a zero mean and standard deviation of ψ_B . All other parameters were the same as the Case I(a) of Table C-1.

The ψ^* , $\tilde{\psi}$ and ψ are shown in Figure C-5. The perturbations of $\tilde{\psi}$ are reduced by the analysis. This means that the analysis filters some high frequency noise of the observations. The trend is toward the solution of Case I(a). The experiment was performed for different sets of E_{ij} , with similar results.

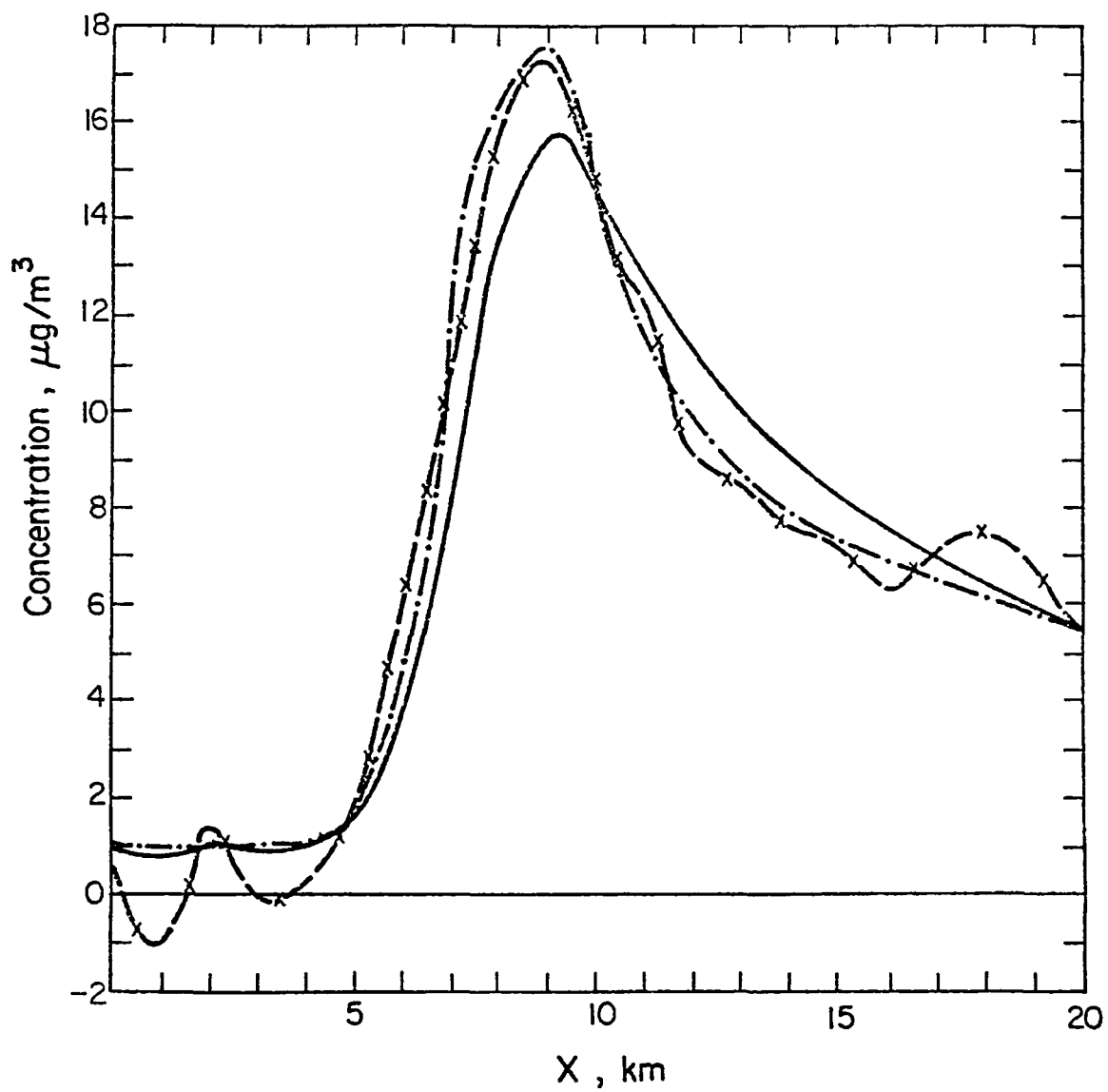


Figure C-5. Concentration distributions with x for Case V showing $\tilde{\psi}(x \text{ --- } x)$, $\psi^*(\text{---} \cdot \text{---} \cdot)$, and $\psi (\text{---})$ along $y = 5 \text{ km}$.

REFERENCES

- Barnes, S. L., 1964: "A Technique for Maximizing Details in Numerical Weather Map Analysis", J. Appl. Meteor., 3, 396-409.
- Busse, A. D. and J. R. Zimmerman, 1973: "User's Guide to the Climatological Dispersion Model", EPA-R4-73-024, (NTIS Accession Number PB-227-346).
- Cressman, G. P., 1959: "An Operational Objective Analysis Systems", Mon. Wea. Rev., 87, 367-374.
- Endlich, R. M. and R. L. Mancuso, 1968: "Objective Analysis of Environmental Conditions Associated with Severe Thunderstorms and Tornadoes", Mon. Wea. Rev., 96, 342-350.
- Gifford, F. A., Jr. and S. R. Hanna, 1973: "Modeling Urban Air Pollution", Atmos. Environ., 7, 131-136.
- Holzman, B., 1943: "The Influence of Stability on Evaporation", Ann. N. Y. Acad. Sci., 44, 13-18.
- Lanczos, C., 1970: The Variational Principles of Mechanics, Fourth Edition, University of Toronto Press, Toronto.
- Lettau, H., 1969: "Note on Aerodynamic Roughness-Parameter Estimation on the Basis of Roughness-Element Description", J. Appl. Meteor., 8, 822-832.
- Martin, D. O., 1976: "The Change of Concentration Standard Deviations with Distance", J. Air Poll. Contr. Asso., 26, 145.
- Rossby, C. G. and R. B. Montgomery, 1935: "The Layer of Frictional Influence in Wind and Ocean Currents", Papers Phys. Oceanog. Meteorol., 3, No. 3.
- Sasaki, Y., 1958: "An Objective Analysis Based on the Variational Method", J. Meteor. Soc., Japan, 36, 77-88.
- _____, 1970a: "Some Basic Formalisms in Numerical Variational Analysis", Mon. Wea. Rev., 98, 875-883.
- _____, 1970b: "Numerical Variational Analysis Formulated Under the Constraints as Determined by Long-Wave Equations and a Low-Pass Filter", Mon. Wea. Rev., 98, 884-898.
- _____, 1970c: "Numerical Variational Analysis with Weak Constraint and Application to Surface Analysis of Severe Storm Gusts", Mon. Wea. Rev., 98, 899-910.

REFERENCES (Cont.)

- _____, and J. M. Lewis, 1970: "Numerical Variational Objective Analysis of the Planetary Boundary Layer in Conjunction with Squall Line Formation", J. Meteor. Soc. of Japan, 48, 381-398.
- Stanford University Aerosol Laboratory and the Ralph M. Parson's Company, 1953: "Behavior of Aerosols within Cities", J. Quar. Reports, Nos. 3, 4, 5 and 6.
- Stephens, J. J., 1970: "Variational Initialization with the Balance Equation", J. Appl. Meteor., 9, 732-739.
- Sweeney, H., 1969: "Development of Sampling Guidelines for Regional and Local Planning", Final Report, NAPCA, Contract No. CPA-22-69-57.
- Thompson, P. D., 1961: Numerical Weather Analysis and Prediction, The MacMillan Company, New York.
- TRW Systems Group, 1969: "Air Quality Displace Model, USDHEW, Public Health Service, NAPCA, Washington, D. C.
- Turner, D. B., 1969: "Workbook of Atmospheric Dispersion Estimates", U.S.D. HEW, PHS, Publication No. 999-AP-26, Cincinnati, Ohio.
- User's Guide to the Statistical Analysis System, 1972: Jolayne Service, North Carolina State University.
- Wilkins, E. M., 1971: "Variational Principle Applied to Numerical Objective Analysis of Urban Air Pollution Distribution", J. Appl. Meteor., 10: 974-981.
- _____, 1972: "Variationally Optimized Numerical Analysis Equations for Urban Air Pollution Monitoring Networks", J. Appl. Meteor., 11: 1334-1341.

TECHNICAL REPORT DATA
(Please read Instructions on the reverse before completing)

1. REPORT NO. EPA-600/4-78-030		2.		3. RECIPIENT'S ACCESSION NO.	
4. TITLE AND SUBTITLE OPTIMUM METEOROLOGICAL AND AIR POLLUTION SAMPLING NETWORK SELECTION IN CITIES Volume I: Theory and Design For St. Louis				5. REPORT DATE June 1978	
				6. PERFORMING ORGANIZATION CODE	
7. AUTHOR(S) Fred M. Vukovich, Walter D. Bach, Jr., and C. Andrew Clayton				8. PERFORMING ORGANIZATION REPORT NO.	
9. PERFORMING ORGANIZATION NAME AND ADDRESS Research Triangle Institute P.O. Box 12094 Research Triangle Park, North Carolina 27709				10. PROGRAM ELEMENT NO. 1HD620	
				11. CONTRACT/GRANT NO. 68-03-2187	
12. SPONSORING AGENCY NAME AND ADDRESS U.S. Environmental Protection Agency-Las Vegas, Nevada Office of Research and Development Environmental Monitoring and Support Laboratory Las Vegas, NV 89114				13. TYPE OF REPORT AND PERIOD COVERED	
				14. SPONSORING AGENCY CODE EPA/600/07	
15. SUPPLEMENTARY NOTES The report is the first in a series on this topic. For further information contact James L. McElroy, Project Officer (702)736-2969, ext. 241 in Las Vegas, NV					
16. ABSTRACT A technique was developed to establish an optimum meteorological and air pollution sampling network in urban areas. The basis of the network is the wind field in the urban area rather than the air pollution distribution because it provided a solution with longer-term stability than the air pollution distribution. Three specific models are required in order to determine the optimum network. These are: a three-dimensional hydrodynamic model; a statistical model; and an objective variational analysis model. The primitive equation model is used to simulate the wind field for a variety of cases. These simulated data were used to determine the form of a regression model which approximates the various wind fields. A regression model form was then used, along with a set of potential network sites, and a criterion for judging alternative networks to derive the sampling network for the winds. The method used to develop the network involved the successive elimination of candidate sites until a reasonably sized network was achieved. The air pollution distribution is obtained through an objective variational analysis model. The model simultaneously minimizes the error variance by comparing observed pollution concentrations with derived pollution concentrations and the error variance of the constraint equation.					
17. KEY WORDS AND DOCUMENT ANALYSIS					
a. DESCRIPTORS		b. IDENTIFIERS/OPEN ENDED TERMS		c. COSATI Field/Group	
Air quality Monitoring		Air monitoring network design Ambient air monitoring Carbon monoxide network design Carbon monoxide monitoring Air network design methodology		04B, 09B, 12A	
18. DISTRIBUTION STATEMENT RELEASE TO PUBLIC		19. SECURITY CLASS (This Report) UNCLASSIFIED		21. NO. OF PAGES 154	
		20. SECURITY CLASS (This page) UNCLASSIFIED		22. PRICE	